

---

Electronic Thesis and Dissertation Repository

---

8-24-2016 12:00 AM

## Nanocarriers for Drug Delivery Applications: From Tunable Morphologies to Glycopolymer-coated Vesicles

Brooke M. Raycraft, *The University of Western Ontario*

Supervisor: Dr. Elizabeth Gillies, *The University of Western Ontario*

A thesis submitted in partial fulfillment of the requirements for the Master of Science degree in Chemistry

© Brooke M. Raycraft 2016

Follow this and additional works at: <https://ir.lib.uwo.ca/etd>

---

### Recommended Citation

Raycraft, Brooke M., "Nanocarriers for Drug Delivery Applications: From Tunable Morphologies to Glycopolymer-coated Vesicles" (2016). *Electronic Thesis and Dissertation Repository*. 4040.  
<https://ir.lib.uwo.ca/etd/4040>

This Dissertation/Thesis is brought to you for free and open access by Scholarship@Western. It has been accepted for inclusion in Electronic Thesis and Dissertation Repository by an authorized administrator of Scholarship@Western. For more information, please contact [wlsadmin@uwo.ca](mailto:wlsadmin@uwo.ca).

## Abstract

Amphiphilic block copolymers are well known to undergo self-assembly in aqueous solution into a variety of core/shell structures making them useful for various health applications. These different architectures are largely a result of the hydrophilic volume or weight fraction of the block copolymer. In drug delivery, differences in morphology can largely impact performance and each provides their individual advantages. Polymer vesicles, commonly referred to as polymersomes, have received significant attention due to their resemblance to biological membranes and multifunctional capabilities. This thesis describes the use of novel polyester block copolymers containing a hydrophilic poly(ethylene oxide) block and a hydrophobic poly(hydroxyalkanoate) block bearing alkene functionality. These polyester block copolymers can be functionalized using orthogonal chemistry with a number of molecules in order to tune their hydrophilic weight fraction and obtain a variety of different desirable morphologies. Additionally, this thesis will describe the synthesis of glycopolymer-coated vesicles using RAFT polymerization for their potential application in targeted drug delivery.

## Keywords

Self-assembly, vesicles, drug delivery, morphology, polyesters, RAFT, vesicles, glycopolymers.

## Co-Authorship Statement

The work presented in this thesis is the result of the author's work as well as the work of coworkers at Western University, collaborators at the University of Edinburgh and supervisor Dr. Elizabeth Gillies whose exact contributions are described here.

Chapter 1 was written by the author and edited by Dr. Elizabeth Gillies.

Chapter 2 describes a project proposed by Dr. Elizabeth Gillies in collaboration with Dr. Michael Shaver at the University of Edinburgh. Synthesis of the parent PEO-*b*-PHEL block copolymers were performed by Jarret MacDonald at the University of Edinburgh. All small molecule synthesis, polymer functionalization, self-assembly, and particle characterization was performed by the author while thermal characterization of the polymers was performed by Trevor McIntosh. The chapter constitutes a manuscript in preparation, which was written by the author and edited by Dr. Gillies.

Chapter 3 describes an ongoing project proposed by Dr. Greg Whitton and Dr. Elizabeth Gillies. All small molecule and polymer synthesis as well as self-assembly and particle functionalization were performed by the author, except for the synthesis of  $\beta$ -D-galactose pentaacetate which was provided by postdoctoral fellow Dr. John Trant. The chapter was written by the author and edited by Dr. Gillies.

Chapter 4, the conclusions, was written by the author and edited by Dr. Gillies.

## Acknowledgments

Firstly, I would like to express my immense gratitude toward my supervisor Dr. Elizabeth Gillies for providing me with the opportunity to learn and develop a number of skills during the two years I have spent in her research group. She has been a great mentor and has provided me with endless support, guidance and leadership.

I would also like to sincerely thank all of my fellow lab mates who I have worked closely with over the past two years. All of you have been so willing to provide help and support whenever I have needed it. In particular, I would like to thank Dr. John Trant for providing me with excellent mentorship and knowledge as a new graduate student.

Lastly, I would like to thank my friends and family for their continuous love and support over the past two years. I wouldn't be where I am today without them.



# Table of Contents

Abstract.....	ii
Co-Authorship Statement.....	iii
Acknowledgements.....	iv
Table of Contents.....	v
List of Tables.....	viii
List of Figures.....	ix
List of Schemes.....	xiv
List of Abbreviations.....	xv
Chapter 1	
1 Nanocarriers for Biomedical Applications.....	1
1.1 Introduction to Polymers.....	1
1.2 Amphiphilic Block Copolymers.....	4
1.2.1 Morphology.....	5
1.2.2 Critical Aggregation Concentration (CAC).....	8
1.2.3 Biocompatibility.....	9
1.2.4 Size and Polydispersity Index (PDI) of Polymer Assemblies.....	10
1.2.5 Drug-Core Stability.....	11
1.3 Carbohydrate-Functionalized Polymersomes for Targeted Delivery.....	12
1.4 Thesis Objectives.....	13

1.5 References.....	16
Chapter 2	
2 Functional Polyester Diblock Copolymers Possessing Encapsulation and Chemical Conjugation Capabilities.....	20
2.1 Introduction.....	20
2.2 Experimental.....	21
2.3 Results and Discussion.....	28
2.4 Conclusions.....	43
2.5 References.....	44
Chapter 3	
3 Glycopolymer-functionalized Vesicles via Azide-Alkyne Click Chemistry.....	48
3.1 Introduction.....	48
3.2 Experimental.....	52
3.3 Results and Discussion.....	60
3.4 Conclusions.....	68
3.5 References.....	70
Chapter 4	
4.1 Conclusions and Future Work.....	72
4.2 References.....	75
Permissions.....	76
Appendix 1.....	79

Appendix 2.....	100
Curriculum Vitae.....	108

## List of Tables

Table 2.1. Composition and properties of the PEO- <i>b</i> -PHEL block copolymers.....	29
Table 2.2. Hydrophilic mass fraction of polymers and their self-assembly properties as determined by TEM and DLS.....	32
Table 2.3. Structures and properties of functionalized PEO <sub>45</sub> - <i>b</i> -PHEL <sub>45</sub> copolymers. ND = none detected.....	35
Table 2.4. Hydrophilic mass fractions of polymers and their self-assembly properties as determined by TEM and DLS.....	37
Table 3.1. Overview of varying density and glycopolymer chain length to afford a small library of glycopolymer-coated vesicles.....	50
Table 3.2. Summary of PAcGal glycopolymers synthesized for this study and their molar mass characteristics.....	65
Table A1.1. Summary of the thermal stabilities of PEO- <i>b</i> -PHELs measured by TGA. T <sub>98%</sub> = maximum temperature at which 98% of mass is still present; T <sub>o</sub> = onset degradation temperature.....	95

## List of Figures

Figure 1.1. Schematic depicting the separation of molecules by size using SEC and resulting chromatograph.....	3
Figure 1.2. Schematic of the phase transition temperatures of polymers.....	4
Figure 1.3. Schematic of a homopolymer, random copolymer, block copolymer, and amphiphilic block copolymer.....	5
Figure 1.4. Schematic of the relationship between hydrophilic volume fraction ( $f_v$ ) and resulting morphology imaged by cryogenic transmission electron microscopy (TEM). The figure was reproduced from Reference 16, permission not required.....	6
Figure 1.5. Cartoon schematic of the structures of various common morphologies seen with amphiphilic block copolymers. Adapted with permission from Reference 4 © 2009 John Wiley & Sons.....	7
Figure 1.6. Graph demonstrating fluorescence intensity of pyrene as a function of polymer concentration.....	8
Figure 1.7. Common hydrophobic blocks of a) PLAAs and b) polyesters used for amphiphilic block copolymers.....	10
Figure 1.8. Schematic representations of two different samples of nanoparticles comparing a monodisperse and polydisperse population obtained from light scattering measurements. The figure was reprinted with permission from Reference 38.....	11
Figure 1.9. Synthesis and self-assembly of polyphosphazenes with different saccharide densities. The figure was reprinted with permission from Reference 42.....	12
Figure 1.10. Schematic representation demonstrating the use of thiol-ene click chemistry for the attachment of small molecules to the backbone of newly synthesized PEO- <i>b</i> -PHCL polymers and subsequent self-assembly.....	14

Figure 1.11. Schematic representation of the two approaches for preparing glycopolymer-coated vesicles explored in this study.....	14
Figure 2.1. <sup>1</sup> H NMR overlay of a) PEO <sub>45</sub> - <i>b</i> -PHEL <sub>45</sub> , b) PEO <sub>45</sub> - <i>b</i> -PHEL <sub>45</sub> -octyl, c) PEO <sub>45</sub> - <i>b</i> -PHEL <sub>45</sub> -TEG d) PEO <sub>45</sub> -PHEL <sub>45</sub> -acid.....	30
Figure 2.2. a-c) TEM images and d) fluorescence confocal microscopy image of assemblies formed from a) PEO <sub>45</sub> - <i>b</i> -PHEL <sub>23</sub> , b) PEO <sub>45</sub> - <i>b</i> -PHEL <sub>45</sub> , and c) PEO <sub>45</sub> - <i>b</i> -PHEL <sub>79</sub> by the solvent switching method and d) PEO <sub>45</sub> - <i>b</i> -PHEL <sub>79</sub> by film hydration.....	33
Figure 2.3. TEM images of assemblies formed by the solvent exchange method from: a) PEO <sub>45</sub> - <i>b</i> -PHEL <sub>45</sub> -octyl; b) PEO <sub>45</sub> - <i>b</i> -PHEL <sub>45</sub> -TEG; c) PEO <sub>45</sub> - <i>b</i> -PHEL <sub>45</sub> -RHD self-assembled using the solvent exchange method.....	38
Figure 2.4. <sup>1</sup> H NMR spectra of a) PEO <sub>45</sub> - <i>b</i> -PHEL <sub>45</sub> -PTX34, b) PEO <sub>45</sub> - <i>b</i> -PHEL <sub>45</sub> -acid, and c) free paclitaxel. The peaks labeled with ‘ indicate peaks corresponding to conjugated molecules.....	41
Figure 3.1. Schematic representation depicting rigidity of a glycodendrimer-functionalized polymersome system compared to a glycopolymer-functionalized system.....	49
Figure 3.2. Two approaches for preparing glycopolymer-coated vesicles explored in this study.....	51
Figure 3.3. SEC data of polymerizations of β-D-galactose from CTA functionalized PEO as a control.....	63
Figure 3.4. <sup>1</sup> H NMR spectra of a) PAGal <sub>6</sub> , b) PAcGal <sub>15</sub> , c) PAcGal <sub>29</sub> , and d) protected β-D-galactose monomer ( <b>5</b> ).....	65
Figure 3.5. a) DLS intensity distribution and b) TEM image of extruded PBD- <i>b</i> -PEO vesicles containing 10% PBD- <i>b</i> -PEO-N <sub>3</sub> before click reaction.....	67
Figure 3.6. FTIR spectra of PBD- <i>b</i> -PEO-N <sub>3</sub> vesicles and click reaction between PGal <sub>15</sub> and 100% azide-functionalized vesicles.....	68
Figure A1.1. <sup>1</sup> H NMR spectrum of <b>2</b> (600 MHz, CDCl <sub>3</sub> ).....	79

Figure A1.2. $^1\text{H}$ NMR spectrum of <b>3</b> (600 MHz, $\text{CDCl}_3$ ).....	80
Figure A1.3. $^1\text{H}$ NMR spectrum of <b>4</b> (600 MHz, $\text{CDCl}_3$ ).....	80
Figure A1.4. $^1\text{H}$ NMR spectrum of $\text{PEO}_{45}$ - <i>b</i> -PHEL <sub>23</sub> (600 MHz, $\text{CDCl}_3$ ).....	81
Figure A1.5. $^1\text{H}$ NMR spectrum of $\text{PEO}_{45}$ - <i>b</i> -PHEL <sub>45</sub> (600 MHz, $\text{CDCl}_3$ ).....	81
Figure A1.6. $^1\text{H}$ NMR spectrum of $\text{PEO}_{45}$ - <i>b</i> -PHEL <sub>79</sub> (600 MHz, $\text{CDCl}_3$ ).....	82
Figure A1.7. $^1\text{H}$ NMR spectrum of $\text{PEO}_{45}$ - <i>b</i> -PHEL <sub>45</sub> -octyl (600 MHz, $\text{CDCl}_3$ ).....	82
Figure A1.8. $^1\text{H}$ NMR spectrum of $\text{PEO}_{45}$ - <i>b</i> -PHEL <sub>45</sub> -TEG (600 MHz, $\text{CDCl}_3$ ).....	83
Figure A1.9. $^1\text{H}$ NMR spectrum of $\text{PEO}_{45}$ - <i>b</i> -PHEL <sub>45</sub> -acid (600 MHz, $\text{CDCl}_3$ ).....	83
Figure A1.10. $^1\text{H}$ NMR spectrum of $\text{PEO}_{45}$ - <i>b</i> -PHEL <sub>45</sub> -PTX34 (600 MHz, $\text{CDCl}_3$ ).....	84
Figure A1.11 $^1\text{H}$ NMR spectrum of $\text{PEO}_{45}$ - <i>b</i> -PHEL <sub>45</sub> -RHD (600 MHz, $\text{CDCl}_3$ ).....	84
Figure A1.12 ATR-FTIR spectra of $\text{PEO}_{45}$ - <i>b</i> -PHEL <sub>23</sub> .....	85
Figure A1.13 ATR-FTIR spectra of $\text{PEO}_{45}$ - <i>b</i> -PHEL <sub>45</sub> .....	85
Figure A1.14 ATR-FTIR spectra of $\text{PEO}_{45}$ - <i>b</i> -PHEL <sub>79</sub> .....	86
Figure A1.15 ATR-FTIR spectra of $\text{PEO}_{45}$ - <i>b</i> -PHEL <sub>45</sub> -octyl.....	86
Figure A1.16 ATR-FTIR spectra of $\text{PEO}_{45}$ - <i>b</i> -PHEL <sub>45</sub> -TEG.....	87
Figure A1.17 ATR-FTIR spectra of $\text{PEO}_{45}$ - <i>b</i> -PHEL <sub>45</sub> -acid.....	87
Figure A1.18 ATR-FTIR spectra of $\text{PEO}_{45}$ - <i>b</i> -PHEL <sub>45</sub> -PTX34.....	88
Figure A1.19 ATR-FTIR spectra of $\text{PEO}_{45}$ - <i>b</i> -PHEL <sub>45</sub> -RHD.....	88
Figure A1.20 SEC trace for $\text{PEO}_{45}$ - <i>b</i> -PHEL <sub>23</sub> .....	89
Figure A1.21 SEC trace for $\text{PEO}_{45}$ - <i>b</i> -PHEL <sub>45</sub> .....	89
Figure A1.22 SEC trace for $\text{PEO}_{45}$ - <i>b</i> -PHEL <sub>79</sub> .....	89

Figure A1.23 SEC trace for PEO <sub>45</sub> - <i>b</i> -PHEL <sub>45</sub> -octyl.....	90
Figure A1.24 SEC trace for PEO <sub>45</sub> - <i>b</i> -PHEL <sub>45</sub> -TEG.....	90
Figure A1.25 SEC trace for PEO <sub>45</sub> - <i>b</i> -PHEL <sub>45</sub> -PTX34.....	90
Figure A1.26 SEC trace for PEO <sub>45</sub> - <i>b</i> -PHEL <sub>45</sub> -RHD.....	91
Figure A1.27 DSC curve for PEO <sub>45</sub> - <i>b</i> -PHEL <sub>23</sub> (obtained from third heating cycle).....	91
Figure A1.28 DSC curve for PEO <sub>45</sub> - <i>b</i> -PHEL <sub>45</sub> (obtained from third heating cycle).....	92
Figure A1.29 DSC curve for PEO <sub>45</sub> - <i>b</i> -PHEL <sub>79</sub> (obtained from third heating cycle).....	92
Figure A1.30 DSC curve for PEO <sub>45</sub> - <i>b</i> -PHEL <sub>45</sub> -octyl (obtained from fourth heating cycle)...	93
Figure A1.31 DSC curve for PEO <sub>45</sub> - <i>b</i> -PHEL <sub>45</sub> -TEG (obtained from fourth heating cycle)...	93
Figure A1.32 DSC curve for PEO <sub>45</sub> - <i>b</i> -PHEL <sub>45</sub> -acid (obtained from third heating cycle).....	94
Figure A1.33 DSC curve for PEO <sub>45</sub> - <i>b</i> -PHEL <sub>45</sub> -PTX34 (obtained from third heating cycle).	94
Figure A1.34 DSC curve for PEO <sub>45</sub> - <i>b</i> -PHEL <sub>45</sub> -RHD (obtained from third heating cycle).....	95
Figure A1.35 TGA curve for PEO <sub>45</sub> - <i>b</i> -PHEL <sub>23</sub> .....	96
Figure A1.36 TGA curve for PEO <sub>45</sub> - <i>b</i> -PHEL <sub>45</sub> .....	96
Figure A1.37 TGA curve for PEO <sub>45</sub> - <i>b</i> -PHEL <sub>79</sub> .....	97
Figure A1.38 TGA curve for PEO <sub>45</sub> - <i>b</i> -PHEL <sub>45</sub> -octyl.....	97
Figure A1.39 TGA curve for PEO <sub>45</sub> - <i>b</i> -PHEL <sub>45</sub> -TEG.....	98
Figure A1.40 TGA curve for PEO <sub>45</sub> - <i>b</i> -PHEL <sub>45</sub> -acid.....	98
Figure A1.41 TGA curve for PEO <sub>45</sub> - <i>b</i> -PHEL <sub>45</sub> -PTX34.....	99
Figure A1.42 TGA curve for PEO <sub>45</sub> - <i>b</i> -PHEL <sub>45</sub> -RHD.....	99



Figure A2.1. $^1\text{H}$ NMR of acrylamide functionalized $\beta$ -D-galactose pentacetate monomer ( <b>5</b> ) immediately before polymerization (600 MHz, $\text{CDCl}_3$ ).....	100
Figure A2.2. $^1\text{H}$ NMR of purified $\beta$ -D-galactose monomer possessing acrylamide functionality ( <b>6</b> ) (600 MHz, $\text{D}_2\text{O}$ ).....	100
Figure A2.3. $^1\text{H}$ NMR spectra of $\beta$ -D-galactose monomer, CTA-functionalized PBD- <i>b</i> -PEO vesicles, polymerization at $t = 18$ h, and $t = 48$ h (bottom to top).....	101
Figure A2.4. $^1\text{H}$ NMR of prop-2-ynyl-2-(butylthiocarbonothiolthio)-2-methylpropanoate alkyne RAFT CTA (600 MHz, $\text{CDCl}_3$ ).....	102
Figure A2.5. $^1\text{H}$ NMR of 2-azidoacetic acid (600 MHz, $\text{CDCl}_3$ ).....	102
Figure A2.6. $^1\text{H}$ NMR of PBD- <i>b</i> -PEO- $\text{N}_3$ (600 MHz, $\text{CDCl}_3$ ).....	103
Figure A2.7. $^1\text{H}$ NMR of PAcGal <sub>6</sub> (600 MHz, $\text{CDCl}_3$ ).....	103
Figure A2.8. $^1\text{H}$ NMR of PAcGal <sub>15</sub> (600 MHz, $\text{CDCl}_3$ ).....	104
Figure A2.9. $^1\text{H}$ NMR of PAcGal <sub>29</sub> (600 MHz, $\text{CDCl}_3$ ).....	104
Figure A2.10. $^1\text{H}$ NMR of PGal <sub>6</sub> (600 MHz, $\text{D}_2\text{O}$ ).....	105
Figure A2.11. $^1\text{H}$ NMR of PGal <sub>15</sub> (600 MHz, $\text{D}_2\text{O}$ ).....	105
Figure A2.12. $^1\text{H}$ NMR of PGal <sub>29</sub> (600 MHz, $\text{D}_2\text{O}$ ).....	106
Figure A2.13. $^1\text{H}$ NMR of click reaction between PGal <sub>15</sub> and 10% azide-functionalized vesicles (600 MHz, $\text{D}_2\text{O}$ ).....	106
Figure A2.14. SEC trace for PAcGal <sub>6</sub> .....	107
Figure A2.15. SEC trace for PAcGal <sub>15</sub> .....	107
Figure A2.16. SEC trace for PAcGal <sub>29</sub> .....	107

## List of Schemes

Scheme 2.1. Synthesis of PEO- <i>b</i> -PHEL block copolymers.....	29
Scheme 2.2. Functionalization of PEO <sub>45</sub> - <i>b</i> -PHEL <sub>45</sub> with octyl chains, TEG, and carboxylic acids.....	35
Scheme 2.3. Synthesis of the PTX conjugate PEO <sub>45</sub> - <i>b</i> -PHEL <sub>45</sub> -PTX34 starting from PEO <sub>45</sub> - <i>b</i> -PHEL <sub>45</sub> -acid. The site of conjugation on PTX is circled.....	40
Scheme 2.4. Synthesis of a thiol-functionalized rhodamine derivative and its conjugation to PEO <sub>45</sub> - <i>b</i> -PHEL <sub>45</sub> .....	43
Scheme 3.1. Synthesis of acrylamide-functionalized $\beta$ -D-galactose monomer ( <b>6</b> ).....	60
Scheme 3.2. Synthesis of PBD- <i>b</i> -PEO-CTA from 2-(butylthiocarbonothioylthio)-2-methylpropanoic acid.....	61
Scheme 3.3. Self-assembly of CTA functionalized vesicles in the presence of Nile red and subsequent polymerization of monomer <b>6</b> from the surface.....	61
Scheme 3.4. Synthesis of PEO <sub>2K</sub> -CTA and control polymerization with <b>6</b> .....	62
Scheme 3.5. Synthesis of PAcGal <sub>n</sub> using RAFT polymerization and subsequent deprotection to give PGal <sub>n</sub> glycopolymers.....	64
Scheme 3.6. Preparation of PBD- <i>b</i> -PEO vesicles with azide functionality presented on the surface.....	66
Scheme 4.1. Preparation of Rhodamine-labeled polymersomes for quantification of glycopolymer chains.....	74

## List of Abbreviations

AIBN	Azobisisobutyronitrile
$\beta$ -6-HEL	$\beta$ -6-heptenolactone
BHT	Butylated hydroxytoluene
CAC	Critical aggregation concentration
CTA	Chain transfer agent
$\bar{D}$	Dispersity
DCC	<i>N,N'</i> -dicyclohexylcarbodiimide
DIPEA	<i>N,N'</i> -diisopropylethylamine
DLS	Dynamic light scattering
DMAP	4-dimethylaminopyridine
DMPA	2,2-dimethoxy-2-phenylacetophenone
DMF	<i>N,N'</i> -dimethylformamide
DMSO	Dimethylsulfoxide
DP	Degree of polymerization
DPTS	4-(dimethylamino)pyridinium-4-toluene sulfonate
DSC	Differential scanning calorimetry
EDC	<i>N</i> -ethyl- <i>N'</i> -(3-dimethylaminopropyl)carbodiimide
EtOAc	Ethyl acetate
$f_v$	Hydrophilic volume fraction

$f_m$	Hydrophilic mass fraction
FDA	Food and Drug Administration
FTIR	Fourier transform infrared
MALS	Multiangle light scattering
$M_i$	Mass of polymers in polymer set i
MWCO	Molecular weight cut off
$N_i$	Number of polymers in polymer set i
NMR	Nuclear magnetic resonance
PEO	Poly(ethylene oxide)
PHEL	Poly(3-hydroxy-6-heptenoate)
RAFT	Reversible addition fragmentation chain transfer
RES	Reticuloendothelial system
SEC	Size exclusion chromatography
TEG	Triethylene glycol
TEM	Transmission electron microscopy
$T_g$	Glass-transition temperature
TGA	Thermogravimetric analysis
THF	Tetrahydrofuran
TLC	Thin layer chromatography
$T_m$	Melting temperature

UATR	Universal attenuated total reflectance
UV	Ultraviolet
$V_e$	Elution volume

## Chapter 1

### 1 Nanocarriers for Biomedical Applications

Nanocarriers have been widely investigated for their use in drug delivery and other biomedical applications.<sup>1-4</sup> A number of drugs that show high potential to be effective therapeutics are hydrophobic and therefore are insoluble in the bloodstream.<sup>5</sup> These drugs may degrade in the bloodstream before reaching their site of action and can also be toxic to healthy tissues.<sup>6</sup> Nanocarriers are promising biomaterials that can be used to solubilize drugs, protect the drug from undergoing unwanted physiochemical reactions or degradation, as well as target the drug to a specific disease site. Various nanocarriers are currently in use today as pharmaceuticals including Doxil (liposomes containing doxorubicin), SMANCS (polymer-drug conjugate of neocarzinostatin), and Abraxane (albumin-bound paclitaxel nanoparticles) which have all been approved by the Food and Drug Administration (FDA) for use as cancer therapeutics.<sup>7</sup> Several other drug delivery systems are currently at various stages in clinical trials.

#### 1.1 Introduction to Polymers

Polymers are macromolecular structures comprised of small monomeric units. These high molecular weight molecules are ubiquitous in nature and include proteins, DNA, and polysaccharides. Polymers can also be made synthetically by a number of different processes to obtain materials with a wide range of desirable properties. Some common examples of synthetic polymers include Teflon, polyethylene, nylon, polystyrene, and poly(vinyl chloride).

In comparison to small molecules, which possess very well-defined molecular weights and physical properties, polymers are generally polydisperse in that they contain polymer chains of unequal length. This is due to the polymerization process, in which chain growth is controlled by the probability of attachment of a given monomer. As a result, polymers have molecular weight distributions and broadly defined physical properties. These properties are primarily dictated by the distribution of polymer chains and the number of repeat units in the chain, also known as the degree of polymerization (DP).

Due to this distribution, the molecular weight of a polymer is described as an average molecular weight calculated from the molecular weights of all the chains in the sample. The most commonly reported molecular weight averages include: the number average molecular weight ( $M_n$ ) and the weight average molecular weight ( $M_w$ ).  $M_n$  describes the statistical average molecular weight of all polymer chains in the sample, and is defined by:

$$M_n = \frac{\sum_i N_i M_i}{\sum_i N_i}$$

where  $M_i$  is the molecular weight of a chain and  $N_i$  is the number of chains of that molecular weight.

Conversely,  $M_w$  takes into account the molecular weight of a chain in determining contributions to the molecular weight average, and is defined by:

$$M_w = \frac{\sum_i N_i M_i^2}{\sum_i N_i M_i}$$

Using these two molecular weight averages, the distribution of size or molecular weight of a given polymer sample can be obtained, known as the dispersity ( $\mathcal{D}$ ):

$$\mathcal{D} = \frac{M_w}{M_n}$$

For an ideal polymer,  $\mathcal{D}$  would be equal to one indicating a completely monodisperse sample. However, in practice, the  $\mathcal{D}$  is always greater than one due to the distributions of molar masses. These molecular weight averages are commonly determined through size exclusion chromatography (SEC), which separates polymer molecules based on their size. A polymer solution is injected into a solvent stream that passes through a column packed with beads containing various pore sizes (Figure 1.1). Smaller molecules are able to pass through the pores in the beads while the larger molecules cannot. As a result, the larger the molecule is in solution the faster it will pass through the column as its passage is not impeded by the pores. In contrast, smaller molecules take the longest to elute as they must travel through numerous pores throughout the column. Thus, fractionation

occurs depending on elution volume  $V_e$ , the volume of solvent required to pass the molecule through the column to the detector. This results in a distribution of the proportions of molecules with different sizes in decreasing order of volume in solution. To convert this information from a distribution of volumes to a distribution of molar masses, a calibration is performed using polymer standards of known molar mass.

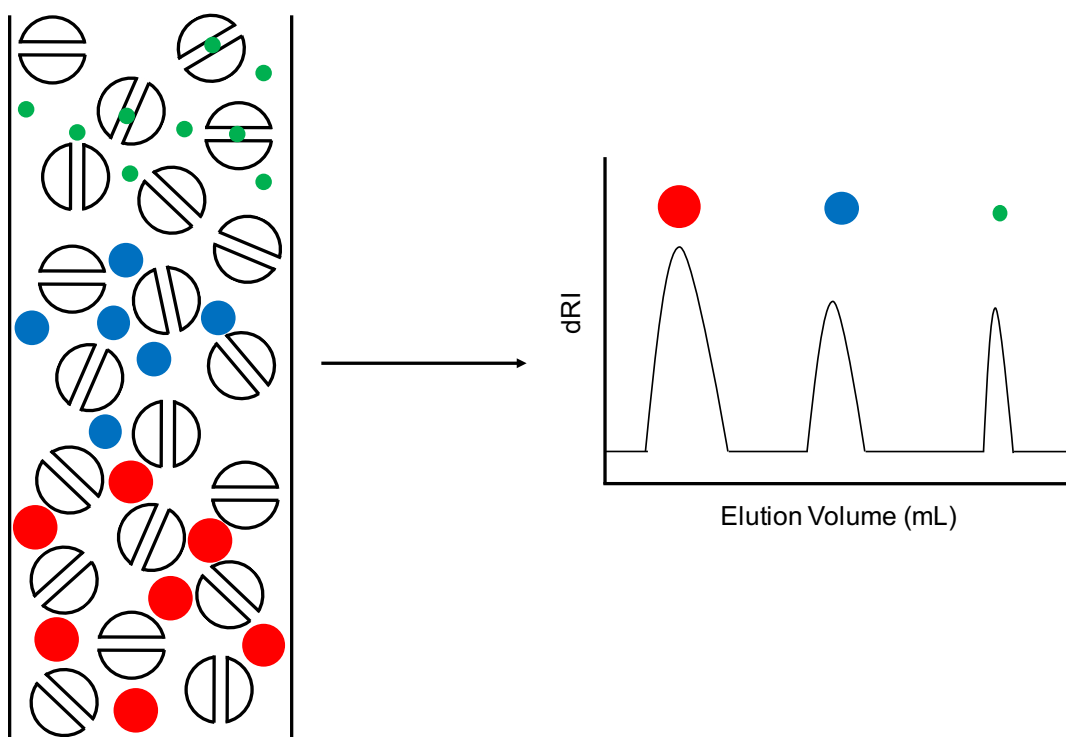


**Figure 1.1.** Schematic depicting the separation of molecules by size using SEC and resulting chromatograph.

Polymers can also be characterized by their state transition temperatures. Unlike small molecules that can exist as solid, liquid or gas separated by phase-transitions occurring at very well-defined temperatures, polymers can exhibit an amorphous glassy state, a crystalline state, rubbery state and melt state. These states are separated by the glass-transition temperature ( $T_g$ ) and melting temperature ( $T_m$ ) (Figure 1.2). Below the  $T_g$ , the polymer is in the glassy state. The polymer chains are static and the polymer is hard and brittle. Above the  $T_g$ , the polymer chains exist in both a static and fluid state resulting in a soft or rubbery material. Below the  $T_m$ , polymer can contain crystalline domains. Above



the  $T_m$ , polymer chains are completely mobile and exhibit fluid-like properties. However, the melting transition is only seen for crystalline polymers and occurs when the polymer chains fall out of their crystal structures and become a disordered liquid. Phase-transition temperatures are determined using differential scanning calorimetry (DSC), a thermoanalytical technique in which the difference in the amount of heat required to increase the temperature of a sample and a reference is measured over multiple heating and cooling cycles. When a phase transition occurs, it will require more or less heat to maintain the sample temperature providing  $T_g$  and  $T_m$ .

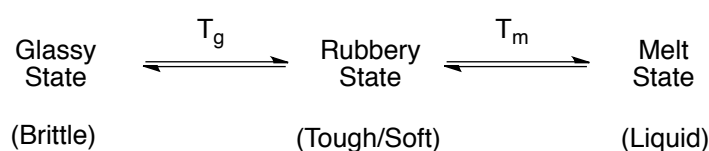


**Figure 1.2.** Schematic of the phase transition temperatures of polymers.

## 1.2 Amphiphilic Block Copolymers

A homopolymer is a polymer composed of repeating units of a single monomer (Figure 1.3). Alternatively, a copolymer is composed of two or more monomers. Block copolymers are linear copolymers formed by alternating homopolymer blocks that differ in composition or structure. In particular, amphiphilic block copolymers consist of at least two regions of distinct chemical nature that undergo phase separation as a result of chain association in solvents that selectively dissolve one of the blocks.<sup>8</sup> Self-assembly of amphiphilic molecules in aqueous solution is driven by the unfavourable interaction of the hydrophobic segment with water, forcing hydrophobic chains to associate with each other to minimize energetically unfavourable hydrophobe-water interactions. Amphiphilic block copolymers can self-assemble in solution, thin-film or bulk and demonstrate a wide range of useful applications including energy storage, biomedical applications, data transfer and storage, catalysis, and separations devices.<sup>9</sup> However, solution self-assembly has received significant attention for its ability to form nanoscale supramolecular core/shell structures. Amphiphilic block copolymers have been shown to

assemble into a vast array of interesting morphologies including spherical micelles,<sup>10</sup> worm-like structures<sup>11</sup> and polymeric vesicles.<sup>12,13</sup> This behavior is analogous to the self assembly of surfactants. However, compared to surfactant micelles, block copolymer aggregates typically have much slower exchange kinetics of individual chains leading to kinetically stagnant systems.<sup>14,15</sup> Additionally, the higher molecular weights and chain entanglements result in more resistant assemblies preventing the leakage of cargo.

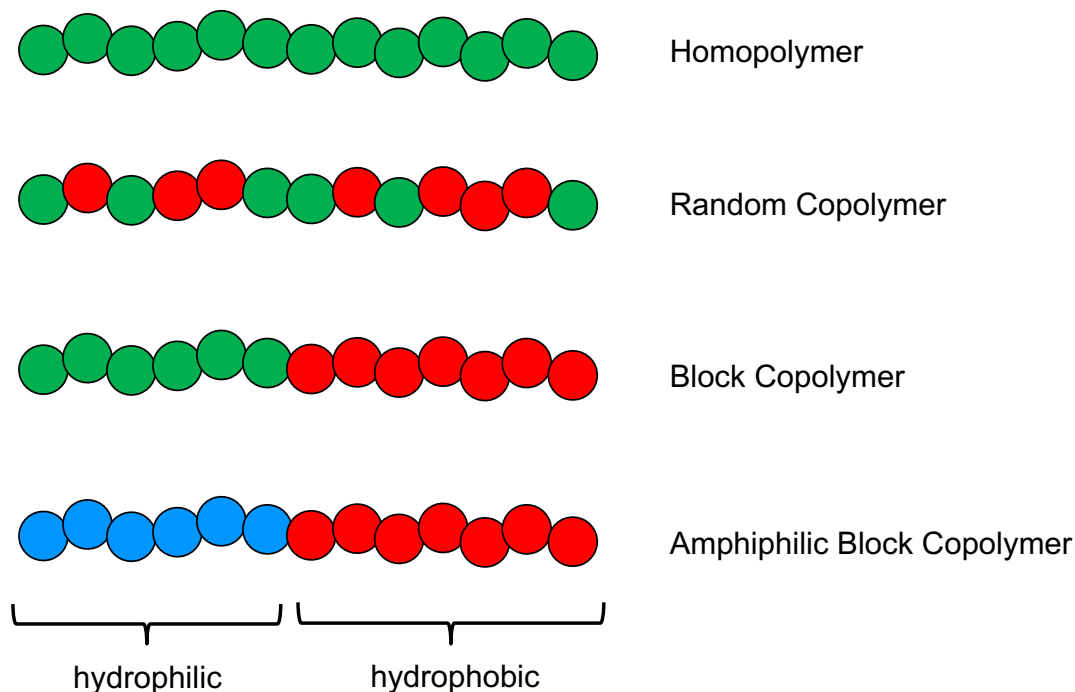


**Figure 1.3.** Schematic of a homopolymer, random copolymer, block copolymer, and amphiphilic block copolymer.

### 1.2.1 Morphology

The morphology of polymer aggregates is primarily the result of the inherent molecular curvature and is largely predicted by the hydrophilic volume fraction ( $f_v$ ) of the block copolymer. Typically, block copolymers with large hydrophilic blocks will assemble into spherical micelles. Lower  $f_v$  values tend to produce vesicles where as  $f_v$  values in the intermediate range produce cylindrical micelles (Figure 1.4). While approximate volume

fractions corresponding to the different morphologies are shown in Figure 1.4, the specific quantities are largely influenced by the chemical structures of the given polymers.

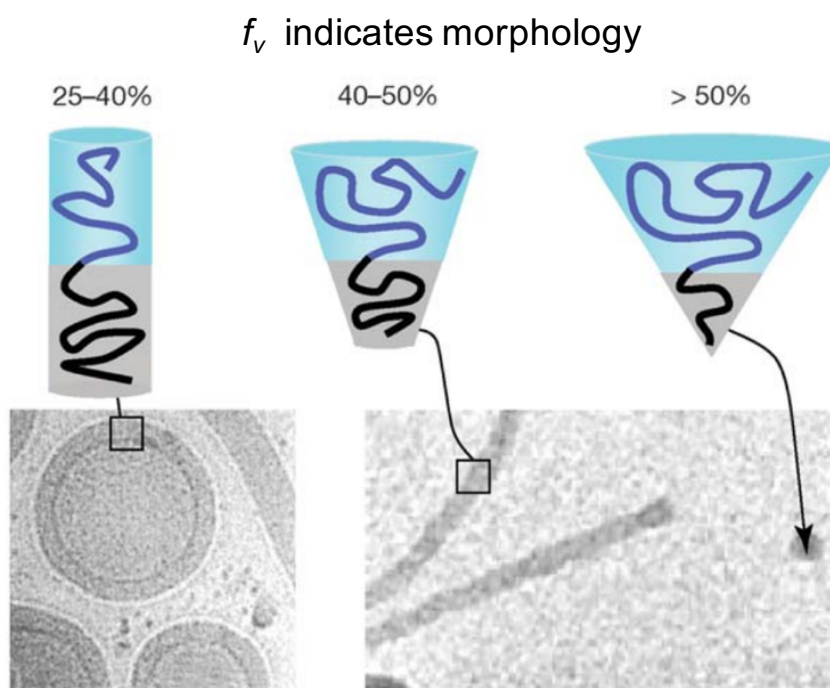


**Figure 1.4.** Schematic of the relationship between hydrophilic volume fraction ( $f_v$ ) and resulting morphology imaged by cryogenic transmission electron microscopy (TEM). The figure was reproduced from Reference 16, permission not required.<sup>16</sup>

Different morphologies can each provide their own advantages in terms of biological applications. In drug delivery, differences in morphology have the ability to largely impact performance.<sup>17</sup> Polymer vesicles, commonly referred to as polymersomes, have received significant attention due to their resemblance to biological membranes. In comparison to biological membranes, polymer vesicles possess increased strength and decreased permeability.<sup>14</sup> Additionally, polymersomes are potentially multifunctional as they possess a hydrophilic core with the ability to encapsulate water-soluble molecules, a hydrophobic membrane that can encapsulate hydrophobic species, and a surface to which various moieties can be conjugated (Figure 1.5). In contrast, micelles possess a hydrophobic core surrounded by a hydrophilic corona that minimizes the interaction of

the hydrophobic block with the aqueous surroundings. As a result, spherical and cylindrical micelles are capable of encapsulating hydrophobic molecules within their cores. However, they lack the capability of encapsulating other types of cargo such as hydrophilic drugs, proteins, and nucleic acids. Although most block copolymer-based systems being studied for drug delivery are spherical in morphology, work done by Discher demonstrated that micelles of cylindrical morphology possess favourable properties including higher drug loading and longer circulation lifetime in the bloodstream.<sup>18,19</sup> Cylindrical micelles provide a larger core volume, allowing the encapsulation of more drug per carrier as well as the ability to easily flow through pores and capillaries due to their flexibility and small diameter.<sup>20</sup> However, only a small number of biocompatible block copolymers have been shown to reproducibly form cylindrical micelles in solution. Due to the various advantages of different morphologies in drug delivery, being able to tune the morphology of biocompatible block copolymer aggregates is of high interest.

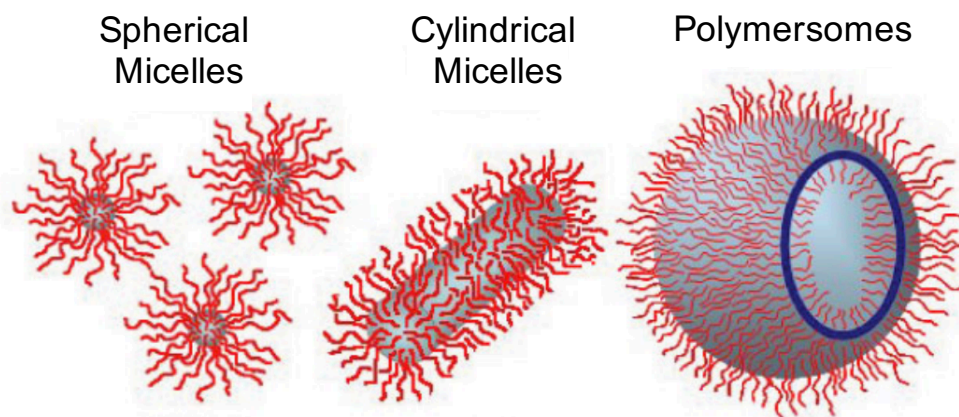


**Figure 1.5.** Cartoon schematic of the structures of various common morphologies seen with amphiphilic block copolymers. Adapted with permission from Reference 4 © 2009 John Wiley & Sons.<sup>4</sup>

### 1.2.2 Critical Aggregation Concentration (CAC)

Polymeric aggregates are in thermodynamic equilibrium with their individual unimers in aqueous solution. The critical aggregation concentration (CAC) is the lowest concentration of copolymer required in order to form an assembly and provides an indirect measure of assembly stability. At low concentrations of polymer, there are an insufficient concentration of polymer chains to assemble and they are instead dispersed in solution. As the concentration of polymer in solution is increased, more chains are able to associate at the aqueous-organic solvent interface and eventually form assembled structures. The CAC can be measured through the use of a fluorescent hydrophobic molecule, commonly pyrene. To do this, the ratio of the fluorescent excitation intensity of pyrene at 338-339 nm to that at 333-334 nm is measured as a function of polymer concentration. As concentration increases and aggregates begin to form, pyrene preferentially localizes in the hydrophobic core of the aggregates resulting in an increase in the excitation intensity ratio due to the less polar environment. The CAC corresponds to the onset of the increase in intensity (Figure 1.6).

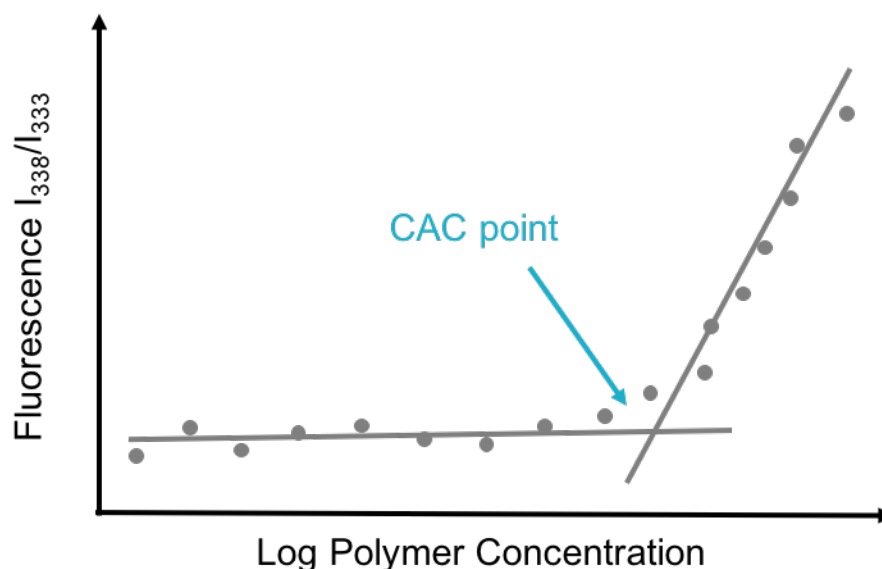


**Figure 1.6.** Graph demonstrating fluorescence intensity of pyrene as a function of polymer concentration.

Aggregate disintegration can occur as a result of significant dilution causing a premature release of cargo. This is a common problem experienced when administering drug-loaded micelles into the bloodstream and is known as the burst release effect.<sup>21,22</sup> Consequently, having assemblies with low CACs or stabilized through crosslinking or other types of interactions is highly desirable.

### 1.2.3 Biocompatibility

An important consideration in the design of materials for biomedical applications is biocompatibility. Among the many different block copolymers designed for drug delivery, those with poly(ethylene oxide) (PEO) as the hydrophilic block have been of broadest interest. It is well established that the conjugation of PEO to biologically relevant molecules typically enhances their water solubility and hydrolytic stability. PEO reduces recognition by the reticuloendothelial system (RES) resulting in longer circulation time.<sup>3</sup> For example, PEO has been shown to extend in vivo circulation lifetimes for insulin, allowing a lower dose frequency and higher patient compliance.<sup>23,24</sup> It is also imperative that the hydrophobic block is biocompatible. Some commonly studied hydrophobic blocks with known biocompatibility include poly(propylene oxide), polyesters, polycarbonates, and poly(L-amino acid)s (PLAAs).<sup>25,26</sup> Of these core-forming blocks, polyesters and PLAAs are of particular interest due to their potential biodegradability. PLAAs are especially advantageous as they possess functional groups allowing chemical conjugation or electrostatic interaction between the amino acid chain and various biologically active molecules. PLAAs have been widely studied for drug delivery and are currently undergoing clinical trials for the delivery of various therapeutics. PLAAs that have been explored as the core-forming block of polymeric micelles include poly( $\beta$ -benzyl L-aspartate) (PBLA), poly( $\gamma$ -benzyl-L-glutamate) (PBGL), poly(*N*-hexyl stearate-L-aspartamide) (PHSA), poly(L-lysine) (PLL), and poly(L-aspartic acid) (PASA) (Figure 1.7).<sup>27</sup> However, the long-term immunogenicity and biodegradability of the polyamide chain must still be established. In contrast, polyesters have shown safe application in humans with well established biodegradability. However, few examples in the literature exist of polyesters with functional groups on the polymer backbone for post-polymerization chemistry.<sup>28-36</sup> The most widely investigated

polyesters for use in polymeric nanocarriers include polycaprolactone (PCL), poly(lactic acid) (PLA) and poly(glycolic acid) (PGA).

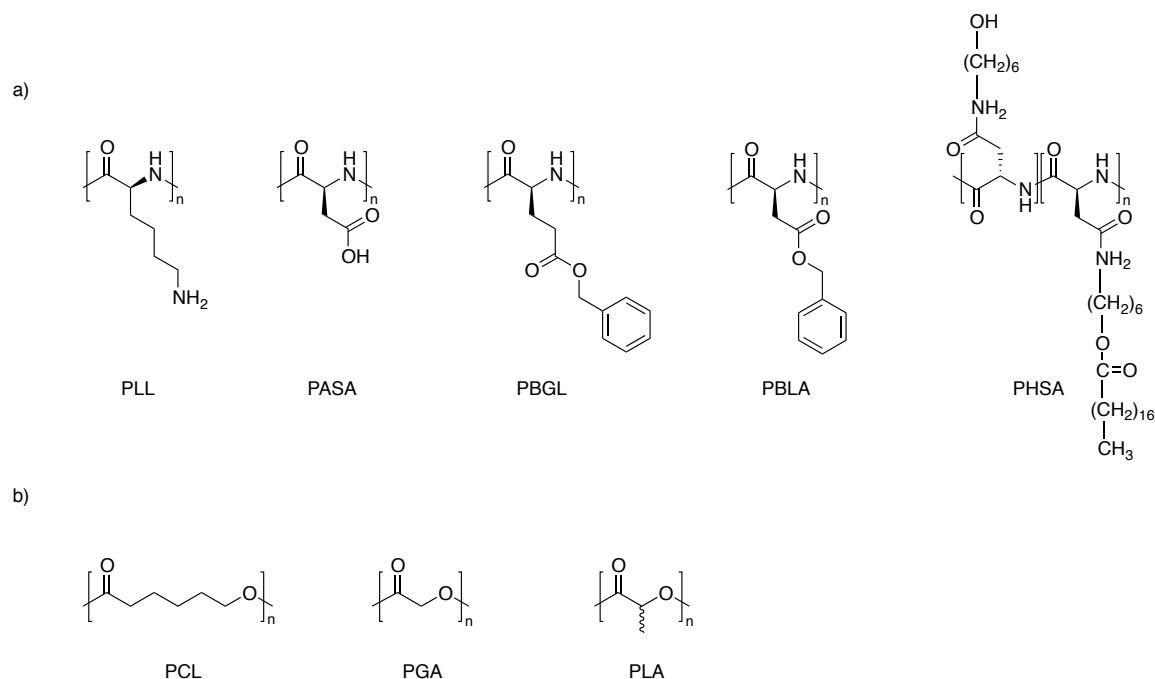


**Figure 1.7.** Common hydrophobic blocks of a) PLAAs and b) polyesters used for amphiphilic block copolymers.

#### 1.2.4 Size and Polydispersity Index (PDI) of Polymer Assemblies

Size influences both the clearance and the biodistribution of drug delivery systems. In order to utilize polymer assemblies for drug delivery applications, an ideal size must be achieved in which particles are large enough to avoid being filtered by the kidneys while small enough that they do not accumulate in the liver. This size range is hypothesized to be somewhere between 70 and 200 nm.<sup>37</sup> When aggregates are less than 200 nm in diameter, uptake by the RES of the liver and spleen is limited.<sup>5</sup> In contrast, small particles (<20-30 nm) are eliminated by the kidneys following administration.<sup>38</sup> Particle size is often measured by light scattering techniques such as dynamic light scattering (DLS) or multiangle light scattering (MALS).

In addition to size, another important consideration is that particles have a low polydispersity index (PDI), meaning there is a narrow distribution in sizes among

assemblies (Figure 1.8). Having aggregates of uniform size is important in controlling the variability in product performance. The PDI of polymeric aggregates is commonly measured by light scattering techniques on a scale of 0.05 to 1 where 0.05 is monodisperse and 1 is very polydisperse.

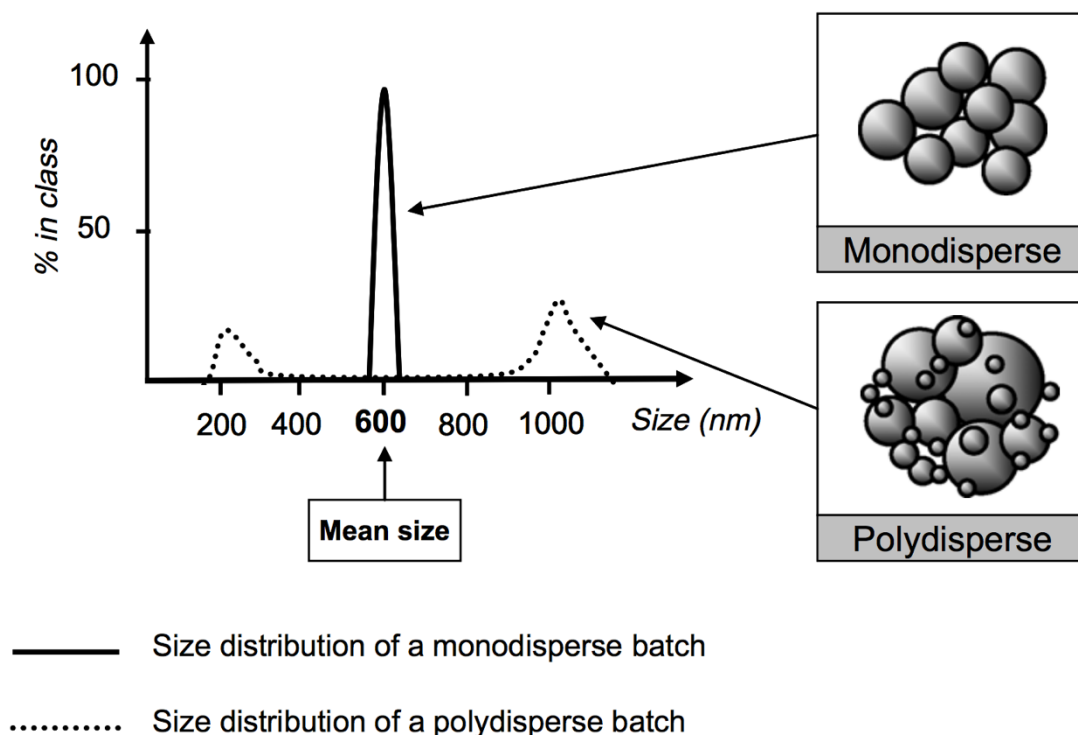


**Figure 1.8.** Schematic representations of two different samples of nanoparticles comparing a monodisperse and polydisperse population obtained from light scattering measurements. The figure was reprinted with permission from Reference 38.

### 1.2.5 Drug-Core Stability

Another important characteristic in designing effective polymeric nanocarriers for drug delivery is the interaction between the drug and the core of the nanoparticle. Favourable drug-core interactions can result in higher drug loading and increased drug solubilization.<sup>39</sup> These interactions can be made more favourable by changing the hydrophobic block length or structure. However, due to the various different structures and properties of pharmaceuticals, optimizations made for one system cannot be universally applied to all.



### 1.3 Carbohydrate-Functionalized Polymersomes for Targeted Delivery

One of the major challenges in optimizing drug delivery vehicles is to selectively target the site of interest.<sup>40</sup> One way this can be achieved is through the incorporation of carbohydrates onto the surface of molecular assemblies as they are involved in many cellular recognition events. Biological saccharides such as glycoproteins, glycolipids and proteoglycans are involved in numerous physiological functions including cell adhesion, protection against pathogen invasion, immune response, fertilization and blood coagulation through sugar-lectin recognition.<sup>41,42</sup> However, the majority of saccharide–protein interactions are generally too weak to be used in biomaterials and devices. These interactions can be amplified through multivalency. Multivalent glycopolymers, or polymers possessing pendant saccharides on the backbones, have been reported to exhibit strong saccharide–protein interactions. Recent advances in controlled polymerization techniques have provided the means to easily access well-defined glycopolymers. In particular, reversible addition fragmentation chain transfer (RAFT) polymerization has been shown to produce glycopolymers with defined end functionalities, controlled molecular weights, low *D* and little toxicity.<sup>43–47</sup>

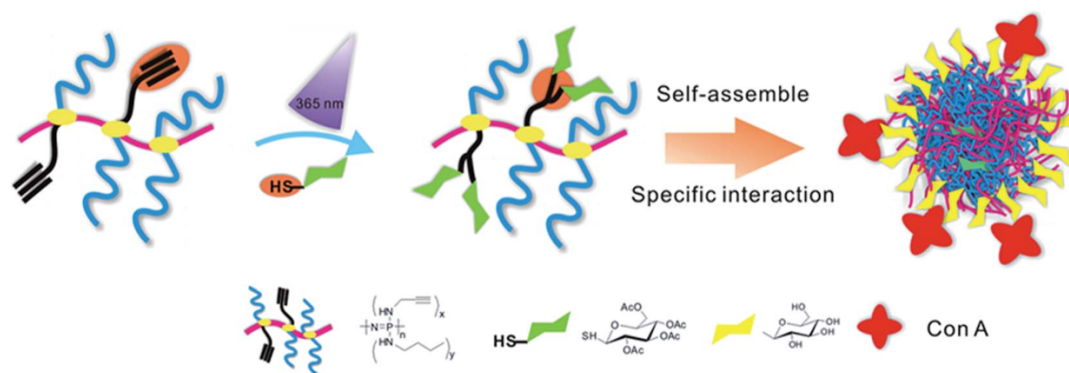


**Figure 1.9.** Synthesis and self-assembly of polyphosphazenes with different saccharide densities. The figure was reprinted with permission from Reference 42.<sup>42</sup>

There are various factors that can influence the binding affinity of glycopolymers to lectin including structure of the saccharide, density of saccharides along the glycopolymer

chain, and relative spatial orientation of the glycopolymers upon the substrates of which they are displayed. In a recent study, Chen and coworkers synthesized an amphiphilic glycosylated polyphosphazene using thiol-yne click chemistry to create polyphosphazenes with different saccharide densities, P-37% and P-58% (Figure 1.9).<sup>42</sup> These amphiphilic glycopolymers were then self-assembled and found to form spherical micelles. The binding affinities of the assemblies toward lectin were studied and it was found that the higher ratio of hydrophobic alkyl groups to  $\beta$ -D-glucose residues considerably enhanced the hydrophobic interactions with the lectin Concanavalin A resulting in higher binding affinity. This study provides evidence that density of glycopolymer on the surface of assemblies influences the strength of binding between saccharides and protein.

In addition to targeted drug delivery, glycopolymers can also serve as therapeutics themselves due to their abundant involvement in many biological processes. Synthetic glycopolymers can function as biological mimics displaying anticoagulant, anti-inflammatory, anti-viral, and anti-tumor properties.<sup>48</sup>

## 1.4 Thesis Objectives

The main goal of this thesis is to present two alternative strategies for obtaining polymeric nanocarriers with the potential to be used in biomedical applications.

Chapter 2 will describe the use of novel polyester block copolymers containing a hydrophilic PEO block and a hydrophobic poly(3-hydroxy-6-heptenoate) (PHEL) block bearing alkene functionality. In this chapter, thiol-ene click chemistry is utilized to conjugate various hydrophilic or hydrophobic species onto the polymer backbone (Figure 1.10). Following solution self-assembly, the effect of changing the polymer's hydrophilic weight fraction on morphology will be investigated. Additionally, this chapter explores the conjugation of biologically relevant molecules to the polymer backbone including drugs and dyes.

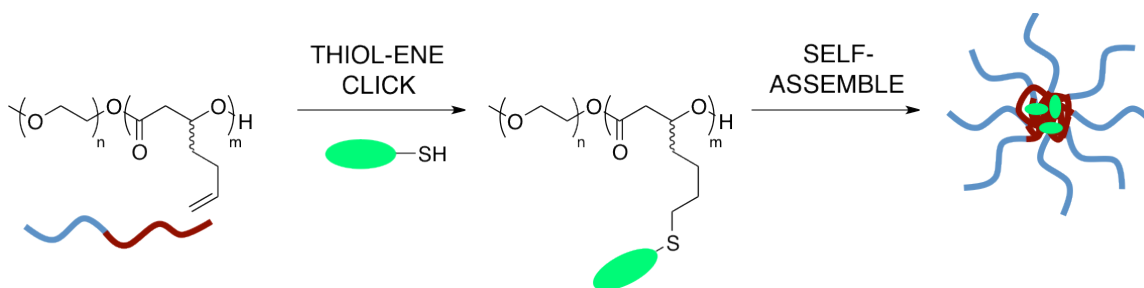


**Figure 1.10.** Schematic representation demonstrating the use of thiol-ene click chemistry for the attachment of small molecules to the backbone of newly synthesized PEO-*b*-PHEL polymers and subsequent self-assembly.

Chapter 3 will describe the synthesis of glycopolymer-coated vesicles using two alternative strategies (Figure 1.11). First, a novel approach is presented for obtaining glycopolymer-functionalized vesicles via aqueous RAFT polymerization of a carbohydrate-based monomer directly from the surface of preassembled vesicles. The second approach involves the synthesis of glycopolymer-coated vesicles through the conjugation of presynthesized glycopolymers bearing alkyne functionality to preassembled azide-functionalized vesicles using orthogonal chemistry.

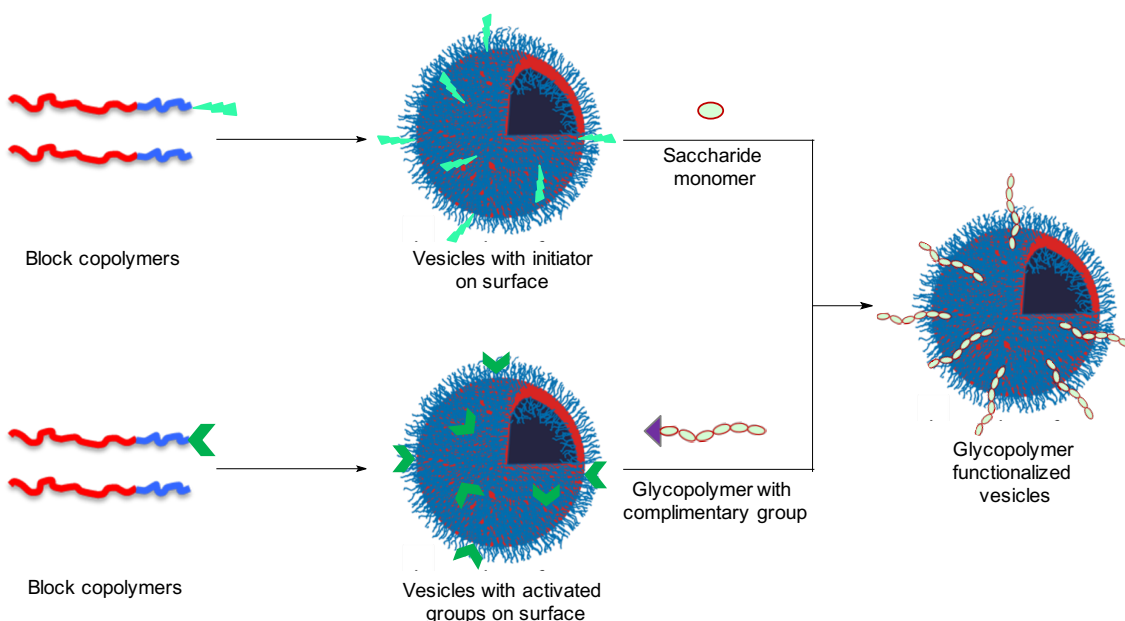


**Figure 1.11.** Schematic representation of the two approaches for preparing glycopolymer-coated vesicles explored in this study.

Chapter 4 will summarize the relevant conclusions obtained from both experimental chapters and will discuss the future goals and directions of each project.

## 1.5 References

- (1) Kataoka, K.; Harada, A.; Nagasaki, Y. *Adv. Drug Deliv. Rev.* **2001**, *47*, 113.
- (2) Cabral, H.; Kataoka, K. *J. Controlled Release* **2014**, *190*, 465.
- (3) Duncan, R. *Nat. Rev. Drug Discov.* **2003**, *2*, 347.
- (4) Blazs, A.; Armes, S. P.; Ryan, A. J. *Macromol. Rapid Commun.* **2009**, *30*, 267.
- (5) Peer, D. *Handbook of Harnessing Biomaterials in Nanomedicine: Preparation, Toxicity and Applications*; Pan Stanford Publishing: Atlanta, 2012.
- (6) Gonsalves, K. E. *Biomedical Nanostructures* Hoboken, N.J, 2008.
- (7) Murphy, E. A.; Majeti, B. K.; Mukthavaram, R.; Acevedo, L. M.; Barnes, L. A.; Cheres, D. A. *Mol. Cancer Ther.* **2011**, *10*, 972.
- (8) Adams, M. L.; Lavasanifar, A.; Kwon, G. S. *J. Pharma. Sci.* **2003**, *92*, 1343.
- (9) Mastroianni, S. E.; Epps, T. H., 3rd *Langmuir* **2013**, *29*, 3864.
- (10) Zhang, L. F.; Eisenberg, A. *Science* **1995**, *268*, 1728.
- (11) Won, Y.; Davis, H. T.; Bates, F. S. *Science* **1999**, *283*, 960.
- (12) Discher, D. E.; Eisenberg, A. *Science* **2002**, *297*, 967.
- (13) Battaglia, G.; Ryan, A. J. *J. Am. Chem. Soc.* **2005**, *127*, 8757.
- (14) Jain, S.; Bates, F. S. *Macromolecules* **2004**, *37*, 1511.
- (15) Fernyhough, C.; Ryan, A. J.; Battaglia, G. *Soft Matter* **2009**, *5*, 1674.
- (16) Discher, D. E.; Ahmed, F. *Annu. Rev. Biomed. Eng.* **2006**, 323.
- (17) Simone, E. A.; Dziubla, T. D.; Muzykantov, V. R. *Expert Opin. Drug Deliv.* **2008**, *5*, 1283.

- (18) Geng, Y.; Discher, D. E. *Polymer* **2006**, *47*, 2519.
- (19) Cai, S.; Vijayan, K.; Cheng, D.; Lima, E. M.; Discher, D. E. *Pharm. Res.* **2007**, *24*, 2099.
- (20) Oltra, N. S.; Nair, P.; Discher, D. E. *Annu. Rev. Chem. Biomol. Eng.* **2014**, *5*, 281.
- (21) Wang, H.; Xu, J.; Wang, J.; Chen, T.; Wang, Y.; Tan, Y. W.; Su, H.; Chan, K. L.; Chen, H. *Angew. Chem. Int. Ed.* **2010**, *49*, 8426.
- (22) Zou, P.; Chen, H.; Paholak, H. J.; Sun, D. *Mol. Pharm.* **2013**, *10*, 4185.
- (23) Alconcel, S. N. S.; Baas, A. S.; Maynard, H. D. *Polym. Chem.* **2011**, *2*, 1442.
- (24) Brocchini, S.; Godwin, A.; Balan, S.; Choi, J.-w.; Zloh, M.; Shaunak, S. *Adv. Drug Deliv. Rev.* **2008**, *60*, 3.
- (25) Zhai, X.; Huang, W.; Liu, J.; Pang, Y.; Zhu, X.; Zhou, Y.; Yan, D. *Macromol. Biosci.* **2011**, *11*, 1603.
- (26) Soo, P. L.; Luo, L.; Maysinger, D.; Eisenberg, A. *Langmuir* **2002**, *18*.
- (27) Lavasanifar, A.; Samuel, J.; Kwon, G. S. *Adv. Drug Deliv. Rev.* **2002**, *54*, 169.
- (28) Mahmud, A.; Xiong, X.; Lavasanifar, A. *Macromolecules* **2006**, *39*, 9419.
- (29) Yan, J.; Ye, Z.; Luo, H.; Chen, M.; Zhou, Y.; Tan, W.; Xiao, Y.; Zhang, Y.; Lang, M. *Polym. Chem.* **2011**, *2*, 1331.
- (30) Wang, X.; Gurski, L. A.; Zhong, S.; Xu, X.; Pochan, D. J.; Farach-Carson, M. C.; Jia, X. *J. Biomater. Sci. Polym. Ed.* **2011**, *22*, 1275.
- (31) Wang, W.; Chang, L.; Li, X.; Wu, Y.; Xing, J.; Deng, L.; Dong, A. *Soft Matter* **2012**, *8*, 1575.
- (32) Surnar, B.; Jayakannan, M. *Biomacromolecules* **2013**, *14*, 4377.

- (33) Deng, H.; Liu, J.; Zhao, X.; Zhang, Y.; Liu, J.; Xu, S.; Deng, L.; Dong, A.; Zhang, J. *Biomacromolecules* **2014**, *15*, 4281.
- (34) Garg, S. M.; Xiong, X.-B.; Lu, C.; Lavasanifar, A. *Macromolecules* **2011**, *44*, 2058.
- (35) Zhang, J.; Xiao, Y.; Xu, H.; Zhou, C.; Lang, M. *Polym. Chem.* **2016**, *7*, 4630.
- (36) Zhang, J.; Zhang, M.; Du, F.-S.; Li, Z.-C. *Macromolecules* **2016**, *49*, 2592.
- (37) Storm, G.; Belliot, S. O.; Daemen, T.; Lasic, D. D. *Adv. Drug Deliv. Rev.* **1995**, *17*, 31.
- (38) Gaumet, M.; Vargas, A.; Gurny, R.; Delie, F. *Eur. J. Pharm. Biopharm.* **2008**, *69*, 1.
- (39) Owen, S. C.; Chan, D. P. Y.; Shoichet, M. S. *Nano Today* **2012**, *7*, 53.
- (40) León, O.; Munoz-Bonilla, A.; Bordegé, V.; Sanchez-Chavez, M.; Fernández-García, M. *J. Polym. Sci. A Polym. Chem.* **2011**, *49*, 2627.
- (41) Miura, Y.; Seto, H.; Fuku, T. *Molecular Recognition of Glycopolymer Interface*; InTech, 2013.
- (42) Chen, C.; Xu, H.; Qian, Y.-C.; Huang, X.-J. *RSC Adv.* **2015**, *5*, 15909.
- (43) Yuan, F.; Wang, S.; Lu, W.; Chen, G.; Tu, K.; Jiang, H.; Wang, L.-Q. *J. Mater. Chem. B* **2015**, *3*, 4546.
- (44) Sun, K.; Bligh, S. W. A.; Nie, H.-l.; Quan, J.; Zhu, L.-m. *RSC Adv.* **2013**, *00*, 1.
- (45) Pasparakis, G.; Alexander, C. *Angew. Chem. Int. Ed.* **2008**, *47*, 4847.
- (46) Shi, H.; Liu, L.; Wang, X.; Li, J. *Polym. Chem.* **2012**, *3*, 1182.
- (47) Ting, S. R. S.; Chen, G.; Stenzel, M. H. *Polym. Chem.* **2010**, *1*, 1392.

- (48) Sunasee, R.; Adokoh, C. K.; Darkwa, J.; Narain, R. *Expert Opin. Drug Deliv.* **2014**, *11*, 867.



## Chapter 2

# 2 Functional Polyester Diblock Copolymers Possessing Encapsulation and Chemical Conjugation Capabilities

## 2.1 Introduction

Molecular self-assembly describes the phenomenon in which molecules spontaneously assemble into complex and ordered structures. The building blocks of life, such as DNA, proteins, and biological membranes, all involve a hierarchical organization of small units into ordered structures formed by non-covalent interactions.<sup>1</sup> The self-assembly of nanostructures is particularly useful as it allows the aggregation of molecules too small to be manipulated independently into ordered entities that have the ability to produce functional materials without human intervention.<sup>2</sup> Block copolymer self-assembly has attracted considerable attention for several decades due to the ability to form ordered structures with various morphologies, including spheres, worms, vesicles, and other structures.<sup>3-7</sup> These aggregates show promise for a number of applications such as catalysis, photoelectric materials, biological imaging, drug delivery, and other areas.

It is well known that morphology can be tuned by varying the block length, thus changing the hydrophilic:hydrophobic ratio of the polymer. The weight fraction of the hydrophilic block of the copolymer ( $f_m$ ) has been shown to predict the morphology of spherical micelles, cylindrical or “worm-like” micelles, and polymersomes.<sup>3,6,8</sup> Additionally, it is also possible to tune solution properties of block copolymers through post-polymerization functionalization. This allows one polymer precursor to be used in obtaining a number of different morphologies through orthogonal chemistry as well as the attachment of cargo. A number of studies have investigated this approach for the functionalization of polyethers.<sup>9-13</sup> In particular, Allen and coworkers recently demonstrated the ability to functionalize methoxypoly(ethylene glycol)-*b*-poly(allyl glycidyl ether) with various lengths of alkyl chains using thiol-ene click chemistry to achieve spheres, long cylindrical micelles, rods, disks and polymersomes.<sup>14</sup>

Block copolymers in which the hydrophobic block is composed of polyesters are also of high interest for use in biomedical applications due to their biodegradability and biocompatibility. Polyesters such PCL have been widely investigated as potential drug delivery candidates.<sup>15-20</sup> However, there are very few examples of polyesters with functional groups on the polymer backbone for post-polymerization chemistry.<sup>21</sup>

Here we report the synthesis of a new small library of amphiphilic poly(ethylene oxide)-*b*-poly(3-hydroxy-6-heptenoate) (PEO-*b*-PHEL) block copolymers possessing allyl groups on the polymer backbone. We demonstrate that using thiol-ene click chemistry, it is possible to tune the  $f_m$  value of the copolymer through post-modification of the allyl groups by the addition of octyl, triethylene glycol (TEG) or acetic acid moieties, thus changing the self-assembling properties of the parent polymers. This approach is also shown to be useful for the attachment of biologically significant molecules such as paclitaxel and Rhodamine B.

## 2.2 Experimental

### General materials and methods

Poly(ethylene oxide) monomethyl ether (PEO,  $M_n = 2000$ ) was purchased from Sigma Aldrich and was dried by three azeotropic distillations from toluene and stored in a nitrogen filled glovebox.  $\beta$ -6-heptenolactone ( $\beta$ -6-HEL) was synthesized by a procedure previously reported for similar lactones<sup>22</sup> and spectral data agreed with those previously reported.<sup>23</sup> The aluminum salen catalyst was synthesized according to a previously reported procedure.<sup>24</sup> 3-Tritylsulfanyl-propionic acid was prepared as previously described.<sup>25</sup> 1-Mercapto-3,6,9,12-tetraoxotridecane (TEG-thiol) was synthesized as previously reported.<sup>26</sup> Rhodamine derivative (**3**) was synthesized as previously reported.<sup>27</sup> 1-Ethyl-3-(3-dimethylaminopropyl) carbodiimide hydrochloride (EDC·HCl) was purchased from Creo Salus (USA). Paclitaxel was purchased from Ontario Chemicals Inc. (Guelph, ON, Canada). Dichloromethane was distilled from calcium hydride before use. Anhydrous tetrahydrofuran (THF), *N,N*-dimethylformamide (DMF)

and toluene were obtained from a solvent purification system using aluminum oxide columns. Deuterated solvents were purchased from Cambridge Isotopes Laboratories (Tewksbury, MA, USA). Solvents were purchased from Caledon Laboratory Chemicals (Georgetown, ON, Canada). All other chemical reagents were purchased from Sigma Aldrich (St. Louis, MO, USA). All solvents and chemicals were used as received unless otherwise noted. Dialysis was performed using Spectra/Por 6 regenerated cellulose membranes from Spectrum Laboratories (Rancho Dominguez, CA, USA). Nuclear Magnetic Resonance (NMR) spectroscopy was conducted on a Varian Inova 600 MHz Spectrometer (Varian, Palo Alto, CA, USA). All  $^1\text{H}$  and  $^{13}\text{C}$  NMR chemical shifts are reported in ppm and referenced relative to the residual solvent peak ( $\text{CHCl}_3$ :  $^1\text{H}$   $\delta$  = 7.26,  $^{13}\text{C}$   $\delta$  = 77). Coupling constants ( $J$ ) are expressed in Hertz (Hz). Fourier transform infrared (FTIR) spectroscopy was conducted using a Perkin Elmer FT-IR Spectrum Two Spectrometer (Waltham, MA, USA) in the universal attenuated total reflectance mode (UATR), using a diamond crystal as well as the UATR sampling accessory (part number L1050231). Differential scanning calorimetry (DSC) and thermogravimetric analysis (TGA) was completed on a DSC Q20 from TA Instruments (Waters, New Castle, DE, USA) at a heating rate of 10  $^{\circ}\text{C}$  per minute, under a  $\text{N}_2$  atmosphere, in an aluminum Tzerot pan with approximately 5 mg of sample. Reported  $T_g$  values were taken as the midpoint temperature of the transition. Size exclusion chromatography (SEC) was performed using a Visotek GPC Max VE2001 solvent module equipped with a Visotek VE3580 RI detector operating at 30  $^{\circ}\text{C}$ , an Agilent Polypore guard column (50x7.5mm) and two Agilent Polypore (300x7.5mm) columns connected in series. Samples were dissolve in THF (glass distilled grade) at a concentration of approximately 5 mg/mL and filtered (pore size: 0.22  $\mu\text{m}$ , ProMax<sup>TM</sup> syringe filter, PTFE) then injected using a 100  $\mu\text{L}$  loop. The THF eluent was filtered and eluted at 1 mL/min for a total of 30 minutes. Molecular weight calibration was carried out using polystyrene standards.

### Synthesis of PEO<sub>45</sub>-*b*-PHEL<sub>23</sub> and general procedure for the synthesis of PEO-*b*-PHEL block copolymers.

In a nitrogen filled glovebox,  $\beta$ -6-HEL (1.80 g, 14.3 mmol, 26 equiv), the aluminum salen catalyst [Al] (Scheme 2.1) (295 mg, 0.54 mmol, 1.0 equiv.) and PEO ( $M_n = 2000$  Da, 1.08 g, 0.54 mmol, 1.0 equiv.) were added to an ampoule with toluene (20 mL). The ampoule was sealed, removed from the glovebox and placed in a preheated oil bath at 85 °C for 20 hours. After 20 hours, 0.5 mL of a 10% MeOH in CH<sub>2</sub>Cl<sub>2</sub> solution was added to quench polymerization. A crude sample was taken for <sup>1</sup>H NMR spectroscopic analysis. The remainder was added to hexanes. Hexanes was decanted and the remaining oil was dried until constant weight. <sup>1</sup>H NMR (600 MHz, CDCl<sub>3</sub>):  $\delta$  1.70-1.71 (m, 48H), 2.02-2.11 (m, 50H), 2.50-2.61 (m, 49H), 3.38 (s, 3H), 3.64 (bs, 180H), 4.21-4.22 (m, 2H), 4.97-5.03 (m, 46H), 5.21-5.22 (m, 22H), 5.74-5.81 (m, 23H).  $M_n$  based on <sup>1</sup>H NMR spectroscopy = 4910 g mol<sup>-1</sup>. SEC (THF):  $M_n = 5140$  g mol<sup>-1</sup>,  $M_w = 5550$  g mol<sup>-1</sup>,  $D = 1.08$ . FTIR: 2891, 1737, 1343, 1103 cm<sup>-1</sup>.  $T_m = 35$  °C.  $T_g = -54$  °C.

#### PEO<sub>45</sub>-*b*-PHEL<sub>45</sub>

This polymer was synthesized as described above for PEO<sub>45</sub>-*b*-PHEL<sub>23</sub> except that the following quantities were used:  $\beta$ -6-HEL (2.00 g, 15.9 mmol, 51 equiv.), [Al] (170 mg, 0.31 mmol, 1.0 equiv.), PEO (620 mg, 0.31 mmol, 1.0 equiv.), toluene (20 mL). <sup>1</sup>H NMR (600 MHz, CDCl<sub>3</sub>):  $\delta$  1.69-1.71 (m, 91H), 2.04-2.07 (m, 95H), 2.47-2.62 (m, 91H), 3.38 (s, 3H), 3.64 (bs, 180H), 4.20-4.22 (m, 2H), 4.96-5.04 (m, 91H), 5.20-5.23 (m, 45H), 5.72-5.82 (m, 45H).  $M_n$  based on <sup>1</sup>H NMR spectroscopy = 7680 g mol<sup>-1</sup>. SEC (THF):  $M_n = 6630$  g mol<sup>-1</sup>,  $M_w = 7860$  g mol<sup>-1</sup>,  $D = 1.19$ . FTIR: 2863, 1829, 1736, 1641, 1168, 1103, 911 cm<sup>-1</sup>.  $T_m = 29$  °C.  $T_g = -59$  °C.

#### PEO<sub>45</sub>-*b*-PHEL<sub>79</sub>

This polymer was synthesized as described above for PEO<sub>45</sub>-*b*-PHEL<sub>23</sub> except that the following quantities were used:  $\beta$ -6-HEL (2.20 g, 17.4 mmol, 92 equiv.), [Al] (106 mg, 0.19 mmol, 1.0 equiv.), PEO (387 mg, 0.19 mmol, 1.0 equiv.), toluene (15 mL). <sup>1</sup>H NMR (600 MHz, CDCl<sub>3</sub>):  $\delta$  1.70 (m, 171H), 2.04-2.09 (m, 170H), 2.48-2.61 (m, 173H), 3.38

(s, 3H), 3.64 (bs, 180H), 4.21 (m, 2H), 4.97-5.03 (m, 158H), 5.21-5.22 (m, 81H), 5.74-5.80 (m, 76H).  $M_n$  based on  $^1\text{H}$  NMR spectroscopy = 11970 g mol<sup>-1</sup>. SEC (THF):  $M_n$  = 12910 g mol<sup>-1</sup>,  $M_w$  = 13340 g mol<sup>-1</sup>,  $D$  = 1.03. FTIR: 2924, 1737, 1642, 1162, 912, 734 cm<sup>-1</sup>.  $T_m$  = 22 °C.  $T_g$  = -46 °C.

**General procedure for functionalization of PEO<sub>45</sub>-*b*-PHEL<sub>45</sub> block copolymers using UV-initiated thiol-ene chemistry.**

To a 10 mL Schlenk tube equipped with a stir bar, a mixture of polymer, thiol and 2,2-dimethoxy-2-phenylacetophenone (DMPA) was added in toluene and degassed by bubbling through argon for 30 minutes. The reaction mixture was then placed in an ACE Glass photochemistry cabinet containing a medium pressure mercury light source (450 W bulb, 2.8 mW/cm<sup>2</sup> measured for UVA radiation at the sample position) and irradiated for 3 hours.

**PEO<sub>45</sub>-*b*-PHEL<sub>45</sub>-octyl**

Polymer = PEO<sub>45</sub>-*b*-PHEL<sub>45</sub> (50.0 mg, 0.006 mmol); thiol = octanethiol (22.0 mg, 0.150 mmol); initiator = DMPA (1.90 mg, 0.007 mmol); solvent = toluene (1 mL). The polymer was purified by precipitation into cold ethanol.  $^1\text{H}$  NMR (600 MHz, CDCl<sub>3</sub>):  $\delta$  0.88 (t, 72H,  $J$  = 7.0 Hz), 1.28 (m, 192H), 1.38 (m, 96H), 1.56-1.61 (m, 144H), 1.71 (m, 40H), 2.08 (m, 40H), 2.47-2.58 (m, 184H), 3.38 (s, 3H), 3.65 (bs, 180H), 4.22 (m, 2H), 4.97-5.04 (m, 40H), 5.20 (m, 44H), 5.75-5.81 (m, 20H).  $M_n$  based on  $^1\text{H}$  NMR spectroscopy = 11190 g mol<sup>-1</sup>. SEC (THF):  $M_n$  = 8150 g mol<sup>-1</sup>,  $M_w$  = 9740 g mol<sup>-1</sup>,  $D$  = 1.19. FTIR: 2926, 2856, 1740, 1116 cm<sup>-1</sup>.  $T_m$  = 34 °C.  $T_g$  = -60 °C.

**PEO<sub>45</sub>-*b*-PHEL<sub>45</sub>-TEG**

Polymer = PEO<sub>45</sub>-*b*-PHEL<sub>45</sub> (50.0 mg, 0.006 mmol); thiol = TEGthiol (27.0 mg, 0.150 mmol); initiator = DMPA (1.90 mg, 0.008 mmol); solvent = toluene (1 mL). The polymer was purified by dialysis using 3500 molecular weight cut off (MWCO) regenerated cellulose membrane in DMF.  $^1\text{H}$  NMR (600 MHz, CDCl<sub>3</sub>):  $\delta$  1.35-1.42 (m, 30H), 1.56-1.60 (m, 60H), 1.70 (m, 58H), 2.07 (m, 58H), 2.51-2.57 (m, 206H), 2.69 (t, 30H,  $J$  = 7.0 Hz), 3.37 (s, 45H), 3.55 (m, 30H), 3.64 (bs, 300H), 4.21 (m, 2H), 4.96-5.03 (m, 58H),

5.20 (m, 44H), 5.73-5.80 (m, 29H).  $M_n$  based on  $^1\text{H}$  NMR spectroscopy = 10200 g mol<sup>-1</sup>. SEC (THF):  $M_n$  = 7710 g mol<sup>-1</sup>,  $M_w$  = 8840 g mol<sup>-1</sup>,  $D$  = 1.15. FTIR: 2865, 1735, 1104 cm<sup>-1</sup>.  $T_m$  = 29 °C.  $T_g$  = -44 °C.

### **PEO<sub>45</sub>-*b*-PHEL<sub>45</sub>-acid**

Polymer = PEO<sub>45</sub>-*b*-PHEL<sub>45</sub> (500 mg, 0.063 mmol); thiol = thioglycolic acid (936 mg, 8.82 mmol); initiator = DMPA (113 mg, 0.441 mmol); solvent = toluene (4 mL). The polymer was purified by dialysis using 3500 MWCO regenerated cellulose membrane in DMF. Yield = 452 mg, 61%.  $^1\text{H}$  NMR (600 MHz, CDCl<sub>3</sub>):  $\delta$  1.31 (m, 94H), 1.51 (m, 197H), 2.44-2.54 (m, 188H), 3.13 (m, 88H), 3.27 (s, 4H), 3.54 (bs, 180H), 4.11 (m, 2H), 5.07 (m, 46H), 11.18 (bs, 41H).  $M_n$  based on  $^1\text{H}$  NMR spectroscopy = 11820 g mol<sup>-1</sup>. FTIR: 3447, 2940, 1726, 1241, 711 cm<sup>-1</sup>.  $T_g$  = -19 °C.

### **Synthesis of PEO<sub>45</sub>-*b*-PHEL-PTX**

In a flame-dried flask equipped with stir bar, PEO<sub>45</sub>-*b*-PHEL<sub>45</sub>-acid (75.0 mg, 0.007 mmol) was dissolved in dry DMF (5 mL). Paclitaxel (550 mg, 0.070 mmol), EDC·HCl (147 mg, 0.710 mmol) and 4-dimethylaminopyridine (DMAP) (33 mg, 0.271 mmol) were added and the reaction mixture was stirred overnight. The polymer was precipitated into cold EtOH and purified by dialysis using 6-8K MWCO regenerated cellulose membrane in DMF.  $^1\text{H}$  NMR (600 MHz, CDCl<sub>3</sub>):  $\delta$  1.10-1.63 (m, 697H), 1.78-2.47 (m, 827H), 3.24 (m, 85H), 3.64 (bs, 190H), 3.76 (m, 34H), 4.15 (m, 34H), 4.25 (m, 33H), 4.39 (m, 30H), 4.92 (m, 35H), 5.13 (m, 45H), 5.33 (m, 36H), 5.64 (m, 41H), 5.95 (m, 34H), 6.17 (m, 40H), 6.28 (s, 29H), 7.27-7.71 (m, 513H), 8.11 (m, 76H).  $M_n$  based on  $^1\text{H}$  NMR spectroscopy = 40030 g mol<sup>-1</sup>. SEC (THF):  $M_n$  = 9010 g mol<sup>-1</sup>,  $M_w$  = 16920 g mol<sup>-1</sup>,  $D$  = 1.88. FTIR: 3447, 2940, 1726, 1241, 711 cm<sup>-1</sup>.  $T_g$  = 131 °C.

### **Synthesis of anhydride 2**

Dicyclohexylcarbodiimide (DCC) (660 mg, 3.2 mmol, 0.6 equiv.) in dry CH<sub>2</sub>Cl<sub>2</sub> (5 mL) was added to a solution of 3-tritylsulfanyl-propionic acid (2.0 g, 5.7 mmol, 1.0 equiv) dissolved in dry CH<sub>2</sub>Cl<sub>2</sub> (15 mL). The reaction mixture was stirred at room temperature for 10 h and filtered to remove dicyclohexylurea byproduct. The resulting solution was

then concentrated, washed with ethyl acetate and dried under vacuum to provide **2** as a white solid. Yield = 86%.  $^1\text{H}$  NMR (600 MHz,  $\text{CDCl}_3$ ):  $\delta$  2.25 (t, 4H,  $J = 7.3$  Hz), 2.50 (t, 4H,  $J = 7.3$  Hz), 7.21-7.24 (m, 6H), 7.30 (t, 12H,  $J = 7.6$  Hz), 7.50 (d, 12H,  $J = 7.6$  Hz).  $^{13}\text{C}$  NMR (600 MHz, DMSO):  $\delta$  166.9, 144.1, 129.2, 127.7, 126.5, 66.7, 34.3, 25.7. FTIR: 3069, 2939, 1819, 1701, 746, 700  $\text{cm}^{-1}$ .

### Synthesis of rhodamine derivative **4**

A solution of rhodamine derivative **3**<sup>27</sup> (500 mg, 1.03 mmol, 1.0 equiv.) in dry THF (14 mL) was added dropwise to a solution of the anhydride **2** (350 mg, 0.516 mmol, 0.5 equiv.) dissolved in dry THF (10 mL). The reaction mixture was stirred overnight at room temperature. The solvent was evaporated and the product was purified by column chromatography using neutral alumina (EtOAc:Hexanes (1:1)). Yield = 26%.  $^1\text{H}$  NMR (600 MHz,  $\text{CDCl}_3$ ,  $\delta$ ): 1.13 (t, 12H,  $J = 7.3$  Hz), 2.01-2.04 (m, 2H), 2.41 (t, 2H  $J = 7.6$  Hz), 2.96-2.97 (m, 2H), 3.25-3.31 (m, 10H), 6.20 (dd, 2H,  $J = 8.8, 2.4$  Hz), 6.35-6.38 (m, 4H), 6.62 (bs, 1H), 7.06 (d, 1H,  $J = 6.5$  Hz), 7.14-7.16 (m, 3H), 7.22 (t, 6H,  $J = 7.6$  Hz), 7.37 (t, 6H,  $J = 7.0$  Hz), 7.41-7.45 (m, 2H), 7.85 (d, 1H,  $J = 6.5$  Hz). MS calcd for  $[\text{M}]^+ \text{C}_{52}\text{H}_{54}\text{N}_4\text{O}_3\text{S}$ , 814.3917; found, 814.3928.

### Synthesis of PEO<sub>45</sub>-*b*-PHEL<sub>45</sub>-RHD

To a solution of rhodamine derivative **4** (215 mg, 0.264 mmol, 1.0 equiv.) dissolved in dry  $\text{CH}_2\text{Cl}_2$  (1 mL) was added a solution of TFA: $\text{CH}_2\text{Cl}_2$  (1:1) (1 mL) dropwise at 0 °C. The reaction mixture was stirred at room temperature for 4 hr and monitored by TLC. The solvent was evaporated, and the resulting thiol product was used immediately without further purification. To a 10 mL Schlenk tube equipped with a stir bar, a mixture of PEO<sub>45</sub>-*b*-PHEL<sub>45</sub> (50.0 mg, 0.007 mmol, 1.0 equiv.), deprotected **4** (145 mg, 0.253 mmol, 36 equiv.) and azobisisobutyronitrile (AIBN) (8 mg, 0.050 mmol, 7.1 equiv.) in toluene (6 mL) were added and degassed by three cycles of freeze pump thaw. The reaction mixture was then stirred at 80 °C for 6 hours. The resulting polymer was purified by dialysis using 6-8K MWCO regenerated cellulose membrane in DMF. Yield = 69%.  $^1\text{H}$  NMR (600 MHz,  $\text{CDCl}_3$ ):  $\delta$  1.15 (t, 65H,  $J = 7.0$  Hz), 1.71 (bs, 94H), 2.02-2.07 (m, 103H), 2.41 (t, 14H,  $J = 7.3$  Hz), 2.50-2.58 (m, 94H), 2.95-2.96 (m, 11H), 3.25-3.32 (m,

51H), 3.64 (bs, 180H), 4.22 (bs, 2H), 4.97-5.04 (m, 84H), 5.21-5.23 (m, 45H), 5.74-5.81 (m, 40H), 6.22 (dd, 9H,  $J = 8.8, 2.4$  Hz), 6.39 (d, 19H,  $J = 9.4$  Hz), 6.62 (bs, 4H), 7.07 (d, 6H,  $J = 7.0$  Hz), 7.15-7.18 (m, 14H), 7.24 (t, 28H,  $J = 7.6$  Hz), 7.38 (d, 28H,  $J = 7.3$  Hz), 7.45 (quin, 12H,  $J = 6.9$  Hz), 7.86 (d, 5H,  $J = 7.0$  Hz).  $M_n$  based on  $^1\text{H}$  NMR spectroscopy = 10550 g mol $^{-1}$ . SEC (THF):  $M_n = 6300$  g mol $^{-1}$ ,  $M_w = 7260$  g mol $^{-1}$ ,  $\bar{D} = 1.15$ . FTIR: 3081, 2930, 2866, 1739, 1515, 913 cm $^{-1}$ .  $T_g = -33$  °C.

**General procedure for self-assembly of PEO<sub>45</sub>-*b*-PHEL<sub>n</sub> block copolymers using a solvent exchange method.**

Copolymer (8 mg) was dissolved in THF (1 mL) and stirred overnight. The resulting solution was filtered (pore size: 0.2  $\mu\text{m}$ , DynaGard® syringe filter, PP) before self-assembly. Polymer self-assembly was achieved by either the addition of polymer dissolved in THF (0.1 mL) to Mili Q water (0.9 mL) while stirring rapidly or vice versa. Assemblies were stirred for 5 hours then purified by dialysis using 6-8K MWCO regenerated cellulose membrane in purified water overnight. The hydrodynamic radius of aggregates was measured by dynamic light scattering (Zetasizer Nano Series, Malvern Instruments, UK) at room temperature (25 °C) in a glass cuvette. Transmission electron microscopy (TEM) imaging was performed using a Phillips CM10 microscope operating at an acceleration voltage of 80 kV.

**Procedure for self-assembly of PEO<sub>45</sub>-*b*-PHEL<sub>79</sub> using film hydration method.**

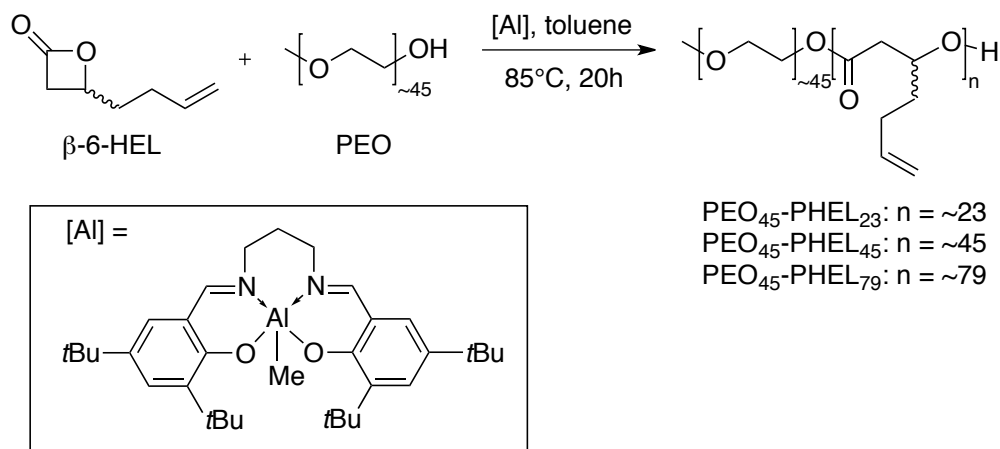
PEO<sub>45</sub>-*b*-PHEL<sub>79</sub> (50 mg) was dissolved in 2 mL of CH<sub>2</sub>Cl<sub>2</sub> in a 25 mL round bottom flask. A Nile red solution in CH<sub>2</sub>Cl<sub>2</sub> was then added to obtain 0.1 w/w/% of Nile red relative to the copolymer. The CH<sub>2</sub>Cl<sub>2</sub> was removed under a stream of nitrogen to produce a film of polymer on the flask. Deionized (DI) water (1 mL/10 mg of polymer) was added and the solution was stirred for 0.5 h at 55 °C. The solution was then sonicated for 0.5 h and finally stirred for 24 h at 55 °C. The resulting vesicles were characterized by confocal fluorescence microscopy using Zeiss LSM 510 DUO Vario using a 63x objective.



## 2.3 Results and Discussion

### Synthesis and characterization of PEO-PHEL block copolymers

$\beta$ -6-Heptenolactone ( $\beta$ -6-HEL) was selected as the monomer for the preparation of functionalizable block copolyesters as it has a pendant terminal alkene that should allow for reactions with thiols *via* well-established thiol-ene chemistry. In addition, recent work in the Shaver group has demonstrated that  $\beta$ -lactones undergo controlled coordination insertion ring opening polymerization using aluminum salen catalysts.<sup>22</sup> Previously,  $\beta$ -6-HEL has been polymerized using zinc and yttrium complexes and the resulting polymers were subsequently functionalized to introduce hydroxyl, epoxide, and pinacolborane moieties.<sup>28,29</sup> To the best of our knowledge,  $\beta$ -6-HEL has not previously been incorporated into block copolymers. This monomer was synthesized using a procedure previously reported for similar lactones via epoxide carbonylation using a chromium porphyrin complex<sup>22</sup> and its identity was confirmed by comparison with previously reported spectral data for the same compound.<sup>30</sup> For the preparation of block copolymers, PEO monomethyl ether with a molar mass of 2000 g mol<sup>-1</sup> was used as an initiator and the polymerization was conducted in toluene at 85 °C for 20 h using an aluminum salen catalyst<sup>31</sup> (Scheme 2.1). In order to investigate block copolymers with varying block ratios, 26, 50, and 90 equivalents of  $\beta$ -6-HEL were used to provide three different PEO-*b*-PHEL block copolymers (Table 2.1). Evaluation of the <sup>1</sup>H NMR spectra prior to purification showed that the conversion of  $\beta$ -6-HEL varied from 86-88%. The polymers were subsequently purified by precipitation into hexanes.



**Scheme 2.1.** Synthesis of PEO-*b*-PHEL block copolymers.

**Table 2.1.** Composition and properties of the PEO-*b*-PHEL block copolymers.

Copolymer	Equiv. of HEL added	DP of HEL (NMR)	M <sub>n</sub> (g mol <sup>-1</sup> ) (NMR)	M <sub>n</sub> (g mol <sup>-1</sup> ) (SEC)	<i>D</i> (SEC)	T <sub>g</sub> (°C)	T <sub>m</sub> (°C)
PEO <sub>45</sub> - <i>b</i> -PHEL <sub>23</sub>	26	23	4910	5140	1.08	-54	35
PEO <sub>45</sub> - <i>b</i> -PHEL <sub>45</sub>	51	45	7680	6630	1.19	-59	29
PEO <sub>45</sub> - <i>b</i> -PHEL <sub>79</sub>	92	79	11970	12910	1.03	-46	22, 29

The block copolymers were characterized by <sup>1</sup>H NMR spectroscopy, FTIR spectroscopy, size exclusion chromatography (SEC), thermogravimetric analysis (TGA) and differential scanning calorimetry (DSC). The degree of polymerization (DP) of the polyester block was determined using <sup>1</sup>H NMR spectroscopy by comparing the integration of the peak at 3.6 ppm corresponding to the hydrogens on the PEO block with that of the multiplet at 5.0 ppm corresponding to the protons on the terminal alkenes of the β-6-HEL block (Figure 2.1d, Figures A1.4-A1.6). The results indicated that DPs of 23, 45, and 79 were

obtained for copolymers PEO<sub>45</sub>-*b*-PHEL<sub>23</sub>, PEO<sub>45</sub>-*b*-PHEL<sub>45</sub>, and PEO<sub>45</sub>-*b*-PHEL<sub>79</sub> respectively. These DPs were in good agreement with the equivalents of  $\beta$ -6-HEL added. From these DPs, the number average molar mass ( $M_n$ ) was calculated for each polymer (Table 2.1). These ranged from 4910 g mol<sup>-1</sup> for PEO<sub>45</sub>-*b*-PHEL<sub>23</sub> to 11970 g mol<sup>-1</sup> for PEO<sub>45</sub>-*b*-PHEL<sub>79</sub>. The molar masses were also measured by SEC in THF relative to polystyrene standards. As illustrated in Table 2.1, the  $M_n$ s were in good agreement with those obtained by NMR spectroscopy and the dispersity ( $\bar{D}$ ) was less than 1.2 for each copolymer (Figures A1.20-A1.22). The SEC traces are included in the Appendix.

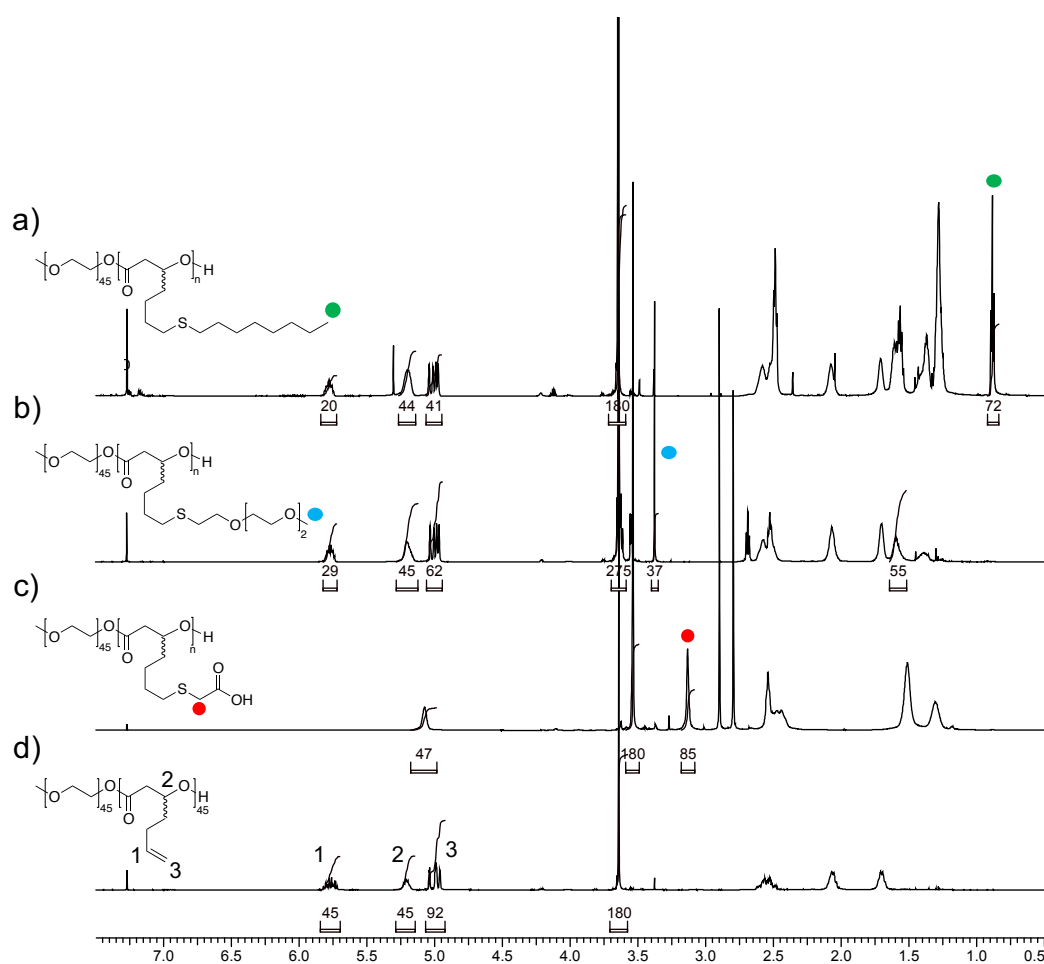


**Figure 2.1.** <sup>1</sup>H NMR overlay of a) PEO<sub>45</sub>-*b*-PHEL<sub>45</sub>-octyl, b) PEO<sub>45</sub>-*b*-PHEL<sub>45</sub>-TEG c) PEO<sub>45</sub>-PHEL<sub>45</sub>-acid d) PEO<sub>45</sub>-*b*-PHEL<sub>45</sub>.

PEO-*b*-PHEL block copolymers were found to be stable up to 400 °C determined by TGA. PEO is a highly crystalline polymer with a  $T_m$  of  $\sim 58$  °C<sup>32</sup> while PHEL is an amorphous polymer with a  $T_g$  of  $\sim -40$  °C.<sup>29</sup> Upon their incorporation into block copolymers, the resulting materials had both amorphous and crystalline domains, suggesting that they undergo phase separation at the nanoscale (Figures A1.27-A1.29). The  $T_m$  of the copolymers decreased from 35 – 22 °C as the PHEL block length increased. This suggests that the crystalline domains became smaller as the PEO content of the copolymers decreased. All three of the copolymers underwent cold crystallization between the  $T_m$  and  $T_g$ . The  $T_g$  ranged from -59 to -46 °C, with no clear trend relating to the changing PHEL block length. However, these  $T_g$ s were lower than the previously reported  $T_g$ s for PHEL of similar DP. This suggests that the presence of non-crystalline PEO at these temperatures prior to cold crystallization may enhance segmental motion.

As one of the main goals of this work was to explore the effects of alkene functionalization on the self-assembly of the block copolymers, the self-assembly of PEO<sub>45</sub>-*b*-PHEL<sub>23</sub>, PEO<sub>45</sub>-*b*-PHEL<sub>45</sub>, and PEO<sub>45</sub>-*b*-PHEL<sub>79</sub> was first explored. The hydrophilic mass fractions ( $f_m$ ) of the copolymers were calculated as molar mass of PEO block/molar mass of copolymer as an estimate of the hydrophilic volume fraction ( $f_v$ ) and the results are summarized in Table 2.2. Self-assembly was performed by a solvent exchange process involving first the dissolution of the copolymer in THF, followed by the addition of water and then dialysis to remove the THF. The resulting assemblies were characterized by dynamic light scattering (DLS) and TEM. As shown in Figure 2.2a, PEO<sub>45</sub>-*b*-PHEL<sub>23</sub> with an  $f_m$  of 0.41 assembled into solid particles that appear to be a mixture of true micelles and compound micelles. The Z-average diameter measured by DLS was 66 nm, which is in reasonable agreement with the TEM images. This result can be compared with those obtained for PEO-PCL block copolymers, whose self-assembly has been well-studied. The number of carbons (7) in the lactone monomer  $\beta$ -6-HEL is similar to that of caprolactone (6). Micelles were also obtained for similar  $f_m$  values in PEO-PCL copolymers.<sup>33</sup> Upon decreasing  $f_m$  to 0.26 in PEO<sub>45</sub>-*b*-PHEL<sub>45</sub>, solid spherical objects with a Z-average diameter of 73 nm were observed (Figure 2.2b). This increasing tendency towards the formation of larger assemblies is consistent with the increasing

length of the hydrophobic block and the formation of more compound micelles. In comparison to PEO-PCL copolymers, typically  $f_v$  values between 0.20 and 0.42 result in vesicular morphology. For  $f_v > 0.42$ , a mixed morphology of both worm micelles and spherical micelles is often observed.<sup>34</sup> Upon further decreasing  $f_m$  to 0.17 in PEO<sub>45</sub>-*b*-PHEL<sub>79</sub>, vesicles were observed in the TEM images (Figure 2.2c) and the Z-average diameter of the assemblies measured by DLS increased to 118 nm.

**Table 2.2.** Hydrophilic mass fraction of polymers and their self-assembly properties as determined by TEM and DLS.

Copolymer	Hydrophilic mass fraction ( $f_m$ )	Z-average diameter (nm)	PDI	Morphology
PEO <sub>45</sub> - <i>b</i> -PHEL <sub>23</sub>	0.41	66 ± 0.5	0.20 ± 0.01	Micelles, compound micelles
PEO <sub>45</sub> - <i>b</i> -PHEL <sub>45</sub>	0.26	73 ± 1.1	0.34 ± 0.05	Compound micelles
PEO <sub>45</sub> - <i>b</i> -PHEL <sub>79</sub>	0.17	118 ± 2.2	0.31 ± 0.01	Vesicles

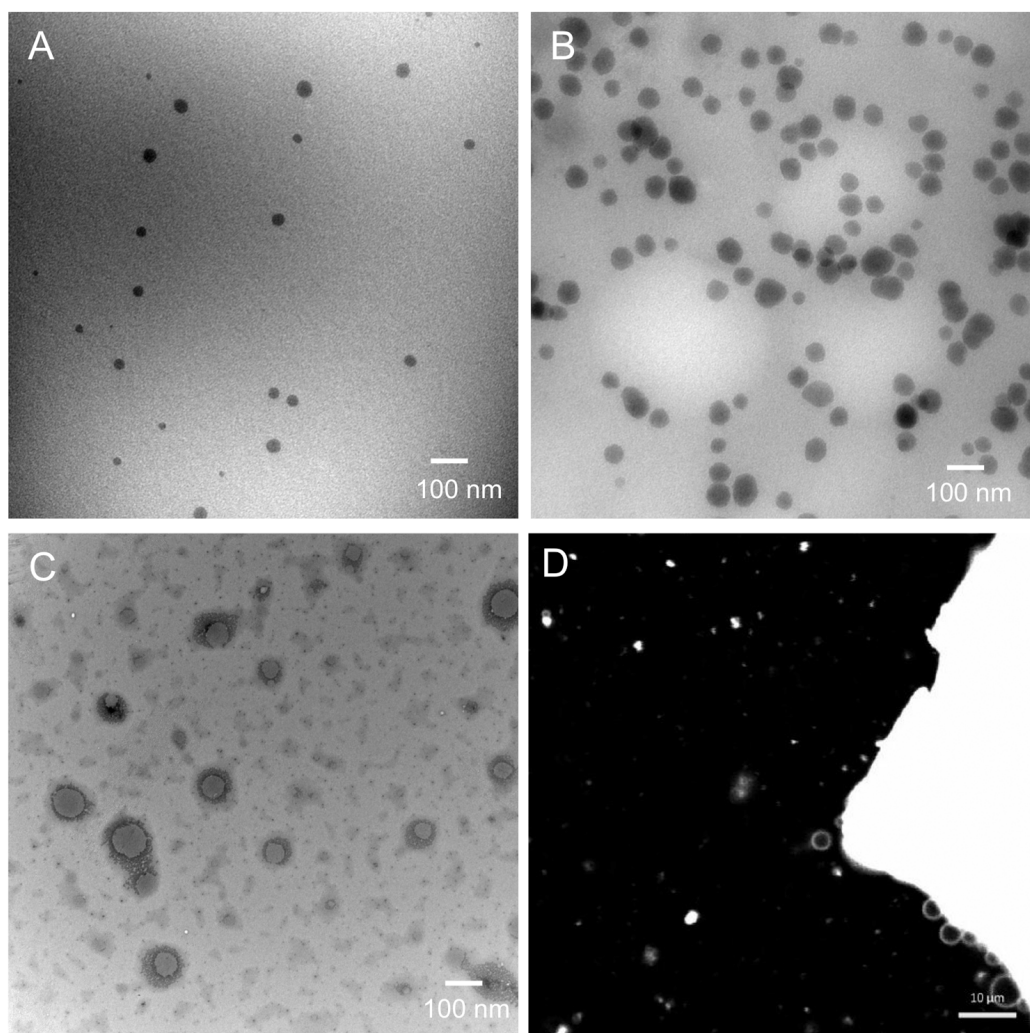


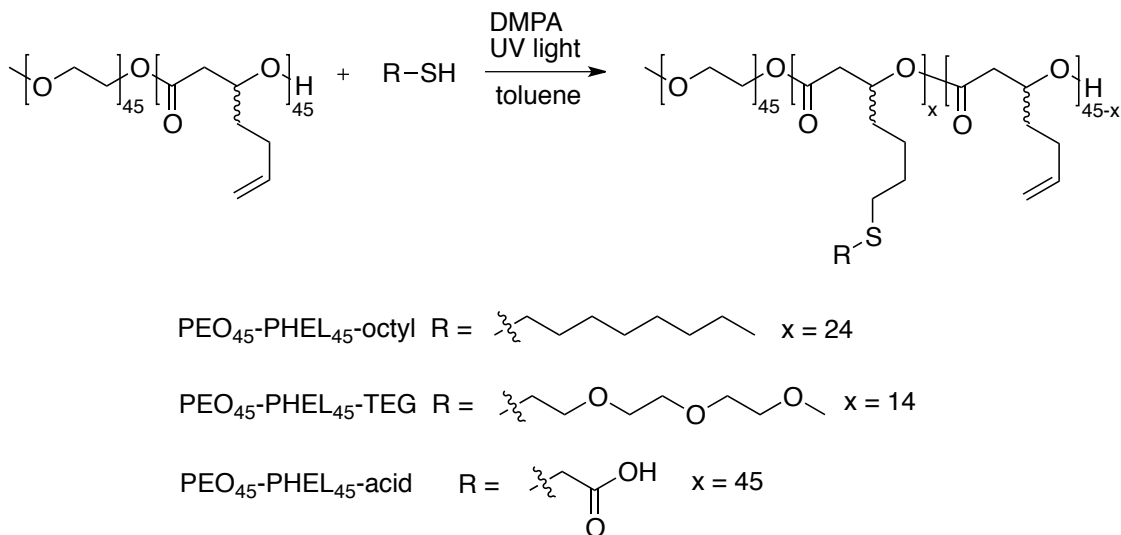
**Figure 2.2.** a-c) TEM images and d) fluorescence confocal microscopy image of assemblies formed from a) PEO<sub>45</sub>-*b*-PHEL<sub>23</sub>, b) PEO<sub>45</sub>-*b*-PHEL<sub>45</sub>, and c) PEO<sub>45</sub>-*b*-PHEL<sub>79</sub> by the solvent switching method and d) PEO<sub>45</sub>-*b*-PHEL<sub>79</sub> by film hydration.

As vesicles are more difficult to image by TEM than solid particles due to their tendency to collapse upon drying, they were also imaged by fluorescence confocal microscopy after incorporation of the hydrophobic dye Nile Red into their membranes. The limitation of this technique is its micrometer-scale resolution, which requires the formation of large micrometer-sized vesicles. Such vesicles can be obtained by the hydration of polymer films.<sup>3,8,34,35</sup> Thus, PEO<sub>45</sub>-*b*-PHEL<sub>79</sub> and 0.1 wt% Nile Red were dissolved in CH<sub>2</sub>Cl<sub>2</sub> and the solution was used to cast a film on a round bottom flask. Water was then added, and the suspension was stirred for 24 hours. As shown in Figure 2.2d, fluorescent vesicles

were clearly observed budding from the polymer surface, confirming the tendency of this polymer to form vesicles.

### **Functionalization of PEO-*b*-PHEL block copolymers to tune their hydrophilic-hydrophobic ratios and self-assemblies**

With the block copolymers in hand, the functionalization of the pendant alkenes by thiol-ene chemistry with the aim of tuning their hydrophilic-hydrophobic ratios was subsequently explored. PEO<sub>45</sub>-*b*-PHEL<sub>45</sub> was chosen as the focus of this work as it had an intermediate  $f_m$  among the three polymers and it was proposed that it would therefore be possible to modify the polymers to achieve assemblies ranging from small micelles to vesicles as well as intermediary structures. First, the modification of the copolymer with hydrophobic 1-octanethiol moieties was investigated. PEO<sub>45</sub>-*b*-PHEL<sub>45</sub> was reacted with 25 equivalents per polymer chain of 1-octanethiol using DMPA as a photoinitiator in combination with UV irradiation in toluene to afford the functionalized copolymer PEO<sub>45</sub>-*b*-PHEL<sub>45</sub>-octyl. The resulting polymer was purified by dialysis in DMF. As shown in Figure 2.1a, a reduction in the integration of the peak corresponding to the alkene protons at 5.0 ppm from 91 to 41 was observed in the <sup>1</sup>H NMR spectrum, which is consistent with the functionalization of approximately 24 of the 45 alkenes with 1-octanethiol. In addition, new peaks appeared at 0.88, 1.28, 1.38 and 1.58 ppm that can be assigned to protons on the alkyl chain. The  $M_n$  of the polymer measured by SEC increased from 6630 to 8150 g mol<sup>-1</sup>, which is consistent with the addition of mass to the polymer. However, it did not increase to the same extent as the actual mass added to the polymer. This can be attributed to the grafted architecture.  $\bar{D}$  remained unchanged. DSC analysis showed that the  $T_g$  and  $T_m$  of the polymers were also relatively unchanged in comparison with PEO<sub>45</sub>-*b*-PHEL<sub>45</sub> at -60 and 34 °C, respectively.



**Scheme 2.2.** Functionalization of  $\text{PEO}_{45}\text{-}b\text{-PHEL}_{45}$  with octyl chains, TEG, and carboxylic acids.

**Table 2.3.** Structures and properties of functionalized  $\text{PEO}_{45}\text{-}b\text{-PHEL}_{45}$  copolymers. ND = none detected.

Sample	Number of functionalized alkenes	$M_n$ (g mol <sup>-1</sup> ) (NMR)	$M_n$ (g mol <sup>-1</sup> ) (SEC)	$\bar{D}$	$T_g$ (°C)	$T_m$ (°C)
$\text{PEO}_{45}\text{-}b\text{-PHEL}_{45}\text{-octyl}$	24	11190	8150	1.19	-60	34
$\text{PEO}_{45}\text{-}b\text{-PHEL}_{45}\text{-TEG}$	14	10200	7710	1.15	-44	29
$\text{PEO}_{45}\text{-}b\text{-PHEL}_{45}\text{-acid}$	45	11820	-	-	-19	ND
$\text{PEO}_{45}\text{-}b\text{-PHEL}_{45}\text{-PTX}$	34 PTX, 11 acid	40030	9010	1.88	131	ND
$\text{PEO}_{45}\text{-}b\text{-PHEL}_{45}\text{-RHD}$	5	10550	6300	1.15	-33	ND



Next, functionalization of PEO<sub>45</sub>-*b*-PHEL<sub>45</sub> with 25 equivalents per polymer chain of hydrophilic 1-mercapto-3,6,9,12-tetraoxotridecane moieties was performed using the same conditions described above to afford PEO<sub>45</sub>-*b*-PHEL<sub>45</sub>-TEG. As shown in Figure 2.1b, a reduction in the integration of the alkene peak at 5.0 ppm from 91 to 62 was observed, suggesting that ~14 alkenes were functionalized with the TEG-SH. In addition, new peaks appeared at 3.37 and 2.69 ppm corresponding to the terminal methoxy group and methylene adjacent to the sulfur of the TEG chain, respectively. The  $M_n$  measured by SEC was 7710 g mol<sup>-1</sup>, similar to that of the octyl derivative and  $\bar{D}$  was also similar at 1.15. In comparison to PEO<sub>45</sub>-*b*-PHEL<sub>45</sub>, PEO<sub>45</sub>-*b*-PHEL<sub>45</sub>-TEG has a somewhat elevated  $T_g$  of -44 °C, suggesting that the TEG grafts reduce segmental motion. However, the  $T_m$  remained unchanged.

An additional approach to tune the hydrophilicity and functionality of the block copolymers involved the conjugation of thioglycolic acid to the alkene pendant groups using the thiol-ene conditions described above. In this case, 140 equivalents per polymer chain were coupled to PEO<sub>45</sub>-*b*-PHEL<sub>45</sub> to afford PEO<sub>45</sub>-*b*-PHEL<sub>45</sub>-acid. When 140 equivalents were added, complete functionalization of the alkenes was achieved as shown in Figure 2.1c by the disappearance of alkene peaks at 5 ppm in the <sup>1</sup>H NMR spectrum and the appearance of a peak at 3.1 ppm corresponding to the protons  $\alpha$  to the carboxylic acid. The presence of carboxylic acids on the polymer made it impossible to obtain measurements by SEC due to interactions with the columns. DSC analysis showed that PEO<sub>45</sub>-*b*-PHEL<sub>45</sub>-acid had a significantly elevated  $T_g$  of -19 °C and no  $T_m$ . It is possible that hydrogen bonding occurs between the carboxylic acids, reducing segmental motion of the polyester block and preventing the crystallization of the PEO block.

As shown in Table 2.4, following the formula of mass of PEO/total mass of the copolymer, the attachment of 24 octyl chains in PEO<sub>45</sub>-*b*-PHEL<sub>45</sub>-octyl results in a decrease in  $f_m$  to 0.18 from 0.26 for PEO<sub>45</sub>-*b*-PHEL<sub>45</sub>. For PEO<sub>45</sub>-*b*-PHEL<sub>45</sub>-TEG,  $f_m$  was calculated as (mass of PEO + mass of TEG)/total mass of copolymer, resulting in 0.44. On the other hand,  $f_m$  values were not calculated for the carboxylic acid-functionalized copolymer as it was not obvious what mass should be deemed to contribute to hydrophilicity and the charge of the ionized acids was anticipated to override any

calculated changes in  $f_m$ . Self-assembly of the resulting functionalized copolymers was studied in the same manner described above. Upon the addition of octyl chains in PEO<sub>45</sub>-*b*-PHEL<sub>45</sub>-octyl, “worm-like” cylindrical micelles as observed by TEM with lengths on the order of a few hundred nm (Figure 2.3a). DLS suggested a Z-average diameter of 143 nm, but the meaning of this number is limited due to the non-spherical nature of the assemblies. Alternatively, the attachment of hydrophilic TEG chains in PEO<sub>45</sub>-*b*-PHEL<sub>45</sub>-TEG led to micellar structures with a Z-average diameter of 59 nm (Figure 2.3b). By TEM, these assemblies were noticeably smaller than those observed for PEO<sub>45</sub>-*b*-PHEL<sub>45</sub> (Figure 2.2b). This is expected based on the higher  $f_m$  for this polymer. On the other hand, PEO<sub>45</sub>-*b*-PHEL<sub>45</sub>-acid did not yield any detectable assemblies by DLS or TEM, suggesting that this polymer is uniformly hydrophilic and dissolves in aqueous solution. Thus, these results show that the morphologies of the polymer assemblies can be readily tuned through functionalization of the polyester block.

**Table 2.4.** Hydrophilic mass fractions of polymers and their self-assembly properties as determined by TEM and DLS.

Copolymer	Hydrophilic mass fraction ( $f$ )	Z-average diameter (nm)	PDI	Morphology
PEO <sub>45</sub> - <i>b</i> -PHEL <sub>45</sub> -octyl	0.18	143 ± 4.0	0.29 ± 0.01	Cylindrical micelles
PEO <sub>45</sub> - <i>b</i> -PHEL <sub>45</sub> -TEG	0.44	59 ± 0.1	0.258 ± 0.002	Micelles, compound micelles
PEO <sub>45</sub> - <i>b</i> -PHEL <sub>45</sub> -acid	NA	-	-	No assembly
PEO <sub>45</sub> - <i>b</i> -PHEL <sub>45</sub> -PTX	0.10	-	-	Macroscopic aggregation
PEO <sub>45</sub> - <i>b</i> -PHEL <sub>45</sub> -RHD	0.19	102 ± 0.4	0.178 ± 0.007	Micelles, compound micelles

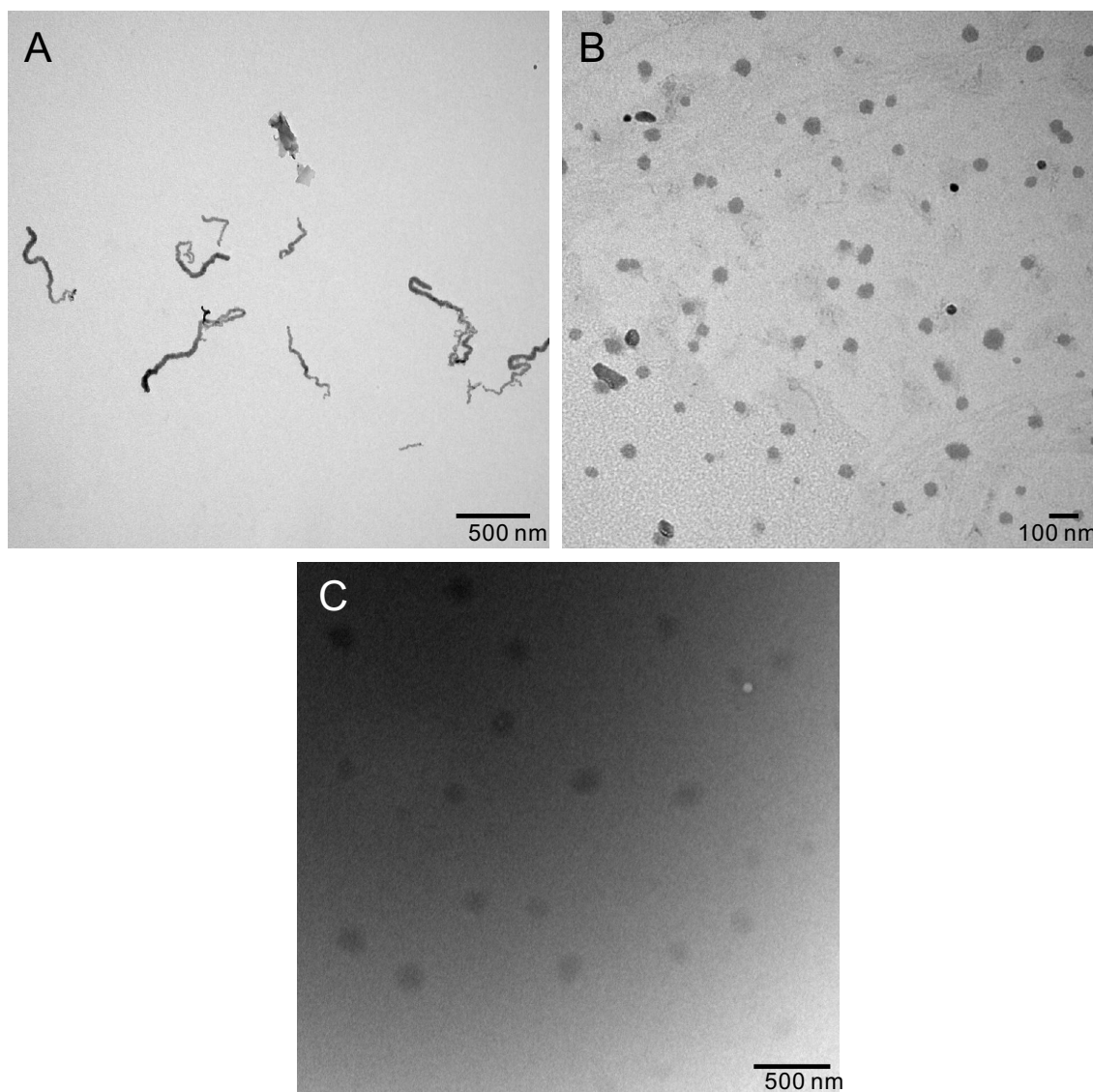


**Figure 2.3.** TEM images of assemblies formed by the solvent exchange method from: a) PEO<sub>45</sub>-*b*-PHEL<sub>45</sub>-octyl; b) PEO<sub>45</sub>-*b*-PHEL<sub>45</sub>-TEG; c) PEO<sub>45</sub>-*b*-PHEL<sub>45</sub>-RHD self-assembled using the solvent exchange method.

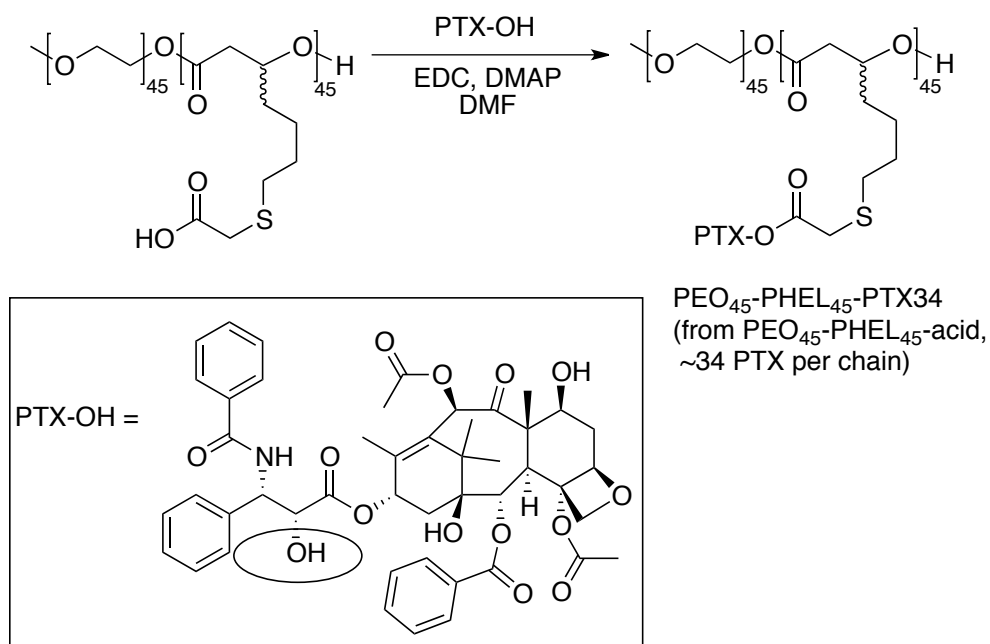
### **Functionalization of PEO-*b*-PHEL block copolymers with drugs and fluorophores**

In addition to altering the hydrophilic-hydrophobic ratios of the polymers, it was also of interest to use the pendant alkene groups to impart new functions to the polymers. To demonstrate this, a drug molecule paclitaxel (PTX) and a fluorescent rhodamine dye (RHD) were conjugated to the copolymers. Block copolymer micelles have been widely

investigated as drug delivery vehicles, in particular for anti-cancer treatment due to the possibility of passively and/or actively targeting these systems to tumors. However, a major challenge with these systems is poor retention of the drug in the delivery vehicle after its administration into the bloodstream. Chemical conjugation of the drug to the delivery system has been demonstrated to eliminate or reduce the burst release effect and to enable slow and prolonged release of drug.<sup>36-39</sup> PTX was selected as the drug to demonstrate functionalization of PEO-*b*-PHEL as it is a widely used anti-cancer therapeutic and it is challenging to administer in the absence of a delivery system due to its high hydrophobicity and consequently poor water solubility. A number of delivery systems for PTX have been developed and covalent conjugation has been shown to slow and control its release.<sup>40,41</sup> In designing a chemical conjugation strategy, a mechanism for release of the active drug should be considered. As PTX possesses three hydroxyl groups, with one selectively undergoing esterification,<sup>42,43</sup> an ester linkage between PTX and PEO<sub>45</sub>-*b*-PHEL<sub>45</sub> was targeted.

Reaction of PEO<sub>45</sub>-*b*-PHEL<sub>45</sub>-acid with 100 equivalents of PTX per polymer chain in the presence of 1-ethyl-3-(3-dimethylaminopropyl) carbodiimide hydrochloride (EDC·HCl) and 4-dimethylaminopyridine (DMAP) afforded PEO<sub>45</sub>-*b*-PHEL<sub>45</sub>-PTX<sub>34</sub> (Scheme 2.3). The amount of paclitaxel coupled to the polymer backbone was determined using <sup>1</sup>H NMR spectroscopy by comparing the integration of the peak corresponding to the hydrogen on the stereocenter of the PHEL block (labeled 1' on the chemical structure in Figure 2.4) at 5.21 ppm with that of the peak corresponding to the proton on the tertiary carbon adjacent to the amide group (labeled b' on the chemical structure in Figure 2.4) at 5.95 ppm. This analysis confirmed that 76% of the pendant carboxylic acid groups on PEO<sub>45</sub>-*b*-PHEL<sub>45</sub>-acid were esterified with PTX, resulting in ~34 PTX molecules per polymer. SEC analysis provided an *M<sub>n</sub>* of 9010 g mol<sup>-1</sup> and a *D* of 1.88. While the *M<sub>w</sub>* clearly increases, consistent with the increasing size of the copolymer upon conjugation of PTX, the significant increase in *D* and underestimation of the molar mass can likely be attributed to tailing due to interactions of the residual carboxylic acids with the column. DSC analysis showed that the copolymers were amorphous, with no melting transition

observed for the PEO block. However, there was a large increase in the  $T_g$  to 131 °C due to the incorporation of PTX, which possesses a relatively rigid structure.



**Scheme 2.3.** Synthesis of the PTX conjugate PEO<sub>45</sub>-*b*-PHEL<sub>45</sub>-PTX<sub>34</sub> starting from PEO<sub>45</sub>-*b*-PHEL<sub>45</sub>-acid. The site of conjugation on PTX is circled.

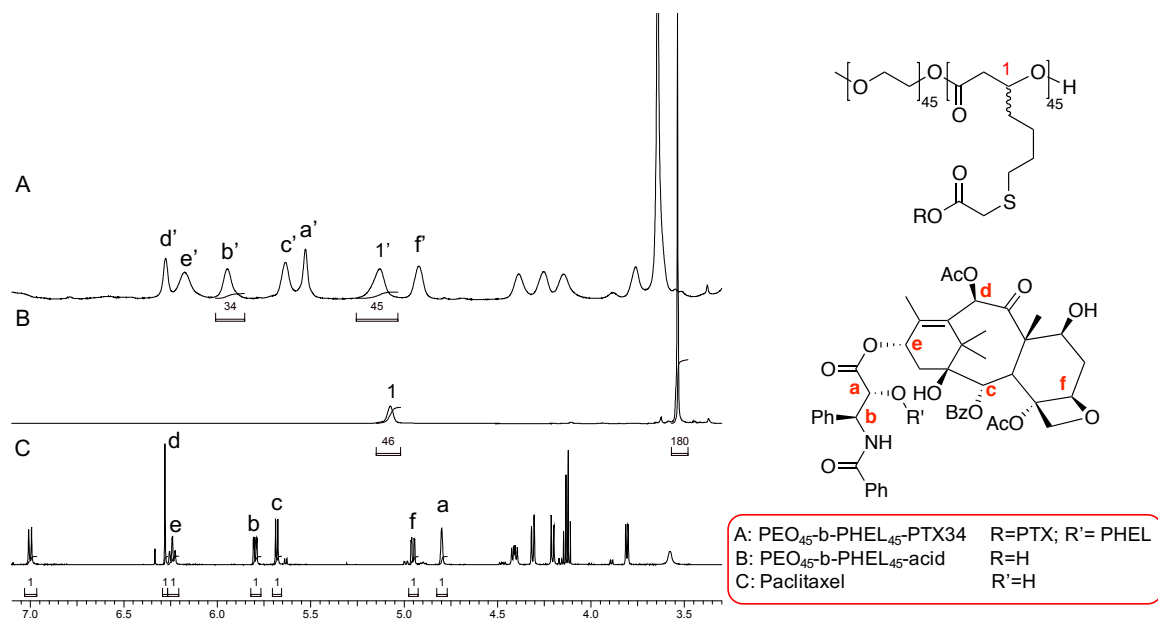


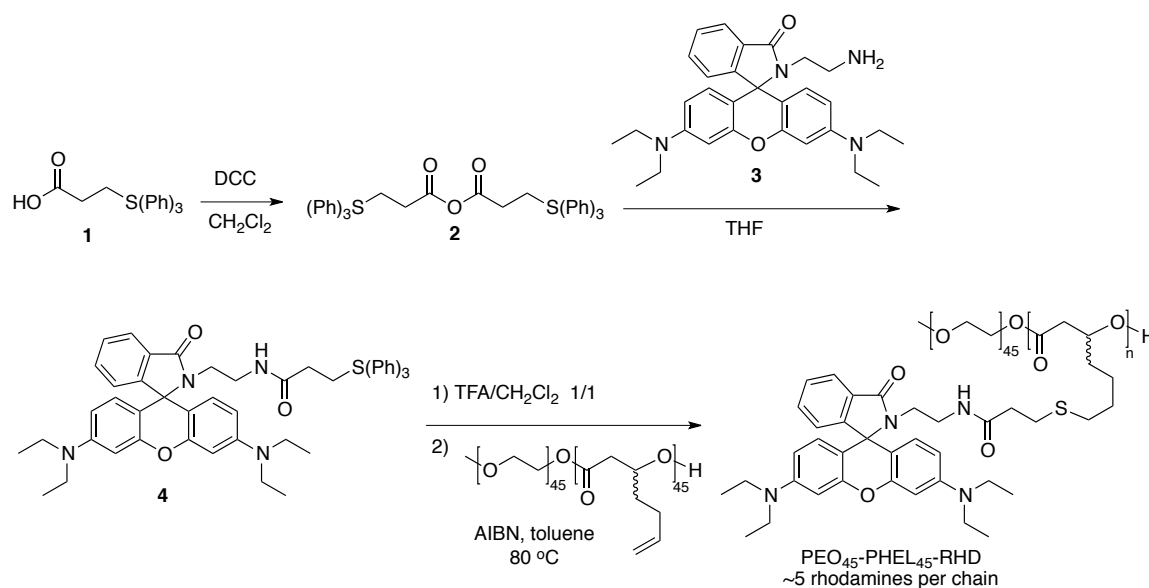
**Figure 2.4.**  $^1\text{H}$  NMR spectra of a)  $\text{PEO}_{45}\text{-}b\text{-PHEL}_{45}\text{-PTX34}$ , b)  $\text{PEO}_{45}\text{-}b\text{-PHEL}_{45}\text{-acid}$ , and c) free paclitaxel. The peaks labeled with ' indicate peaks corresponding to conjugated molecules.

The self-assembly of  $\text{PEO}_{45}\text{-}b\text{-PHEL}_{45}\text{-PTX34}$  was studied by the solvent exchange method involving THF and water. Unfortunately, macroscopic precipitation occurred under all of the conditions investigated. This can be attributed to the very low  $f_m$  value of 0.10 for this polymer as PTX contributes significantly to the hydrophobic fraction.

The labeling of polymeric assemblies with fluorophores is also of significant interest for monitoring their cell uptake, intracellular trafficking, and biodistribution.<sup>44-46</sup> The covalent conjugation of the fluorophore ensures that the fluorophore does not diffuse out of the assembly and partition into hydrophobic environments such as cell membranes. In the current work, the dye selected for conjugation to the polymer is a rhodamine B derivative because of its relatively high fluorescence quantum yield and ease of modification.<sup>27,47</sup> To install a thiol onto the rhodamine for thiol-ene reaction with the polymer, 3-tritylsulfanylpropionic acid **1**<sup>25</sup> was first condensed using *N*, *N'*-dicyclohexylcarbodiimide (DCC) to form the anhydride **2** (Scheme 2.4). An amine-functionalized rhodamine (**3**), was synthesized as previously reported,<sup>48</sup> then reacted with anhydride **2** in  $\text{CH}_2\text{Cl}_2$  to afford the protected thiol derivative of rhodamine (**4**).

Compound **4** was very sensitive to acid and required purification on neutral alumina rather than silica gel to avoid the loss of the trityl protecting group. The trityl protecting group was then cleaved using trifluoroacetic acid (TFA) to afford the free thiol, which was used immediately in the conjugation reaction due to its susceptibility to oxidation and other degradation pathways.

First, conjugation of the dye to PEO<sub>45</sub>-*b*-PHEL<sub>45</sub> was attempted using the photochemically-initiated thiol-ene reaction described above. This approach was unsuccessful, likely due to strong absorbance of the light by the rhodamine. However, thermal initiation using azobisisobutyronitrile (AIBN) and 38 equivalents of thiol per polymer chain in toluene at 80 °C was successful, yielding PEO<sub>45</sub>-*b*-PHEL<sub>45</sub>-RHD with 5 fluorophores per polymer chain as determined by <sup>1</sup>H NMR spectroscopy (Figure A1.11). SEC analysis provided an  $M_n$  of 6300 g mol<sup>-1</sup> and a  $D$  of 1.15, which are very similar to those of PEO<sub>45</sub>-*b*-PHEL<sub>45</sub>. The addition of the small percentage of rhodamine units to the PHEL block had a relatively significant effect on the thermal properties of the copolymer. DSC analysis showed that PEO<sub>45</sub>-*b*-PHEL<sub>45</sub>-RHD was amorphous, with no melting transition observed for the PEO block. There was also an increase in the  $T_g$  to -33 °C from -59 °C of PEO<sub>45</sub>-*b*-PHEL<sub>45</sub>. Self-assembly of PEO<sub>45</sub>-*b*-PHEL<sub>45</sub>-RHD was investigated using the solvent exchange method with THF and water as described above. As shown in Figure 2.3c and Table 2.4, this copolymer self-assembled to form solid spherical assemblies that were likely compound micelles with a Z-average diameter of 102 nm. The larger size of these assemblies relative to those formed by PEO<sub>45</sub>-*b*-PHEL<sub>45</sub> can likely be attributed to the decreased  $f_m$  of PEO<sub>45</sub>-*b*-PHEL<sub>45</sub>-RHD. This demonstrates that these new copolymers with pendant alkene groups can also be readily used to provide fluorescently-labeled polymer assemblies.



**Scheme 2.4.** Synthesis of a thiol-functionalized rhodamine derivative and its conjugation to PEO<sub>45</sub>-*b*-PHEL<sub>45</sub>.

## 2.4 Conclusions

In this work, a small library of novel PEO-*b*-PHEL block copolymers possessing pendant allyl groups and varying degrees of polymerization for the hydrophobic block were synthesized. The parent polymers were studied for the formation of different morphologies and were found to produce spherical micelles (PEO<sub>45</sub>-*b*-PHEL<sub>23</sub> and PEO<sub>45</sub>-*b*-PHEL<sub>45</sub>) as well as vesicles (PEO<sub>45</sub>-*b*-PHEL<sub>79</sub>). It was also found that PEO<sub>45</sub>-*b*-PHEL<sub>45</sub> could be functionalized with octyl, TEG or acid groups to significantly alter  $f_m$ , in turn influencing their self-assembly behaviour and resulting morphologies. In addition, the successful attachment of paclitaxel and rhodamine B using thiol-ene chemistry to the PHEL block afforded biologically interesting polymers capable of forming various morphologies upon self-assembly in aqueous media. This technique afforded well-defined polymers with high rates of conversion and low dispersities, making them ideal candidates for biological applications.



## 2.5 References

- (1) Lehn, J.-M. *Science* **2002**, *295*, 2400.
- (2) Ikkala, O.; Brinke, G. *Science* **2002**, *295*, 2407.
- (3) Discher, D. E.; Eisenberg, A. *Science* **2002**, *297*, 967.
- (4) Blanz, A.; Madsen, J.; Battaglia, G.; Ryan, A. J.; Armes, S. P. *J. Am. Chem. Soc.* **2011**, *133*, 16581.
- (5) Warren, N. J.; Mykhaylyk, O. O.; Mahmood, D.; Ryan, A. J.; Armes, S. P. *J. Am. Chem. Soc.* **2014**, *136*, 1023.
- (6) Jain, S.; Bates, F. S. *Science* **2003**, *300*, 460.
- (7) Mai, Y.; Eisenberg, A. *Chem. Soc. Rev.* **2012**, *41*, 5969.
- (8) Ahmed, F.; Discher, D. E. *J. Controlled Release* **2004**, *96*, 37.
- (9) Zhang, Y.; Lundberg, P.; Diether, M.; Porsch, C.; Janson, C.; Lynd, N. A.; Ducani, C.; Malkoch, M.; Malmstrom, E.; Hawker, C. J.; Nystrom, A. M. *J. Mater. Chem. B* **2015**, *3*, 2472.
- (10) Barthel, M. J.; Mansfeld, U.; Hoeppener, S.; Czaplewska, J. A.; Schacher, F. H.; Schubert, U. S. *Soft Matter* **2013**, *9*, 3509.
- (11) Ozdemir, F.; Keul, H.; Mourran, A.; Moeller, M. *Macromol. Rapid Commun.* **2011**, *32*, 1007.
- (12) Koyama, Y.; Umehara, M.; Mizuno, A.; Itaba, M. *Bioconjug. Chem.* **1996**, *7*, 298.
- (13) Obermeier, B.; Frey, H. *Bioconjug. Chem.* **2011**, *22*, 436.
- (14) Le Devedec, F.; Won, A.; Oake, J.; Houdaihed, L.; Bohne, C.; Yip, C. M.; Allen, C. *ACS Macro Lett.* **2016**, *5*, 128.
- (15) Aliabadi, H. M.; Brocks, D. R.; Lavasanifar, A. *Biomaterials* **2005**, *26*, 7251.

- (16) Aliabadi, H. M.; Mahmud, A.; Sharifabadi, A. D.; Lavasanifar, A. *J. Controlled Release* **2005**, *104*, 301.
- (17) Allen, C.; Eisenberg, A.; Masic, J.; Maysinger, D. *Drug Deliv.* **2000**, *7*, 139.
- (18) Forrest, M. L.; Won, C. Y.; Malick, A. W.; Kwon, G. S. *J. Controlled Release* **2006**, *110*, 370.
- (19) Kim, S. Y.; Lee, Y. M. *Biomaterials* **2001**, *22*, 1697.
- (20) Kim, S. Y.; Lee, Y. M.; Shin, H. J.; Kang, J. S. *Biomaterials* **2001**, *22*, 2049.
- (21) Mahmud, A.; Xiong, X.; Lavasanifar, A. *Macromolecules* **2006**, *39*, 9419.
- (22) MacDonald, J. P.; Parker, M. P.; Greenland, B. W.; Hermida-Merino, D.; Hamley, I. W.; Shaver, M. P. *Polym. Chem.* **2015**, *6*, 1445.
- (23) Lee, J. T.; Thomas, P. J.; Alpher, H. *J. Org. Chem.* **2001**, *66*, 5424.
- (24) Atwood, D. A.; Hill, M. S.; Jegier, J. A.; Rutherford, D. *Organometallics* **1997**, *16*, 2659.
- (25) Sharma, K. S.; Durand, G.; Giusti, F.; Olivier, B.; Fabiano, A.; Bazzacco, P.; Dahmane, T.; Ebel, C.; Popot, J.; Pucci, B. *Langmuir* **2008**, *24*, 13581.
- (26) Snow, A. W.; Foos, E. E. *Synthesis* **2003**, *4*, 509.
- (27) Rull-Barrull, J.; d'Halluin, M.; Le Grogneec, E.; Felpin, F.-X. *Chem. Commun.* **2016**, *52*, 2525.
- (28) Guillaume, C.; Ajellal, N.; Carpentier, J.-F.; Guillaume, S. M. *J. Polym. Sci. A Polym. Chem.* **2011**, *49*, 907.
- (29) Ajellal, N.; Thomas, C. M.; Carpentier, J.-F. *J. Polym. Sci. A Polym. Chem.* **2009**, *47*, 3177.
- (30) Lee, J. T.; Thomas, P. J.; Alper, H. *J. Org. Chem.* **2001**, *66*, 5424.

- (31) Cross, E. D.; Allan, L. E. N.; Decken, A.; Shaver, M. P. *J. Polym. Sci. A Polym. Chem.* **2013**, *51*, 1137.
- (32) Wei, T.; Zheng, B.; Yi, H.; Gao, Y.; Guo, W. *Polym. Eng. Sci.* **2014**, *54*, 2872.
- (33) Savic, R.; Luo, L.; Eisenberg, A.; Maysinger, D. *Science* **2003**, *25*, 615.
- (34) Discher, D. E.; Ahmed, F. *Annu. Rev. Biomed. Eng.* **2006**, 323.
- (35) Blanz, A.; Armes, S. P.; Ryan, A. J. *Macromol. Rapid Commun.* **2009**, *30*, 267.
- (36) Bader, H.; Ringsdorf, H.; Schmidt, B. *Angew. Makromol. Chem.* **1984**, *123*, 457.
- (37) Bae, Y.; Nishiyama, N.; Fukushima, S.; Koyama, Y.; Yasuhiro, M.; Kataoka, K. *Bioconjug. Chem.* **2005**, *16*, 122.
- (38) Ulbrich, K.; Subr, V. *Adv. Drug Deliv. Rev.* **2010**, *62*, 150.
- (39) Trivedi, R.; Kompella, U. B. *Nanomed.* **2010**, *5*, 485.
- (40) Hu, X.; Li, J.; Lin, W.; Huang, Y.; Jing, X.; Xie, Z. *RSC Adv.* **2014**, *4*, 38405.
- (41) Xu, X.; Zhang, X.; Wang, X.; Li, Y.; Jing, X. *Polym. Adv. Technol.* **2009**, *20*, 843.
- (42) Lataste, H.; Senilh, V.; Wright, M.; Guénard, D.; Potier, P. *Proc. Natl. Acad. Sci. USA* **1984**, *81*, 4090.
- (43) Deutsch, H. M.; Glinski, J. A.; Hernandez, M.; Haugwitz, R. D.; Narayanan, V. L.; Suffness, M.; Zalkow, L. H. *J. Med. Chem.* **1989**, *32*, 788.
- (44) Robin, M. P.; O'Reilly, R. K. *Polym. Int.* **2015**, *64*, 174.
- (45) Rapoport, N.; Marin, A.; Luo, Y.; Prestwich, G. D.; Muniruzzaman, M. *J. Pharm. Sci.* **2002**, *91*, 157.

- (46) Lai, C. P.; Kim, E. Y.; Badr, C. E.; Weissleder, R.; Mempel, T. R.; Tannous, B. A.; Breakefield, X. O. *Nat. Commun.* **2015**, *6*, 7029.
- (47) Nguyen, T.; Francis, M. B. *Org. Lett.* **2003**, *5*, 3245.
- (48) Zhang, X.; Shiraishi, Y.; Hirai, T. *Org. Lett.* **2007**, *9*, 5039.

## Chapter 3

### 3 Glycopolymer-functionalized Vesicles via Azide-Alkyne Click Chemistry

#### 3.1 Introduction

Amphiphilic block copolymers have been shown to assemble into a vast array of interesting morphologies including spherical micelles,<sup>1</sup> cylindrical “worm-like” micelles and vesicles.<sup>2,3</sup> In particular, polymer vesicles, commonly referred to as polymersomes, have received significant attention due to their resemblance to biological membranes. In comparison to biological membranes, polymer vesicles possess increased strength and decreased permeability. Additionally, polymersomes are potentially multifunctional as they possess a hydrophilic core with the ability to encapsulate water-soluble molecules, a hydrophobic membrane that can encapsulate hydrophobic species, and a surface to which various moieties can be conjugated. Based on these properties, there has been specific interest in the use of polymersomes in biomedical applications, particularly in drug delivery.<sup>4,5</sup> However, one of the major challenges in optimizing drug delivery vehicles is to selectively target the site of interest.<sup>6</sup> One way this can be achieved is through the incorporation of carbohydrates onto the surface of molecular assemblies as they are involved in many cellular recognition events. Although saccharide–protein interactions are generally too weak to be used in biomaterials and devices, the interactions can be amplified through multivalency. Multivalent glycopolymers have been reported to exhibit strong saccharide–protein interactions.<sup>7</sup>

Previous work in our group has involved the functionalization of polymersomes with glycodendrimers designed to interact with influenza viruses thereby intercepting the infection process.<sup>8</sup> This was achieved through the conjugation of *N*-acetylneuraminic acid (Neu5Ac, commonly referred to as sialic acid) to the peripheries of polyester dendrons and then their subsequent conjugation to the polymersome surface in order to inhibit the binding of viral hemagglutinin to sialic acids on host cells, thus preventing viral uptake. Additionally, the water-soluble drug zanamivir was incorporated into the core of the polymersome to prevent the release of progeny virus from the host cells, inhibiting viral

replication. It was shown that incorporation of carbohydrate-functionalized dendrons onto the polymersome surface led to a 2000-fold enhancement in protein binding compared to that of a small-molecule analogue.<sup>8</sup> However, when tested *in vitro*, these assemblies were shown to be ineffective against the influenza virus. It is presumed that this ineffectiveness may be due to the rigidity of the dendrimers on the polymersome periphery making it difficult for their functionalities to easily surround the virus. It is hypothesized that using a system with more molecular flexibility may improve multivalent binding. This may be achieved by using a linear glycopolymer system as opposed to glycodendrimers as they possess much more flexibility (Figure 3.1).

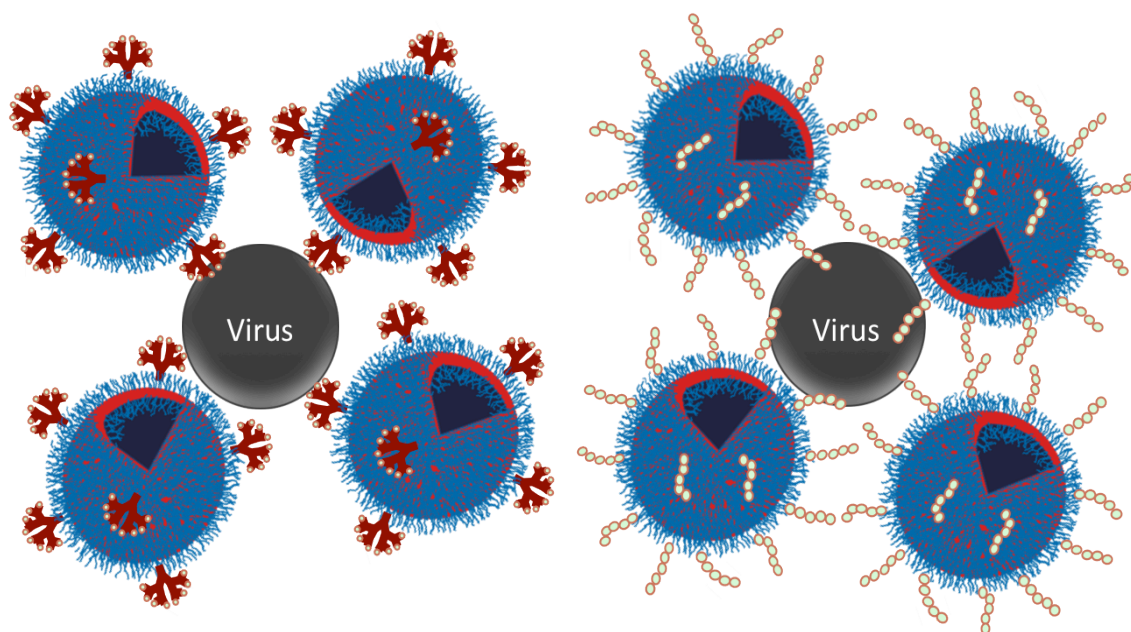


**Figure 3.1.** Schematic representation depicting rigidity of a glycodendrimer-functionalized polymersome system compared to a glycopolymer-functionalized system.

Although numerous studies have shown that glycodendrimers exhibit better protein interactions compared to their linear counterparts, few studies have explored the performance of glycopolymer-functionalized micelles compared to glycodendrimer micelles.<sup>9,10</sup> In addition to structure, there are several other factors that may influence the affinity and specificity of multivalent binding. Some examples include the density of glycopolymer chains as well as glycopolymer chain length. However, few reports have explored the effect of glycopolymer density<sup>11</sup> and glycopolymer chain length<sup>12</sup> on protein

binding interactions. The goal of this study was to create a small library of glycopolymer-coated vesicles with varying densities and chain lengths of glycopolymer on the vesicle surface (Table 3.1). The saccharide-protein binding of these glycopolymer-coated vesicles can then be determined and compared using a lectin binding assay.

**Table 3.1.** Overview of varying density and glycopolymer chain length to afford a small library of glycopolymer-coated vesicles.

		Percentages of functionalized terminal groups present on glycopolymer surface	
		100%	10%
Glycopolymer chain length	8	High density, short chain glycopolymer-coated vesicles	Low density, short chain glycopolymer-coated vesicles
	20	High density, medium chain glycopolymer-coated vesicles	Low density, medium chain glycopolymer-coated vesicles
	40	High density, long chain glycopolymer-coated vesicles	Low density, long chain glycopolymer-coated vesicles

Three general approaches can be envisioned for the incorporation of glycopolymers onto the surface of vesicles. One approach involves the synthesis of amphiphilic block copolymers with a hydrophilic block containing saccharide units, followed by their assembly into vesicles. The majority of existing studies utilize this linear approach to afford glycopolymer-decorated vesicles.<sup>6,13-17</sup> Another possible approach involves the assembly of vesicles containing functional groups on the surface followed by their reaction with glycopolymers possessing complimentary groups at their terminus using orthogonal chemistry.<sup>9,11</sup> The third approach involves the assembly of vesicles in which saccharide monomer can be polymerized directly from the vesicle surface which, to the best of our knowledge, has not yet been explored in the literature. This work will describe the efforts towards obtaining glycopolymer-coated vesicles using the latter two methods described above (Figure 3.2).

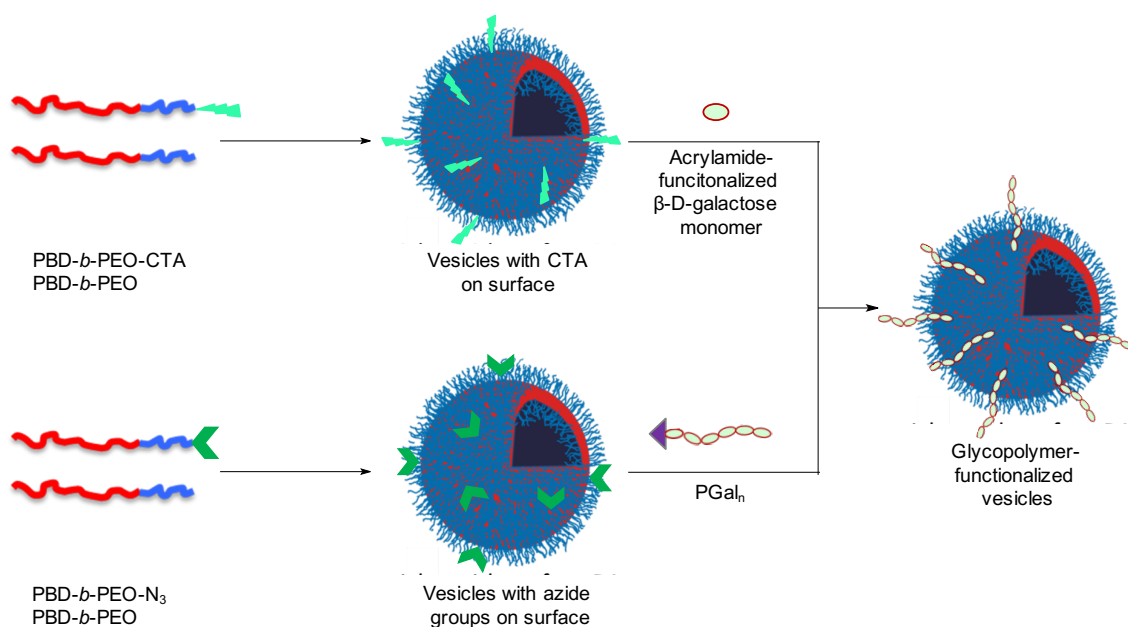


**Figure 3.2.** Two approaches for preparing glycopolymer-coated vesicles explored in this study.

In the first approach, glycopolymer-functionalized vesicles will be accessed using a novel method involving reversible addition-fragmentation chain transfer (RAFT) polymerization of carbohydrate-based monomers directly from the surface of preassembled vesicles. This can be achieved using a commercially available amphiphilic



block copolymer poly(butadiene-*b*-ethylene oxide) (PBD-*b*-PEO) and functionalizing the terminus with a RAFT chain-transfer agent (CTA). Following self-assembly of the functionalized block copolymers into vesicles in aqueous solution, it is then possible to polymerize a monomer using RAFT polymerization from the vesicle surface. Vesicles with varying glycopolymer chain length and chain density can be achieved by varying the equivalents of PBD-*b*-PEO chains functionalized with CTA, the equivalents of monomer, and adjusting reaction time.

In the second approach, glycopolymer-functionalized vesicles will be obtained using alkyne-azide click chemistry. This can be achieved through the functionalization of PBD-*b*-PEO with an azide moiety. These block copolymers can undergo self-assembly in aqueous solution with varying equivalents of PBD-*b*-PEO and PBD-*b*-PEO-N<sub>3</sub> to provide vesicles with varying equivalents of azide on the surface. Additionally, glycopolymers can be synthesized via RAFT polymerization from a CTA possessing alkyne functionality. Orthogonal chemistry can then be used in aqueous conditions to functionalize the azide groups on the vesicle surface with glycopolymer. This study will use a  $\beta$ -D-galactose based monomer possessing acrylamide functionality as a simple model. The incorporation of Nile red into assemblies will allow assays to be performed on the resulting glycopolymer-functionalized vesicles to determine and compare their protein-binding capabilities.

## 3.2 Experimental

### General Materials and Methods

Poly(butadiene-*b*-ethylene oxide) (PBD-*b*-PEO) (PDI = 1.15) with a composition of 6000 g mol<sup>-1</sup> PBD (>80% 1,2 addition) and 4000 g mol<sup>-1</sup> PEO was purchased from Polymer Source (Dorval, QC, Canada) and dried by three azeotropic distillations from toluene before use. Alkyne-functionalized CTA (7),<sup>18</sup> D-galactose pentaacetate,<sup>19</sup> and PBD-*b*-PEO-N<sub>3</sub><sup>20</sup> were prepared as previously reported. Anhydrous CH<sub>2</sub>Cl<sub>2</sub> and triethylamine (NEt<sub>3</sub>) were distilled from calcium hydride (CaH<sub>2</sub>). Anhydrous acetonitrile and methanol

(MeOH) were obtained from a solvent purification system using aluminum oxide columns. Deuterated solvents were purchased from Cambridge Isotopes Laboratories (Tewksbury, MA, USA). Solvents were purchased from Caledon Laboratory Chemicals (Georgetown, ON, Canada). All other chemical reagents were purchased from Sigma Aldrich (St. Louis, MO, USA). All solvents and chemicals were used as received unless otherwise noted. Dialysis was performed using Spectra/Por 6 regenerated cellulose membranes from Spectrum Laboratories (Rancho Dominguez, CA, USA). Nuclear Magnetic Resonance (NMR) spectroscopy was conducted on a Varian Inova 600 MHz Spectrometer (Varian, Palo Alto, CA, USA). All  $^1\text{H}$  and  $^{13}\text{C}$  NMR chemical shifts are reported in ppm and referenced relative to the residual solvent peak ( $\text{CHCl}_3$ :  $^1\text{H}$   $\delta$  = 7.26,  $^{13}\text{C}$   $\delta$  = 77.2,  $(\text{CD}_3)_2\text{SO}$ :  $^1\text{H}$   $\delta$  = 2.50,  $^{13}\text{C}$   $\delta$  = 39.5,  $\text{D}_2\text{O}$ :  $^1\text{H}$   $\delta$  = 4.79,  $\text{CD}_3\text{OD}$ :  $^1\text{H}$   $\delta$  = 3.31). Coupling constants ( $J$ ) are expressed in Hertz (Hz). Size exclusion chromatography (SEC) was performed using a Waters Separations Module 2695 equipped with a Refractive Index Detector (Waters 2414) and three PLaquagel-OH 40  $\mu\text{m}$  (300x7.5mm) columns (Polymer Laboratories) connected in series and to a PLaquagel-OH 8  $\mu\text{m}$  guard column. The calibration was performed using poly(methyl methacrylate) standards. DLS was performed on a ZetaSizer Nano instrument from Malvern. Fourier transform infrared (FTIR) spectroscopy was conducted using a Perkin Elmer FT-IR Spectrum Two Spectrometer (Waltham, MA, USA) in the universal attenuated total reflectance mode (UATR), using a diamond crystal as well as the UATR sampling accessory (part number L1050231).

### Synthesis of 2-azidoethanol (**2**)

A mixture of 2-bromoethanol (50 g, 0.40 mol, 1.0 equiv.) and sodium azide (26 g, 0.40 mol, 1.0 equiv.) was heated to reflux overnight with stirring. The resulting mixture was put under vacuum for 4 hours followed by dilution with 200 mL diethyl ether. The solution was filtered through celite and concentrated. Purification was performed by distillation at 140  $^\circ\text{C}$  (190 mbar) to provide compound **2** as a light yellow liquid. Yield = 86%.  $^1\text{H}$  NMR (600 MHz,  $\text{CDCl}_3$ ):  $\delta$  3.34 (t, 2H,  $J$  = 5.28 Hz), 3.56 (s, 1H), 3.69 (t, 2H,  $J$  = 5.28 Hz). Spectral data agreed with those previously reported.<sup>19</sup>

### Synthesis of galactose derivative 3

Galactose derivative **1**<sup>19</sup> (20.0 g, 51.0 mmol, 1.0 equiv.) was dissolved in 120 mL of anhydrous CH<sub>2</sub>Cl<sub>2</sub> and azidoethanol (**2**) (6.69 g, 76.9 mmol, 1.5 equiv.) was added via syringe. The resulting solution was cooled to 0 °C and BF<sub>3</sub>·OEt<sub>2</sub> (25.4 g, 179 mmol, 3.5 equiv.) was added dropwise. The reaction mixture was stirred overnight under argon. After dilution with CH<sub>2</sub>Cl<sub>2</sub>, the reaction mixture was washed with 1M HCl, saturated NaHCO<sub>3</sub> and water. The organic phase was dried over MgSO<sub>4</sub>, filtered and concentrated. Purification was performed by flash chromatography on silica gel (ethyl acetate/hexane 1/1) yielding compound **3** as a yellow syrup. Yield = 69%. <sup>1</sup>H NMR: (600 MHz, CDCl<sub>3</sub>, δ): 1.97 (s, 3H), 2.03 (s, 3H), 2.04 (s, 3H), 2.14 (s, 3H), 3.28-3.31 (m, 1H), 3.47-3.51 (m, 1H), 3.66-3.70 (m, 1H), 3.91-3.93 (m, 1H), 4.02-4.05 (m, 1H), 4.09- 4.13 (m, 1H), 4.10-4.19 (m, 1H), 4.55-4.56 (d, 1H, *J* = 8.2 Hz), 5.00-5.03 (dd, 1H, *J* = 10.6, 3.5 Hz), 5.21-5.24 (dd, 1H, *J* = 10.3, 7.9 Hz), 5.38-5.39 (dd, 1H, *J* = 3.5, 1.2 Hz). Spectral data agreed with those previously reported.<sup>19</sup>

### Synthesis of galactose derivative 4

Lindlar catalyst (0.5 g) and *p*-toluenesulfonic acid-H<sub>2</sub>O (0.52 g, 2.7 mmol, 1.1 equiv.) were added to a solution of compound **3** (1.0 g, 2.4 mmol, 1.0 equiv.) in methanol (17 mL) under argon. The reaction mixture was stirred under H<sub>2</sub> for 8 hours. The reaction mixture was filtered through a plug of celite and concentrated to yield compound **4** as an orange viscous liquid. <sup>1</sup>H NMR (400 MHz, DMSO-d<sub>6</sub>): δ 1.91 (s, 3H), 2.01 (s, 3H), 2.03 (s, 3H), 2.11 (s, 3H), 3.72-3.89 (m, 2H), 4.06 (d, 2H, *J* = 6.3 Hz), 4.24 (t, 1H, *J* = 6.4 Hz), 4.79 (d, 1H, *J* = 8.2 Hz), 4.98 (dd, 1H, *J* = 10.4, 8 Hz), 5.17 (dd, 1H, *J* = 10.2, 3.5 Hz), 5.28 (d, 1H, *J* = 3.5 Hz). Spectral data is consistent with published values.<sup>19</sup>

### Synthesis of protected galactose monomer 5

A suspension of compound **4** (14 g, 35 mmol, 1.0 equiv.) was dissolved in 215 mL of anhydrous CH<sub>2</sub>Cl<sub>2</sub> and cooled to 0 °C while stirring. Acryloyl chloride (6.4 g, 70 mmol, 2.1 equiv.), diisopropylethylamine (DIPEA) (48 mL, 280 mmol, 8 equiv.) and 4-dimethylaminopyridine (DMAP) (0.15 g) were added to the reaction mixture. The

solution was stirred at room temperature under argon overnight. The reaction mixture was washed with saturated  $\text{NH}_4\text{Cl}$ ,  $\text{NaHCO}_3$  and water. The organic phase was dried over magnesium sulphate, filtered and butylated hydroxytoluene (BHT) was added to the solution as an inhibitor before being concentrated. The resulting material was purified by flash chromatography on silica (ethyl acetate/hexanes 3/1) to provide compound **5** as a yellow syrup. Yield = 40%.  $^1\text{H}$  NMR (600 MHz,  $\text{CDCl}_3$ ):  $\delta$  2.00 (s, 3H), 2.05 (s, 3H), 2.06 (s, 3H), 2.17 (s, 3H), 3.48-3.53 (m, 1H), 3.60-3.65 (m, 1H), 3.73-3.77 (m, 1H), 3.90-3.94 (m, 2H), 4.11-4.19 (m, 2H), 4.49 (d, 1H,  $J$  = 8.2 Hz), 5.03 (dd, 1H,  $J$  = 10.6, 3.5 Hz), 5.19 (dd, 1H,  $J$  = 10.6, 8.2 Hz), 5.41 (d, 1H,  $J$  = 3.5 Hz), 5.67 (d, 1H,  $J$  = 10.0 Hz), 6.12 (dd, 1H,  $J$  = 17.0, 10.0 Hz). Spectral data is consistent with published values.<sup>19</sup>

### Synthesis of deprotected galactose monomer **6**

To a solution of compound **5** (0.50 g, 1.1 mmol) in anhydrous methanol (10 mL), 25% sodium methoxide in methanol (230  $\mu\text{L}$ , 1.1 mmol) was added dropwise. The reaction mixture was stirred at room temperature for 1.5 hours. Dowex cation exchange resin (H-form) was added until a pH of 6 was obtained and then the solution was filtered and concentrated using a rotary evaporator. The residue was dissolved in water, filtered and freeze-dried to provide **6** as an off white solid. Yield = 76 %.  $^1\text{H}$  NMR (600 MHz,  $\text{D}_2\text{O}$ ):  $\delta$  3.48-3.52 (m, 3H), 3.62 (dd, 1H,  $J$  = 9.9, 3.5 Hz) 3.66 (dd, 1H,  $J$  = 7.6, 4.1 Hz), 3.72-3.81 (m, 3H), 3.90 (d, 1H,  $J$  = 3.5 Hz), 3.97-4.00 (m, 1H), 4.38 (d, 1H,  $J$  = 8.2 Hz), 5.74 (d, 1H,  $J$  = 10.6 Hz), 6.18 (d, 1H,  $J$  = 17.6 Hz), 6.26 (dd, 1H,  $J$  = 17.3, 10.3 Hz). Spectral data is consistent with published values.<sup>19</sup>

### Preparation of RAFT chain-transfer agent (CTA) functionalized PBD-*b*-PEO (PBD-*b*-PEO-CTA)

A solution of 2-(butylthiocarbonothioylthio)-2-methylpropanoic acid<sup>18</sup> (200 mg, 0.79 mmol, 1.0 equiv.) in anhydrous  $\text{CH}_2\text{Cl}_2$  (4 mL) was added to a flame-dried flask and the flask was fitted with a magnetic stir bar and reflux condenser. Thionyl chloride (230  $\mu\text{L}$ , 4.0 mmol, 5.0 equiv.) was added dropwise using a needle and syringe. The reaction mixture was heated at reflux for 2 hours.  $\text{CH}_2\text{Cl}_2$  was removed under vacuum. PBD-*b*-PEO (50 mg) was dried through azeotrope formation with toluene (x3) and redissolved in

0.5 mL of freshly distilled  $\text{CH}_2\text{Cl}_2$  in a separate flame-dried flask. Next,  $\text{NEt}_3$  (3 mL) was added to the dissolved PBD-*b*-PEO and the mixture was cooled to 0 °C. The acid chloride RAFT agent was then dissolved in  $\text{CH}_2\text{Cl}_2$  (0.5 mL) and added to the reaction mixture dropwise. The reaction was slowly brought to room temperature and stirred overnight. The solvent was then removed using a rotary evaporator and replaced with a minimal amount of DMF. The resulting solution was then dialyzed using a 6-8 kg mol<sup>-1</sup> MWCO membrane. After 48 hours of dialysis with changing the solvent reservoir every 12 hours, the DMF was removed *in vacuo*. Based on <sup>1</sup>H NMR spectroscopy, 85% of the polymer termini were functionalized. Yield = 79 %. <sup>1</sup>H NMR (600 MHz,  $\text{CDCl}_3$ ):  $\delta$  0.92-0.95 (m, 3H), 1.05-1.45 (m, 243H), 1.70 (s, 6H), 1.90-2.12 (m, 173H), 3.52-3.77 (m, 364H), 4.25-4.27 (m, 2H), 4.87-5.4.94 (m, 231H), 5.31-5.57 (m, 138 H).

### Synthesis of CTA functionalized PEO 2K

To a flame-dried round bottom flask fitted with a magnetic stir bar, methoxy poly(ethylene oxide) (PEO) ( $M_n$  = 2000 Da, 500 mg, 0.25 mmol, 1.0 equiv.), 2-(butylthiocarbonothioylthio)-2-methylpropanoic acid<sup>18</sup> (340 mg, 1.3 mmol, 5.2 equiv.), DMAP (30 mg, 0.25 mmol, 1.0 equiv.), 4-(dimethylamino)pyridinium-4-toluene sulfonate (DPTS) (140 mg, 0.48 mmol, 1.9 equiv.) was added to dry  $\text{CH}_2\text{Cl}_2$  (10 mL). While stirring, *N,N'*-Dicyclohexylcarbodiimide (DCC) (600 mg, 2.9 mmol, 12 equiv.) was added and the reaction mixture was stirred for 48 hours at 30 °C. The reaction mixture was filtered through celite to remove insoluble byproduct. The resulting product was then purified by dialysis against DMF using a 6-8 kg mol<sup>-1</sup> MWCO membrane. After 48 hours of dialysis with changing the solvent reservoir every 12 hours, the DMF was removed *in vacuo*. Based on <sup>1</sup>H NMR spectroscopy, 100% of the polymer termini were functionalized. Yield = 60 %. <sup>1</sup>H NMR (600 MHz,  $\text{CDCl}_3$ ):  $\delta$  0.90 (t, 3H,  $J$  = 7.3 Hz), 1.23 (bs, 2H), 1.36-1.43 (m, 3H), 1.60-1.65 (m, 3H), 1.67 (s, 6H), 3.25 (t, 2H,  $J$  = 7.6 Hz), 3.35 (s, 3H), 3.49-3.74 (m, 164H), 4.22-4.24 (m, 2H).

### Synthesis of PAcGal<sub>6</sub> from alkyne-functionalized CTA and general procedure for the synthesis of PAcGal<sub>n</sub> glycopolymers.

Acetonitrile was subjected to three cycles of freeze pump thaw. Before use,  $\beta$ -D-galactose pentaacetate monomer **5** was dissolved in CH<sub>2</sub>Cl<sub>2</sub> and added to the top of a silica plug. BHT was eluted with CH<sub>2</sub>Cl<sub>2</sub> and discarded. The plug was washed with methanol. The filtrate was concentrated using a rotary evaporator and compound **5** was used immediately. In a Schlenk tube fitted with a magnetic stir bar, alkyne-functionalized CTA **7** (23 mg, 0.08 mmol, 1.0 equiv.), **5** (450 mg, 1.0 mmol, 13 equiv.) and azobisisobutyronitrile (AIBN) (4.9 mg, 0.03 mmol, 0.38 equiv.) were combined in acetonitrile (3 mL) and degassed by bubbling argon through the reaction mixture for 30 minutes at 0 °C. The reaction was then heated at 75 °C for 3 hours. The resulting filtrate was concentrated, dissolved in minimal amount of DMF and purified by dialysis against methanol using a 2 kg mol<sup>-1</sup> MWCO membrane. <sup>1</sup>H NMR (600 MHz, CDCl<sub>3</sub>):  $\delta$  0.94 (t, 3H,  $J$  = 7.2 Hz), 1.17-1.20 (m, 6H), 1.42-1.44 (m, 5H), 1.50-1.69 (m, 8H), 1.99-2.17 (m, 96H), 3.37-4.15 (m, 48H), 4.55-4.67 (m, 8H), 5.06-5.14 (m, 12H), 5.40 (bs, 6H).  $M_n$  based on <sup>1</sup>H NMR spectroscopy = 2970 g mol<sup>-1</sup>. SEC (DMF):  $M_n$  = 4160 g mol<sup>-1</sup>,  $M_w$  = 5480 g mol<sup>-1</sup>,  $D$  = 1.32. FTIR: 1745, 1218, 1046 cm<sup>-1</sup>.

### PAcGal<sub>15</sub>

This polymer was synthesized as described above for PAcGal<sub>6</sub> except that the following quantities were used: CTA **7** (14 mg, 0.05 mmol, 1.0 equiv.), **5** (550 mg, 1.2 mmol, 25 equiv.) and AIBN (2.7 mg, 0.02 mmol, 0.40 equiv.), acetonitrile (2.8 mL). Reaction time = 12 hours. Yield = 47%. <sup>1</sup>H NMR (600 MHz, CDCl<sub>3</sub>):  $\delta$  0.87 (t, 3H,  $J$  = 7.0 Hz), 1.10-1.65 (m, 43H), 1.91-2.09 (m, 194H), 2.39 (m, 9H), 3.60-4.08 (m, 72H), 4.49-4.57 (m, 14H), 4.96-5.04 (m, 29H), 5.33 (bs, 15H). Yield = 47%.  $M_n$  based on <sup>1</sup>H NMR spectroscopy = 7000 g mol<sup>-1</sup>. SEC (DMF):  $M_n$  = 9040 g mol<sup>-1</sup>,  $M_w$  = 11030 g mol<sup>-1</sup>,  $D$  = 1.22. FTIR: 1745, 1218, 1046 cm<sup>-1</sup>.

### PAcGal<sub>29</sub>

This polymer was synthesized as described above for PAcGal<sub>6</sub> except that the following quantities were used: CTA **7** (14 mg, 0.05 mmol, 1.0 equiv.), **5** (1.06 g, 2.38 mmol, 48 equiv.) and AIBN (2.7 mg, 0.02 mmol, 0.4 equiv.), acetonitrile (2.65 mL). Reaction time = 17 hours. Yield = 47%. <sup>1</sup>H NMR (600 MHz, CDCl<sub>3</sub>): δ 0.88 (m, 3H), 1.11-1.72 (m, 75H), 1.92-2.11 (m, 380H), 2.99 (bs, 10H), 3.31-4.10 (m, 205H), 4.56-4.59 (m, 30H), 5.01-5.05 (m, 58H), 5.34 (bs, 29H). *M<sub>n</sub>* based on <sup>1</sup>H NMR spectroscopy = 13260 g mol<sup>-1</sup>. SEC (DMF): *M<sub>n</sub>* = 10900 g mol<sup>-1</sup>, *M<sub>w</sub>* = 13290 g mol<sup>-1</sup>, *D* = 1.22. FTIR: 1745, 1218, 1046 cm<sup>-1</sup>.

### Synthesis of PGal<sub>6</sub> and general procedure for synthesis of PGal<sub>n</sub>

PAcGal<sub>6</sub> (170 mg, 0.057 mmol) was dissolved in anhydrous MeOH (3 mL) in a flame-dried flask fitted with a magnetic stir bar. To the flask, 25% sodium methoxide in MeOH (0.34 mL) was added dropwise and then stirred at room. The reaction was stirred for approximately 4 hours. The pH of the reaction mixture was then adjusted to 7 using saturated NH<sub>4</sub>Cl and then concentrated under reduced pressure. PAcGal<sub>6</sub> was purified by dialysis against pure water using a 2 kg mol<sup>-1</sup> MWCO membrane and then was lyophilized to provide a fluffy white solid. Yield = 82%. <sup>1</sup>H NMR (600 MHz, D<sub>2</sub>O): δ 1.03-1.15 (m, 6H), 1.25-1.28 (m, 2H), 1.32-1.35 (m, 2H), 1.55-2.26 (m, 22H), 3.33-4.06 (m, 75H), 4.41 (bs, 6H). *M<sub>n</sub>* based on <sup>1</sup>H NMR spectroscopy = 1950 g mol<sup>-1</sup>. FTIR: 3301, 1646, 1072, 1041 cm<sup>-1</sup>.

### PGal<sub>15</sub>

This polymer was synthesized as described above for PGal<sub>6</sub> except that the following quantities were used: PAcGal<sub>15</sub> (100 mg, 0.034 mmol), 25% sodium methoxide in MeOH (0.146 mL) and anhydrous MeOH (2 mL). Yield = 78%. <sup>1</sup>H NMR (600 MHz, D<sub>2</sub>O): δ 1.14-1.15 (m, 2H), 1.25-1.27 (m, 2H), 1.33-1.36 (m, 1H), 1.50-2.41 (m, 45H), 3.43-4.07 (m, 151H), 4.42 (bs, 15H). *M<sub>n</sub>* based on <sup>1</sup>H NMR spectroscopy = 4450 g mol<sup>-1</sup>. FTIR: 3301, 1646, 1072, 1041 cm<sup>-1</sup>.

## **PGal<sub>29</sub>**

This polymer was synthesized as described above for PGal<sub>6</sub> except that the following quantities were used: PAcGal<sub>29</sub> (574 mg, 0.043 mmol), 25% sodium methoxide in MeOH (0.356 mL) and anhydrous MeOH (10 mL). Yield = 85%. <sup>1</sup>H NMR (600 MHz, D<sub>2</sub>O):  $\delta$  1.15-1.17 (m, 4H), 1.25-1.27 (m, 6H), 1.48-2.23 (m, 91H), 3.42-3.97 (m, 315H), 4.42 (bs, 29H).  $M_n$  based on <sup>1</sup>H NMR spectroscopy = 8330 g mol<sup>-1</sup>. FTIR: 3301, 1646, 1072, 1041 cm<sup>-1</sup>.

## **Preparation of functionalized PBD-*b*-PEO-N<sub>3</sub> vesicles**

For the 100% functionalized vesicles, PBD-*b*-PEO-N<sub>3</sub> (50 mg) was dissolved in 1 mL of CH<sub>2</sub>Cl<sub>2</sub> in a 25 mL round bottom flask. For the 10% functionalized vesicles, PBD-*b*-PEO-N<sub>3</sub> (5 mg) and PBD *b*-PEO (45 mg) were used. A Nile red solution in CH<sub>2</sub>Cl<sub>2</sub> was then added to obtain an accurate loading of 0.1 w/w% of Nile red relative to the copolymers. The CH<sub>2</sub>Cl<sub>2</sub> was removed under a stream of argon to produce a film of polymer on the flask. Deionized (DI) water (1 mL/10 mg of polymer) was then added and the solution was stirred for 0.5 h at 45 °C. The solution was then sonicated for 0.5 h and finally stirred for 24 h at 45 °C. The polymersomes were then extruded two times through each of 1000 nm, 400 nm, 200 nm and 100 nm polycarbonate membranes (Whatman, Nuclepore) at 45 °C using a pressure driven Lipex Thermobarrel Extruder (1.5 mL capacity, Northern Lipids). The resulting vesicles were characterized by dynamic light scattering (DLS) and transmission electron microscopy (TEM).

## **TEM**

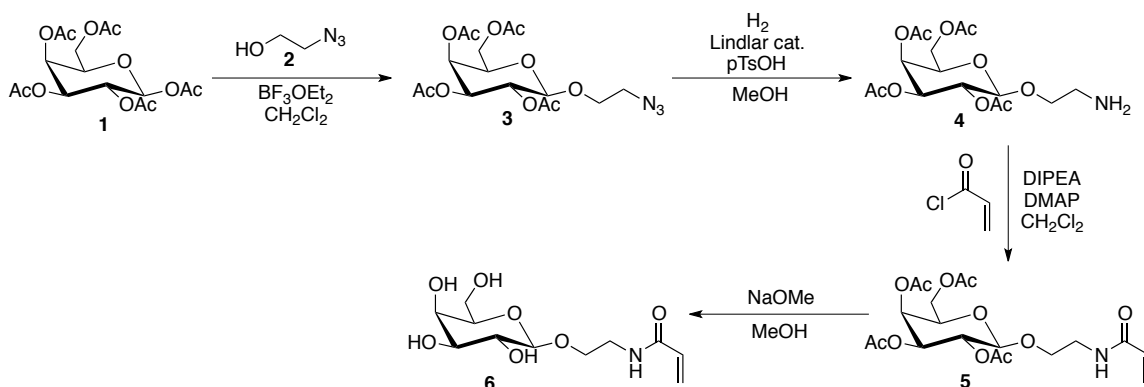
The vesicle suspension (prepared as described above, 10  $\mu$ L of 0.1 mg mL<sup>-1</sup>) was placed on a Formvar®/carbon grid and was left to stand 5 min. The excess solution was then blotted off using a piece of filter paper. The resulting sample was consecutively imaged using a Phillips CM10 microscope operating at 80 kV with a 40  $\mu$ m aperture.



### General procedure for surface conjugation by click chemistry

Vesicles were prepared as described above at a concentration of 10 mg/mL of polymer. A solution of copper (II) sulfate pentahydrate ( $\text{CuSO}_4 \cdot 5\text{H}_2\text{O}$ ), sodium ascorbate, bathophenanthrolinedisulfonic acid disodium salt hydrate, and  $\text{PGal}_n$  was added in sequence such that the reaction mixture contained 1 mM  $\text{CuSO}_4$ , 25 mM sodium ascorbate, 2.3 mM bathophenanthrolinedisulfonic acid and 4 equivalents of  $\text{PGal}_n$  with respect to  $\text{PBD-}b\text{-PEO-N}_3$ . The reaction mixture was stirred at room temperature overnight and then dialyzed against water overnight using a 25 kg  $\text{mol}^{-1}$  MWCO membrane. The resulting suspension was lyophilized and the product was characterized by FTIR spectroscopy.

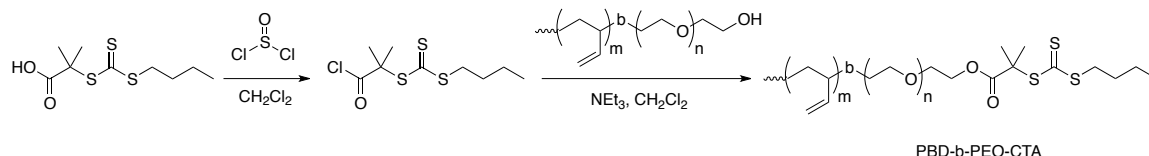
### 3.3 Results and Discussion



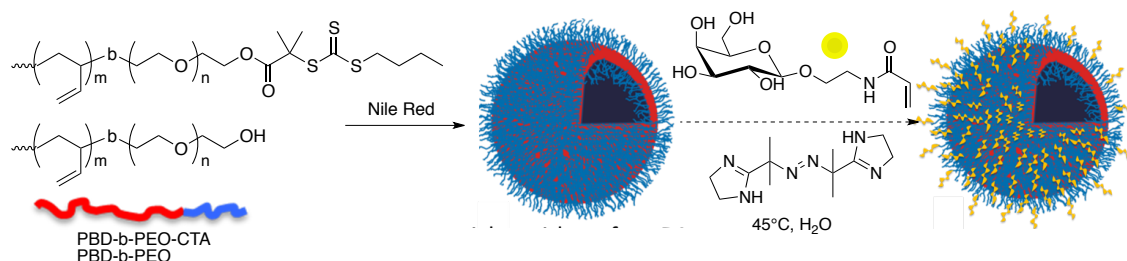
**Scheme 3.1.** Synthesis of acrylamide-functionalized  $\beta$ -D-galactose monomer (**6**).

An acrylamide-functionalized  $\beta$ -D-galactose monomer was synthesized as shown in Scheme 3.1. A selective glycosylation of D-galactose pentaacetate (**1**)<sup>19</sup> with 2-azidoethanol (**2**) in the presence of  $\text{BF}_3 \cdot \text{OEt}_2$  yielded compound **3** as only the  $\beta$  anomer.<sup>19</sup> The azide group in compound **3** was then reduced to an amine using a Lindlar-catalyzed hydrogenation. The resulting compound (**4**) was treated with acryloyl chloride in the presence of DIPEA and DMAP to yield compound **5** bearing acrylamide functionality. It was discovered that compound **5** readily polymerizes and as a result, small amounts of

BHT was added to the product as a radical inhibitor before solvent was evaporated from the product. During purification by column chromatography, BHT was also added to the eluent to prevent polymerization. Lastly, a deprotection of compound **5** was performed using sodium methoxide to yield compound **6**.<sup>19</sup>

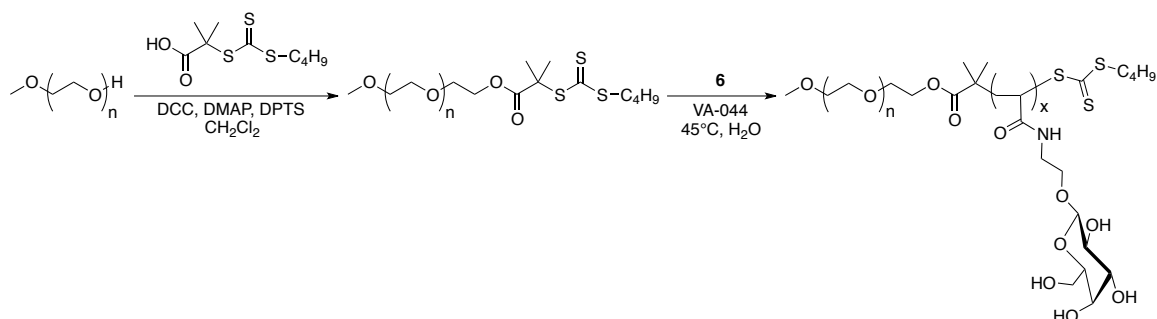


**Scheme 3.2.** Synthesis of PBD-*b*-PEO-CTA from 2-(butylthiocarbonothioylthio)-2-methylpropanoic acid.



**Scheme 3.3.** Self-assembly of CTA functionalized vesicles in the presence of Nile Red and subsequent polymerization of monomer **6** from the surface.

Following the synthesis of monomer, PBD-*b*-PEO was functionalized with CTA. This was achieved by first preparing the acid chloride derivative of 2-(butylthiocarbonothioylthio)-2-methylpropanoic acid using thionyl chloride in order to produce a highly reactive acylating reagent (Scheme 3.2). The acid chloride derivative was then reacted with PBD-*b*-PEO resulting in functionalization of ~85% of the terminal hydroxyl groups according to <sup>1</sup>H NMR spectroscopy.



**Scheme 3.4.** Synthesis of PEO2K-CTA and control polymerization with **6**.

Characterization of glycopolymers polymerized from vesicles is complex and problematic due to their assembled nature and lack of a common solvent for PBD, PEO and the glycopolymer (see Figure A2.3). As a result, a control study was performed using PEO ( $M_n = 2000 \text{ g mol}^{-1}$ ) functionalized with CTA to provide a fully water-soluble polymer. Functionalization of PEO with 2-(butylthiocarboethioylthio)-2-methylpropanoic acid was performed via a DCC coupling. The resulting PEO-CTA, **6** (100 equiv.), and the water-soluble initiator VA-044 were combined and heated at  $45^\circ\text{C}$ . Half of the reaction mixture was removed after 10 hours and quenched by exposure to air. The other half of the reaction was polymerized for 24 hours and then quenched by exposure to air. Size exclusion chromatography (SEC) data shown in Figure 3.3 indicated that a 10-hour polymerization lead to glycopolymers with 8 saccaride units whereas polymerizing for 24 hours yielded glycopolymers with 21 saccaride units with low dispersities ( $D = 1.13$ ). These results indicate only a 20% conversion after 24 hours, which is unusual and undesirable using this technique. Additionally, SEC data indicated a broad shoulder suggesting the presence of a high molecular weight impurity (Figure 3.3). This impurity is likely from uncontrolled polymerization of the monomer before use. This impurity may also help to explain the low conversion of monomer as there would be less monomer available to undergo controlled RAFT polymerization. Due to the low conversion of monomer and high molecular weight impurity present in the control study, an alternative strategy was taken to provide glycopolymer-coated vesicles. This alternative approach instead involved a more traditional strategy in which premade glycopolymers could be conjugated to the surface of preassembled azide-functionalized vesicles using alkyne-azide click chemistry.

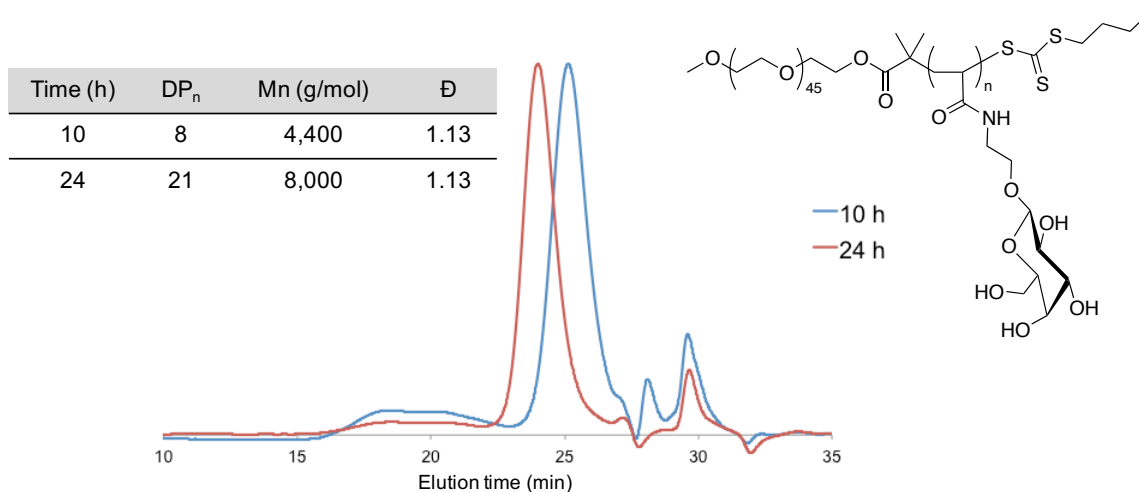
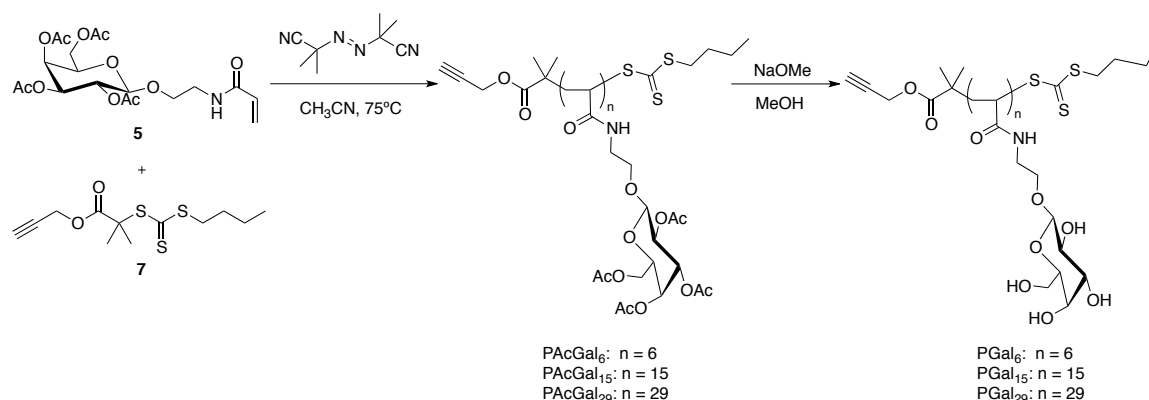


**Figure 3.3.** SEC data of polymerizations of  $\beta$ -D-galactose from CTA functionalized PEO as a control.

For this second approach,  $\beta$ -D-galactose pentaacetate possessing acrylamide functionality (**5**) was selected as the monomer to afford acetylated glycopolymers due to the tendency of the deprotected  $\beta$ -D-galactose monomer (**6**) to undergo uncontrolled radical polymerization resulting in a high molecular weight impurity. For the preparation of the acetylated glycopolymers using RAFT polymerization, CTA **7**<sup>18</sup> possessing a terminal alkyne moiety was used along with AIBN as the initiator and the polymerization was conducted in acetonitrile at 75 °C (Scheme 3.5). During preliminary polymerizations, it was discovered that glycopolymer degree of polymerization plateaus at ~35 units even at monomer equivalents as high as 100, relative to CTA. This plateau is likely due to the bulky nature of the monomer. As a result, no more than 48 equivalents of monomer was used for further polymerizations. In order to investigate the effect of glycopolymer length on protein binding, 12, 25, and 48 equivalents of monomer **5** relative to CTA were used to provide three glycopolymers of varying lengths (Table 3.2). Evaluation of the <sup>1</sup>H NMR spectra prior to purification showed that the conversion of **5** varied from 50-60%. The polymers were subsequently purified by dialysis against methanol using a 3500 g mol<sup>-1</sup> MWCO membrane.



**Scheme 3.5.** Synthesis of  $\text{PAcGal}_n$  using RAFT polymerization and subsequent deprotection to provide  $\text{PGal}_n$  glycopolymers.

The resulting glycopolymers were characterized by  $^1\text{H}$  NMR spectroscopy, FTIR spectroscopy, and SEC. The DP was determined using  $^1\text{H}$  NMR spectroscopy by comparing the integration of the peak at 0.94 ppm corresponding to the 3 hydrogens on the terminal methyl group of the CTA with that of the multiplet at 5.4 ppm corresponding to the anomeric proton on the galactose. This indicated that DPs of 6, 15, and 29 were obtained for glycopolymers  $\text{PAcGal}_6$ ,  $\text{PAcGal}_{15}$  and  $\text{PAcGal}_{29}$ , respectively. These values are in agreement with the number of equivalents and the conversion observed by NMR spectroscopy. From these DPs, the number average molar mass ( $M_n$ ) was calculated for each polymer (Table 3.2). These ranged from  $2970 \text{ g mol}^{-1}$  for  $\text{PAcGal}_6$  to  $13290 \text{ g mol}^{-1}$  for  $\text{PAcGal}_{29}$ . The molar masses were also measured by SEC in DMF relative to poly(methyl methacrylate) standards. As shown in Table 3.2, the  $M_n$ s were in good agreement with those obtained by NMR spectroscopy and the  $D$  was less than 1.4 for each glycopolymer. The SEC traces are included in the appendix (Figures A2.14-A2.16). The acetylated glycopolymers were then deprotected using sodium methoxide in methanol. Successful deprotection was indicated by the absence of the acetate peaks at 1.99-2.17 ppm (Figures A2.10-A12). The deprotected glycopolymers were characterized by  $^1\text{H}$  NMR and FTIR spectroscopy.

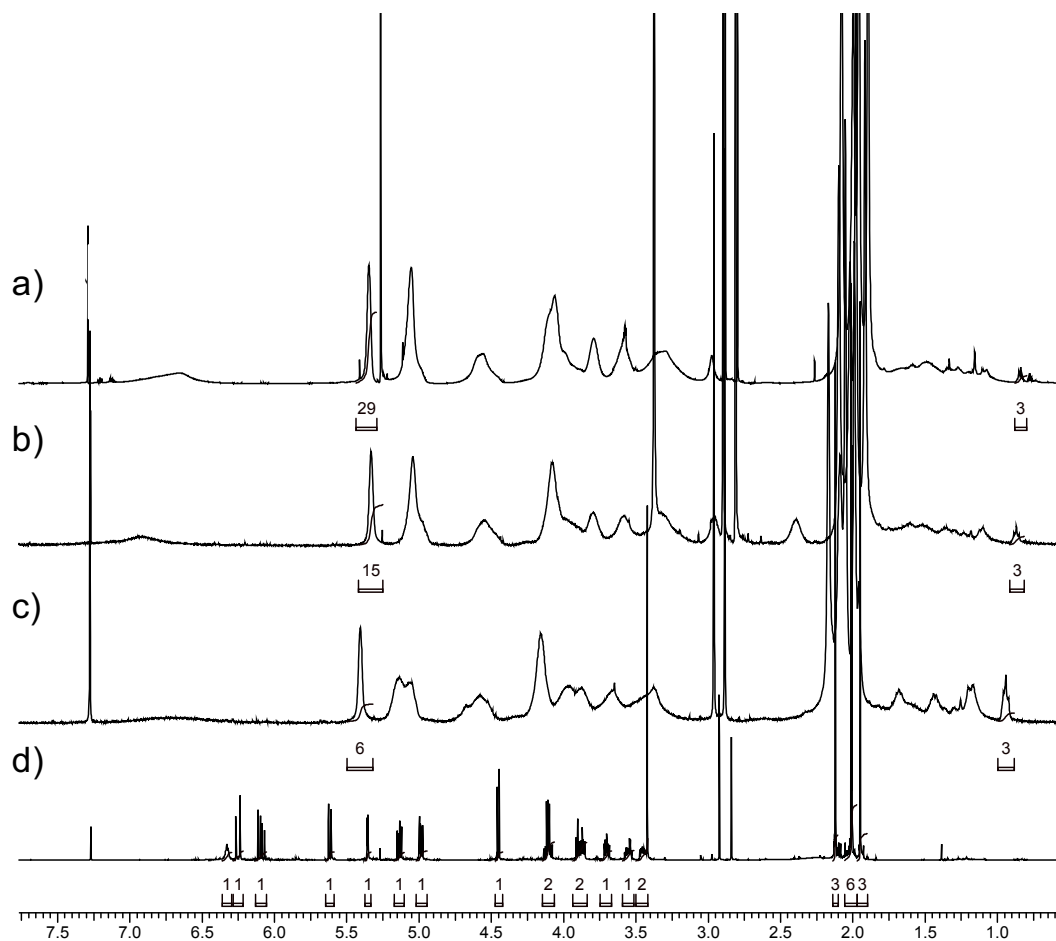
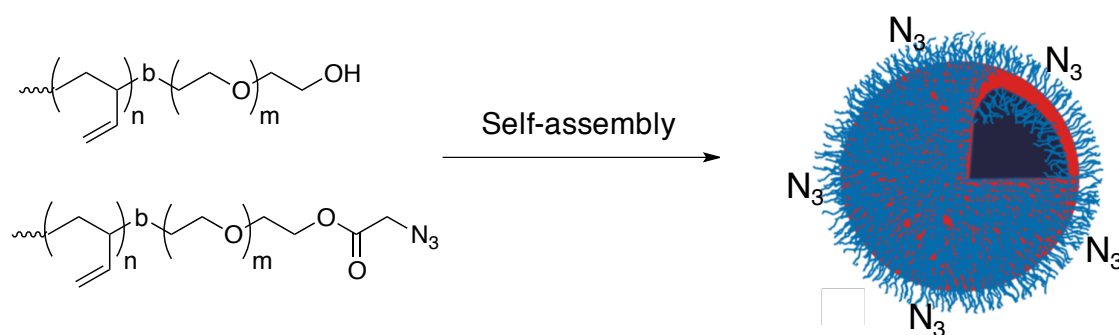


**Figure 3.4.**  $^1\text{H}$  NMR spectra of a)  $\text{PAGal}_6$ , b)  $\text{PAcGal}_{15}$ , c)  $\text{PAcGal}_{29}$ , and d) protected  $\beta$ -D-galactose monomer (**5**).

**Table 3.2.** Summary of PAcGal glycopolymers synthesized for this study and their molar mass characteristics.

Glycopolymer	Equiv. of <b>5</b> added	DP of <b>5</b> (NMR)	% Conversion (NMR)	$M_n$ ( $\text{g mol}^{-1}$ ) (NMR)	$M_n$ ( $\text{g mol}^{-1}$ ) (SEC)	$\bar{D}$ (SEC)
PAcGal <sub>6</sub>	12	6	50	2970	4160	1.32
PAcGal <sub>15</sub>	25	15	60	7000	9040	1.22
PAcGal <sub>29</sub>	48	29	60	13260	10900	1.22

Following the synthesis and characterization of PGal<sub>n</sub> glycopolymers, vesicles with surface azide groups were prepared as previously reported (Scheme 3.3).<sup>21</sup> In order to control the percentage of glycopolymer on the vesicle surface, vesicles of PBD-*b*-PEO and PBD-*b*-PEO-N<sub>3</sub> with either 10 or 100% PBD-*b*-PEO-N<sub>3</sub> were prepared by hydration of a thin film in the presence of the hydrophobic dye Nile red. The vesicles were then extruded through a 100 nm pore diameter membrane to reduce their diameters. The resulting vesicles were characterized using DLS and TEM (Figure 3.6). This showed that the diameters were approximately 200 nm. The larger diameter relative to the extrusion pore size can likely be attributed to the flexibility of the vesicles. Ambient temperature at which the extrusion was performed is above the T<sub>g</sub> of the PBD, meaning that it would exist in a flexible rubbery state.



**Scheme 3.6.** Preparation of PBD-*b*-PEO vesicles with azide functionality presented on the surface.

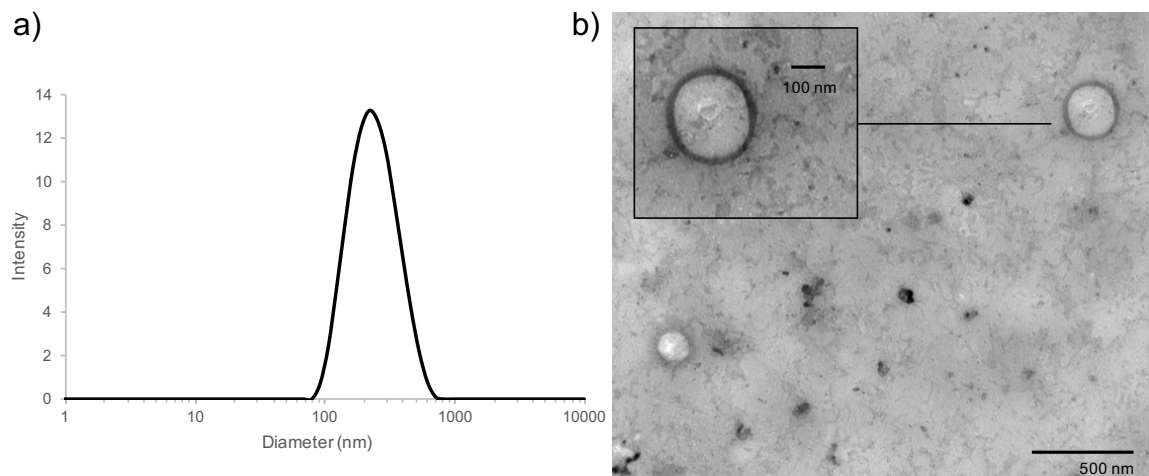


**Figure 3.5.** a) DLS intensity distribution and b) TEM image of extruded PBD-*b*-PEO vesicles containing 10% PBD-*b*-PEO-N<sub>3</sub> before click reaction.

Cycloaddition reactions between the azide-functionalized vesicles and alkyne-terminated glycopolymers were performed over 24 hours using 1 mM CuSO<sub>4</sub>, 25 mM sodium ascorbate, 2.3 mM bathophenanthrolinedisulfonic acid and 4 equivalents of PGal<sub>n</sub> with respect to PBD-*b*-PEO-N<sub>3</sub>. Excess PGal<sub>n</sub> was then removed by dialysis against purified water. The resulting glycopolymer-coated vesicles were analyzed using <sup>1</sup>H NMR spectroscopy in D<sub>2</sub>O. However, quantification of glycopolymer on the vesicle surface was not possible due to the extent of overlapping peaks from the glycopolymer and PEO. As a result, the efficacy of the click reaction between PGal<sub>n</sub> and azide was approximated through FTIR spectroscopy (Figure 3.6). The percent reduction of the azide peak at 2110 cm<sup>-1</sup> was used to quantify the coupling efficacy. However, for the click reaction between PGal<sub>15</sub> and 100% azide-functionalized vesicles, a complete disappearance of the azide peak was observed. It should be noted that approximately 50% of the azides should be located in the interior of the vesicles and thus inaccessible to the glycopolymer, which is unlikely to diffuse through the vesicle membrane. However, a conjugation yield higher than 50% was obtained, which is consistent with previous studies.<sup>21,22</sup> This may be explained by the dynamic nature of the vesicles, allowing polymer chains functionalized with azide contained in the vesicle interior to migrate to the vesicle exterior during the 24-hour reaction period. The attachment of glycopolymer to the PBD-*b*-PEO-N<sub>3</sub> vesicles can further be confirmed by the appearance of a broad OH stretch at 2930 cm<sup>-1</sup>. However,



for the click reaction between PGal<sub>15</sub> and 10% azide-functionalized vesicles, FTIR spectroscopy was not a viable strategy for the quantification of coupling efficacy as no azide peak from the vesicles could be detected before the reaction with glycopolymer. This is likely due to the high molecular weight (10 kg mol<sup>-1</sup>) of PBD-*b*-PEO and low abundance of making the azide peak undetectable. This finding demonstrates that quantification using FTIR should be used with caution as disappearance of the azide peak does not infer complete conversion but rather that the azide peak is too weak to be detected.

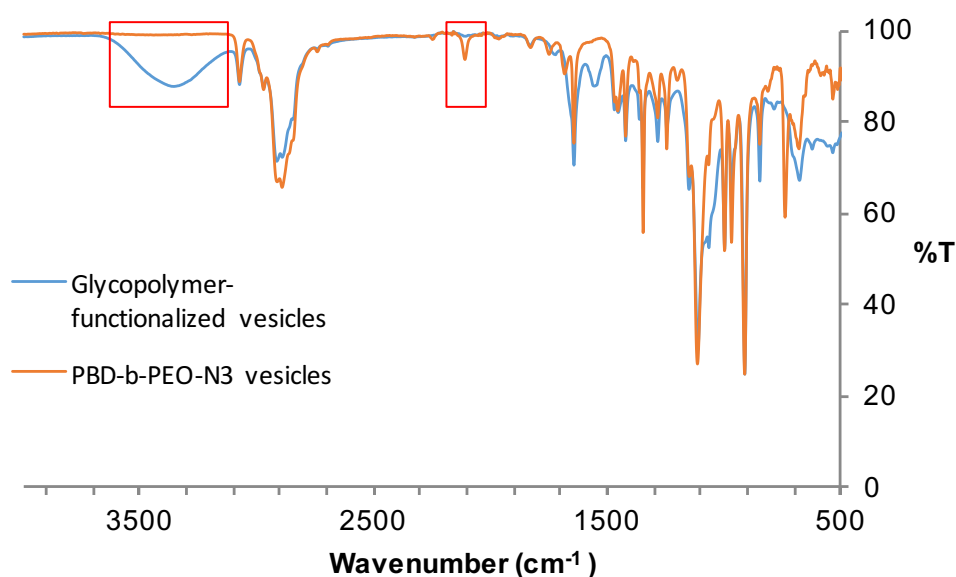


**Figure 3.6.** FTIR spectra of PBD-*b*-PEO-N<sub>3</sub> vesicles and click reaction between PGal<sub>15</sub> and 100% azide-functionalized vesicles.

### 3.4 Conclusions

Synthesis of a  $\beta$ -D-galactose monomer with an acrylamide functionality was achieved over 4 steps. First, an approach involving the polymerization of the monomer from the vesicle surface via RAFT polymerization was explored. However, difficulties involving homopolymerization of the deprotected galactose monomer **6** and separation of the resulting high molecular weight homopolymer were encountered. Thus another approach

involving the conjugation of pre-synthesized glycopolymers to the vesicle surface was explored. Alkyne-functionalized glycopolymer with low, medium and high degree of polymerization and relatively low dispersities (1.22-1.32) were synthesized by RAFT polymerization. PBD-*b*-PEO was functionalized with an azide moiety followed by its self-assembly into vesicles to give loadings of either 10 or 100% azide on the surface. Glycopolymer was then conjugated to the azide-functionalized vesicles by a copper(I) catalyzed 3 + 2 “click” cycloaddition. FTIR spectroscopy suggested a high conjugation yield. However, further work will be required to better quantify this reaction, characterize the resulting vesicles and evaluate their capacities to bind to lectin.

### 3.5 References

- (1) Zhang, L. F.; Eisenberg, A. *Science* **1995**, 268, 1728.
- (2) Discher, D. E.; Eisenberg, A. *Science* **2002**, 297, 967.
- (3) Battaglia, G.; Ryan, A. J. *J. Am. Chem. Soc.* **2005**, 127, 8757.
- (4) Ahmed, F.; Pakunlu, R. I.; Srinivas, G.; Brannan, A.; Bates, F.; Klein, M. L.; Minko, T.; Discher, D. E. *Mol. Pharm.* **2006**, 3, 340.
- (5) Brown, M. D.; Schätzlein, A.; Brownlie, A.; Jack, V.; Wang, W.; Tetley, L.; Gray, A. I.; Uchegbu, I. F. *Bioconjug. Chem.* **2000**, 11.
- (6) León, O.; Muñoz-Bonilla, A.; Bordegé, V.; Sánchez-Chaves, M.; Fernández-García, M. *J. Polym. Sci. A Polym. Chem.* **2011**, 49, 2627.
- (7) Taylor, M. E.; Bezouska, K.; Drickamer, K. *J. Biol. Chem.* **1992**, 267, 1719.
- (8) Nazemi, A.; Haeryfar, S. M.; Gillies, E. R. *Langmuir* **2013**, 29, 6420.
- (9) Kumar, J.; Bousquet, A.; Stenzel, M. H. *Macromol. Rapid Commun.* **2011**, 32, 1620.
- (10) Martin, A. L.; Li, B.; Gillies, E. R. *J. Am. Chem. Soc.* **2009**, 131, 734.
- (11) Chen, C.; Xu, H.; Qian, Y.-C.; Huang, X.-J. *RSC Adv.* **2015**, 5, 15909.
- (12) Trinadh, M.; Govindaraj, K.; Rajasekhar, T.; Dhayal, M.; Sainath, A. V. S. *Polym. Int.* **2015**, 64, 795.
- (13) Lu, J.; Fu, C.; Wang, S.; Tao, L.; Yan, L.; Haddleton, D. M.; Chen, G.; Wei, Y. *Macromolecules* **2014**, 47, 4676.
- (14) Sun, K.; Bligh, S. W. A.; Nie, H.-l.; Quan, J.; Zhu, L.-m. *RSC Adv.* **2013**, 00, 1.
- (15) Menon, S.; Ongungal, R. M.; Das, S. *Polym. Chem.* **2013**, 4, 623.

- (16) Li, Z.-C.; Shen, Y.; Liang, Y.-Z.; Li, F.-M. *Chin. J. Poly. Sci.* **2001**, *19*, 297.
- (17) Pasparakis, G.; Alexander, C. *Angew. Chem. Int. Ed.* **2008**, *47*, 4847.
- (18) Hossain, M. D.; Valade, D.; Jia, Z.; Monteiro, M. J. *Polym. Chem.* **2012**, *3*, 2986.
- (19) Yu, K.; Kizhakkedathu, J. N. *Biomacromolecules* **2010**, *11*, 3073.
- (20) Amos, R. C.; Nazemi, A.; Bonduelle, C. V.; Gillies, E. R. *Soft Matter* **2012**, *8*, 5947.
- (21) Li, B.; Martin, A. L.; Gillies, E. R. *Chem. Commun.* **2007**, 5217.
- (22) Nazemi, A.; Amos, R. C.; Bonduelle, C. V.; Gillies, E. R. *J. Polym. Sci. A Polym. Chem.* **2011**, *49*, 2546.

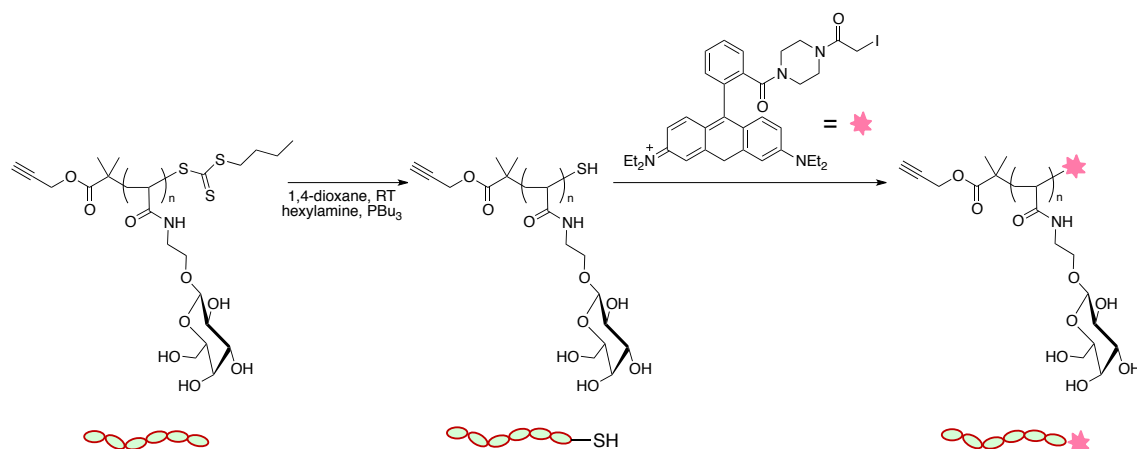
## Chapter 4

### 4.1 Conclusions and Future Work

The work described in this thesis presented the synthesis of novel polymeric systems for potential use in drug delivery and other biomedical applications. The development of functional polymeric nanocarriers that are biocompatible, biodegradable and possess targeting capabilities are highly desirable. Shown here is the synthesis of novel polyester block copolymers PEO-*b*-PHEL bearing pendant alkenes that can be easily functionalized using thiol-ene click chemistry. It has been demonstrated that the morphology of the parent PEO-*b*-PHEL copolymers can be tuned through the attachment of various small molecules to obtain a variety of desirable morphologies including spherical micelles, cylindrical micelles and vesicles. This provides a flexible platform for the synthesis of copolymers that vary in the composition of their core-forming blocks from a single polymer precursor which has not been previously described for polyesters. It was also shown that this strategy can be used for the attachment of an anticancer drug and fluorescent dye, paclitaxel and rhodamine B, respectively. PEO-*b*-PHEL-RHD was found to self-assemble into spherical compound micelles while the self-assembly of PEO-*b*-PHEL-PTX34 resulted in macroscopic precipitation. Further studies will investigate the effect of lowering the amount of paclitaxel conjugated to PEO-*b*-PHEL on the self-assembly behavior in order to obtain paclitaxel-loaded polymeric assemblies for use in drug delivery. In theory, once administered into the body the synthesized paclitaxel-loaded nanocarriers would accumulate in the extracellular matrix (ECM) of the tumor cells as a result of the enhanced permeability and retention (EPR) effect of tumor tissue. The ester linkage connecting paclitaxel to the polymer backbone could then undergo enzymatic hydrolysis by biological enzymes rendering the original paclitaxel structure unaltered. However, this linkage is not very selective. Due to the increased acidity of the ECM of tumor cells, changing the linkage to something pH sensitive such as an acetal could provide a stimuli-responsive release of the drug cargo at the tumor site.<sup>1</sup>

Also described in this thesis was the synthesis of glycopolymer-functionalized vesicles to afford vesicles with varying glycopolymer lengths and densities on the surface. The first approach presented involving polymerization of a  $\beta$ -D-galactose monomer (**6**) from the

surface of preassembled vesicles functionalized with CTA proved to be challenging due to their assembled nature and lack of a common solvent for the three blocks, leading to incomplete characterization. The second approach described the synthesis of well-defined glycopolymers possessing alkyne functionality obtained using RAFT polymerization. These glycopolymers were then conjugated to preassembled azide-functionalized vesicles using a copper(I) catalyzed 3 + 2 “click” cycloaddition. However, quantification of glycopolymer on the vesicle surface was problematic for similar reasons as seen with the previous system investigated. Due to the problems associated with characterization of the glycopolymer-coated vesicles using standard techniques, another approach should be utilized in order to more accurately quantify the amount of glycopolymer being added to the vesicle surface. One method by which this could be achieved is through the utilization of the trithiocarbonate group present in the CTA which becomes incorporated into the terminus of the glycopolymers. It has been demonstrated that these terminal functionalities are easily converted to thiols<sup>2</sup> that can be further reacted with other molecules such as proteins<sup>3,4</sup> or dyes.<sup>5</sup> Attachment of a fluorescent dye to the terminus of the glycopolymers surrounding the vesicles would allow quantification using fluorescence spectroscopy. Rhodamine B would be a good candidate for this purpose as it is water-soluble, inexpensive and synthetically versatile.<sup>6</sup> Cleavage of the terminal trithiocarbonate end group could be accomplished by reacting 1-hexylamine in the presence of tributylphosphine resulting in a thiol (Scheme 4.1).<sup>4</sup> The resulting polymer could then be treated with a reactive Rhodamine B derivative to obtain fluorescently labelled glycopolymer, which when conjugated to the vesicles would be quantifiable by fluorescence spectroscopy. This fluorescent labelling combined with FTIR spectroscopy should provide an estimation for the amount of glycopolymer that was successfully attached to the vesicles.



**Scheme 4.1.** Preparation of Rhodamine-labeled polymersomes for quantification of glycopolymer chains.

Once proper characterization has been achieved, the biological properties of the resulting glycopolymer-coated vesicles will be explored. As a first step, lectin-binding studies will be performed on agarose bound lectin in order to examine the effect of glycopolymer density and length on protein binding which has not previously been investigated. The findings of these binding studies will provide valuable insight into how glycopolymer chain length and density influence saccharide-protein binding strength in order to develop biomaterials with optimal binding capabilities.

### 3.6 References

- (1) Gillies, E. R.; Goodwin, A. P.; Fréchet, J. M. *Bioconjug Chem* **2004**, *15*, 1254.
- (2) Willcock, H.; O'Reilly, R. K. *Polym. Chem.* **2010**, *1*, 149.
- (3) Roth, P. J.; Jochum, F. D.; Zentel, R.; Theato, P. *Biomacromolecules* **2010**, *11*, 238.
- (4) Li, M.; De, P.; Li, H.; Sumerlin, B. S. *Polym. Chem.* **2010**, *1*, 854.
- (5) Beija, M.; Charreyre, M.-T.; Martinho, J. M. G. *Prog. Polym. Sci.* **2011**, *36*, 568.
- (6) Nguyen, T.; Francis, M. B. *Org. Lett.* **2003**, *5*, 3245.



## Permissions

This Agreement between Brooke Raycraft ("You") and Royal Society of Chemistry ("Royal Society of Chemistry") consists of your license details and the terms and conditions provided by Royal Society of Chemistry and Copyright Clearance Center.

License Number	3918400963963
License date	Jul 29, 2016
Licensed Content Publisher	Royal Society of Chemistry
Licensed Content Publication	RSC Advances
Licensed Content Title	Glycosylation of polyphosphazenes by thiol-yne click chemistry for lectin recognition
Licensed Content Author	Chen Chen,Huang Xu,Yue-Cheng Qian,Xiao-Jun Huang
Licensed Content Date	Feb 3, 2015
Licensed Content Volume Number	5
Licensed Content Issue Number	21
Type of Use	Thesis/Dissertation
Requestor type	academic/educational
Portion	figures/tables/images
Number of figures/tables/images	1
Format	print and electronic
Distribution quantity	4
Will you be translating?	no
Order reference number	
Title of the thesis/dissertation	NANOCARRIERS FOR DRUG DELIVERY APPLICATIONS: FROM TUNABLE MORPHOLOGIES TO GLYCOPOLYMER-COATED VESICLES
Expected completion date	Aug 2016
Estimated size	120
Requestor Location	Brooke Raycraft 7 Prescott Cr  Bracebridge, ON P1L0B7 Canada Attn: Brooke Raycraft
Billing Type	Invoice
Billing Address	Brooke Raycraft

This Agreement between Brooke Raycraft ("You") and Elsevier ("Elsevier") consists of your license details and the terms and conditions provided by Elsevier and Copyright Clearance Center.

License Number	3918341424462
License date	Jul 29, 2016
Licensed Content Publisher	Elsevier
Licensed Content Publication	European Journal of Pharmaceutics and Biopharmaceutics
Licensed Content Title	Nanoparticles for drug delivery: The need for precision in reporting particle size parameters
Licensed Content Author	Marie Gaumet,Angelica Vargas,Robert Gurny,Florence Delie
Licensed Content Date	May 2008
Licensed Content Volume Number	69
Licensed Content Issue Number	1
Licensed Content Pages	9
Start Page	1
End Page	9
Type of Use	reuse in a thesis/dissertation
Portion	figures/tables/illustrations
Number of figures/tables/illustrations	1
Format	both print and electronic
Are you the author of this Elsevier article?	No
Will you be translating?	No
Order reference number	
Original figure numbers	figure 2
Title of your thesis/dissertation	NANOCARRIERS FOR DRUG DELIVERY APPLICATIONS: FROM TUNABLE MORPHOLOGIES TO GLYCOPOLYMER-COATED VESICLES
Expected completion date	Aug 2016
Estimated size (number of pages)	120
Elsevier VAT number	GB 494 6272 12
Requestor Location	Brooke Raycraft

This Agreement between Brooke Raycraft ("You") and John Wiley and Sons ("John Wiley and Sons") consists of your license details and the terms and conditions provided by John Wiley and Sons and Copyright Clearance Center.

License Number	3917200568830
License date	Jul 27, 2016
Licensed Content Publisher	John Wiley and Sons
Licensed Content Publication	Macromolecular Rapid Communications
Licensed Content Title	Self-Assembled Block Copolymer Aggregates: From Micelles to Vesicles and their Biological Applications
Licensed Content Author	Adam Blanz, Steven P. Armes, Anthony J. Ryan
Licensed Content Date	Jan 22, 2009
Licensed Content Pages	11
Type of Use	Dissertation/Thesis
Requestor type	University/Academic
Format	Print and electronic
Portion	Figure/table
Number of figures/tables	1
Original Wiley figure/table number(s)	Figure 1
Will you be translating?	No
Title of your thesis / dissertation	NANOCARRIERS FOR DRUG DELIVERY APPLICATIONS: FROM TUNABLE MORPHOLOGIES TO GLYCOPOLYMER-COATED VESICLES
Expected completion date	Aug 2016
Expected size (number of pages)	120
Requestor Location	Brooke Raycraft 7 Prescott Cr  Bracebridge, ON P1L0B7 Canada Attn: Brooke Raycraft
Publisher Tax ID	EU826007151
Billing Type	Invoice
Billing Address	Brooke Raycraft 7 Prescott Cr

## Appendix 1

This appendix and compounds 1-4 included within correspond to the molecules described in Chapter 2.

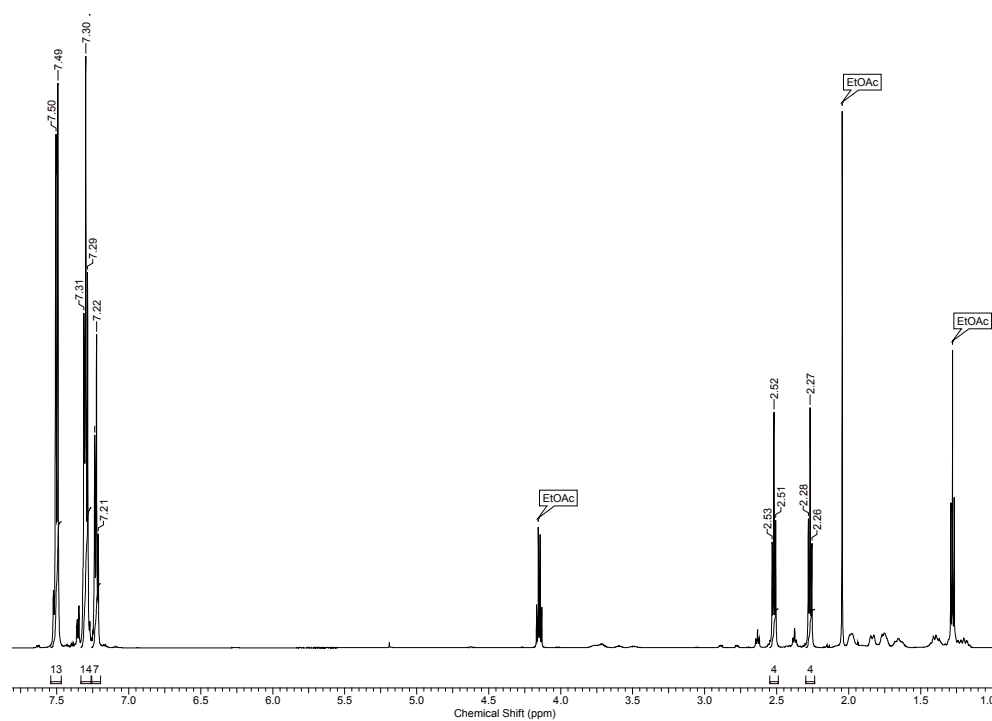


**Figure A1.1.**  $^1\text{H}$  NMR spectrum of **2** (600 MHz,  $\text{CDCl}_3$ ).

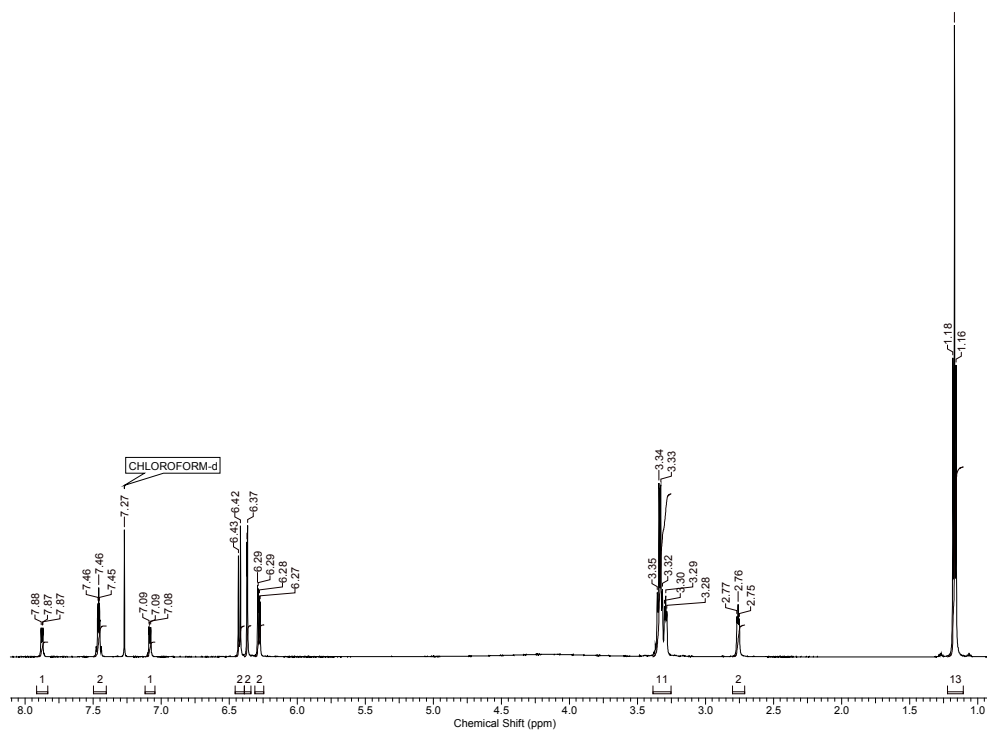


**Figure A1.2.** <sup>1</sup>H NMR spectrum of **3** (600 MHz, CDCl<sub>3</sub>).

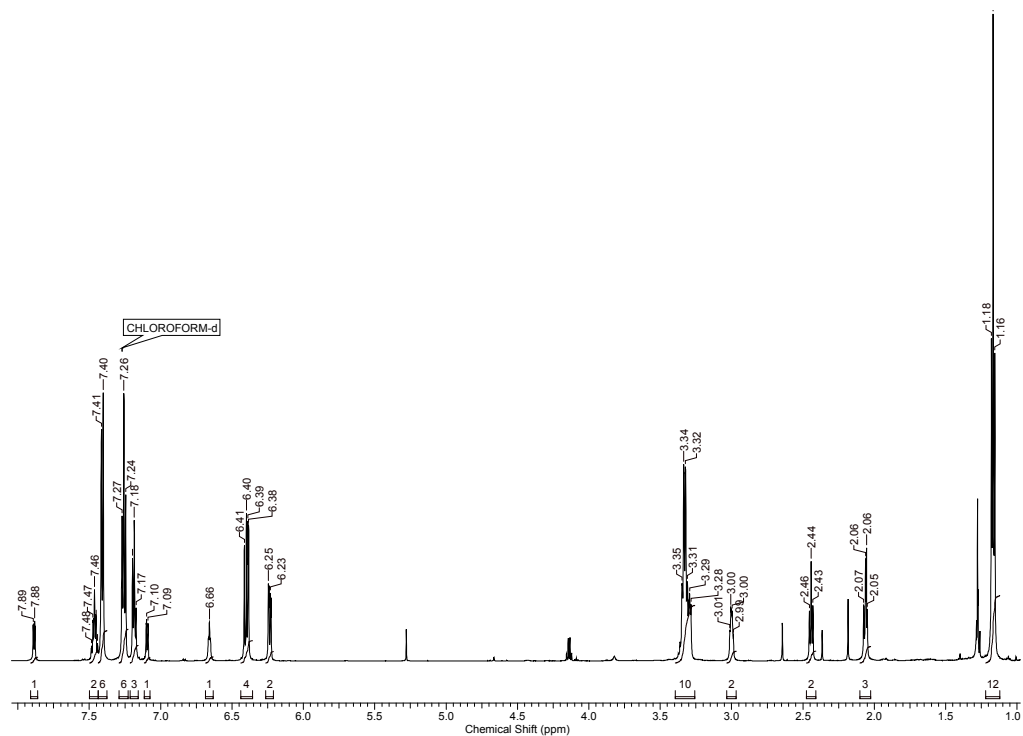


**Figure A1.3.** <sup>1</sup>H NMR spectrum of **4** (600 MHz, CDCl<sub>3</sub>).

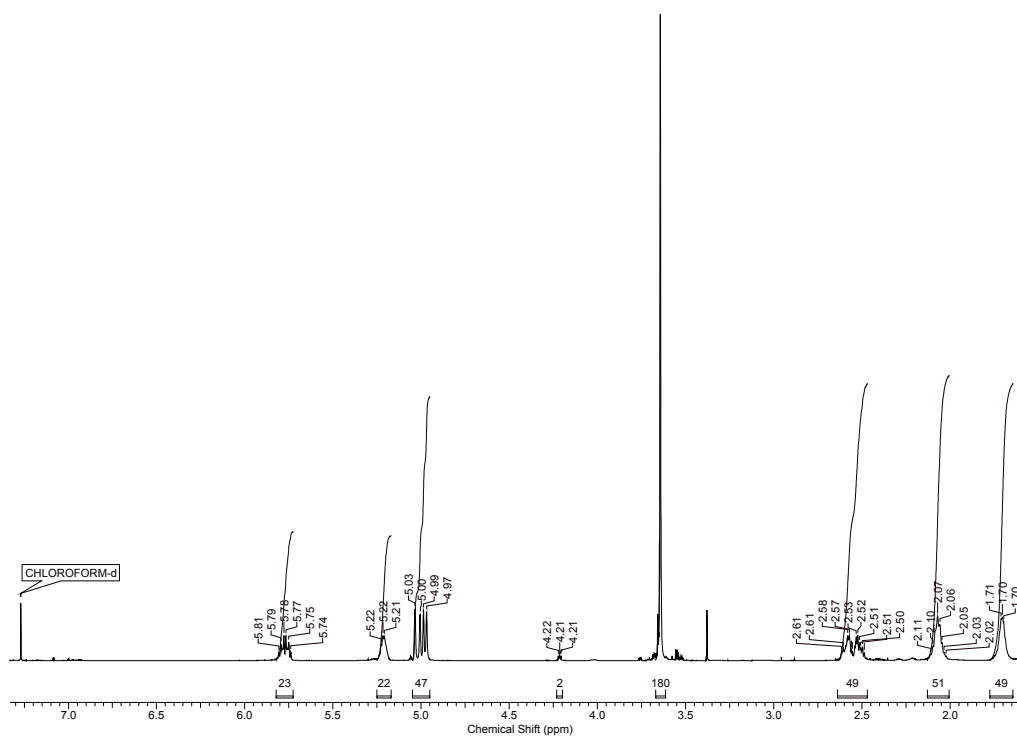


**Figure A1.4.**  $^1\text{H}$  NMR spectrum of  $\text{PEO}_{45}\text{-b-PHEL}_{23}$  (600 MHz,  $\text{CDCl}_3$ ).

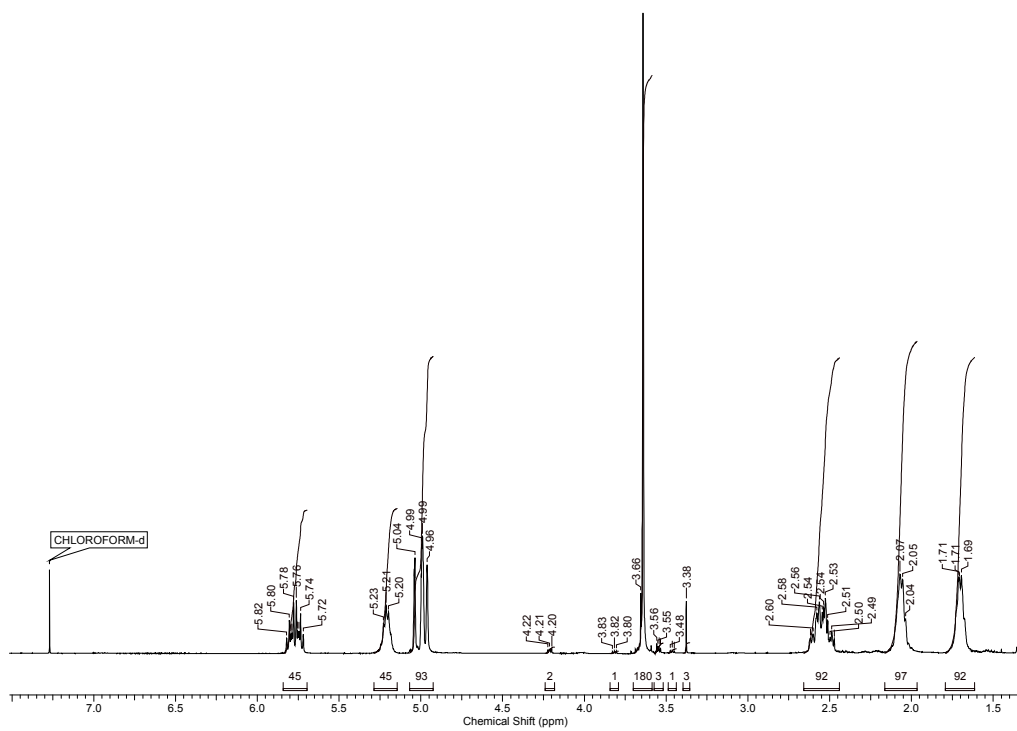


**Figure A1.5.**  $^1\text{H}$  NMR spectrum of  $\text{PEO}_{45}\text{-b-PHEL}_{45}$  (600 MHz,  $\text{CDCl}_3$ ).

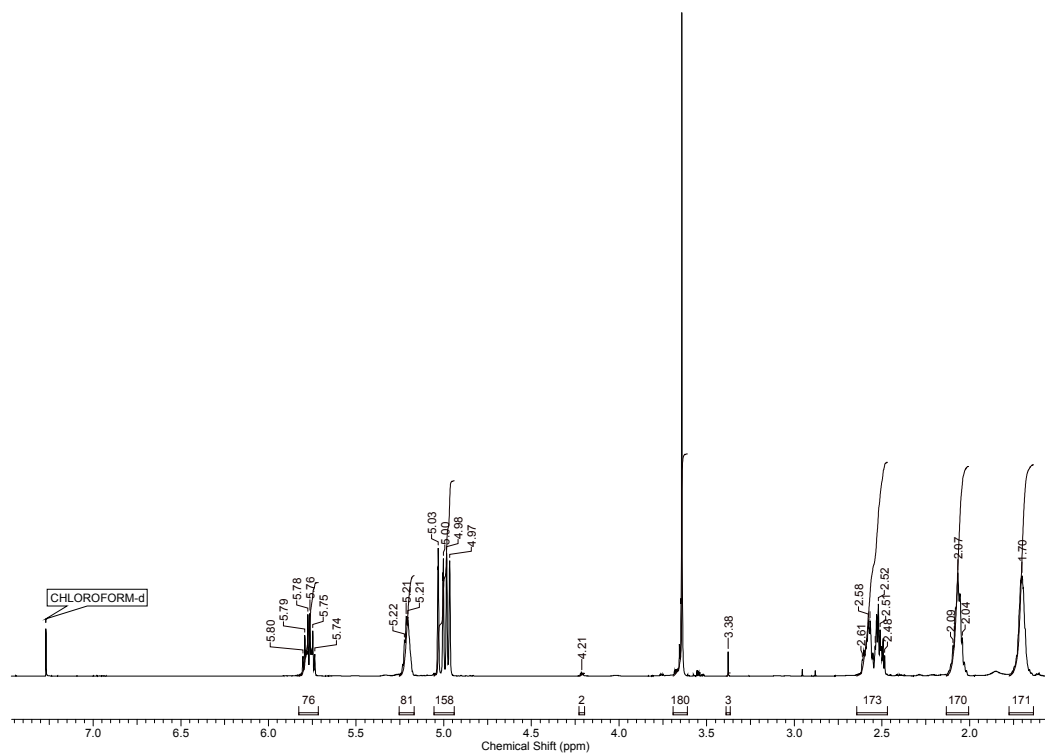


**Figure A1.6.** <sup>1</sup>H NMR spectrum of PEO<sub>45</sub>-b-PHEL<sub>79</sub> (600 MHz, CDCl<sub>3</sub>).

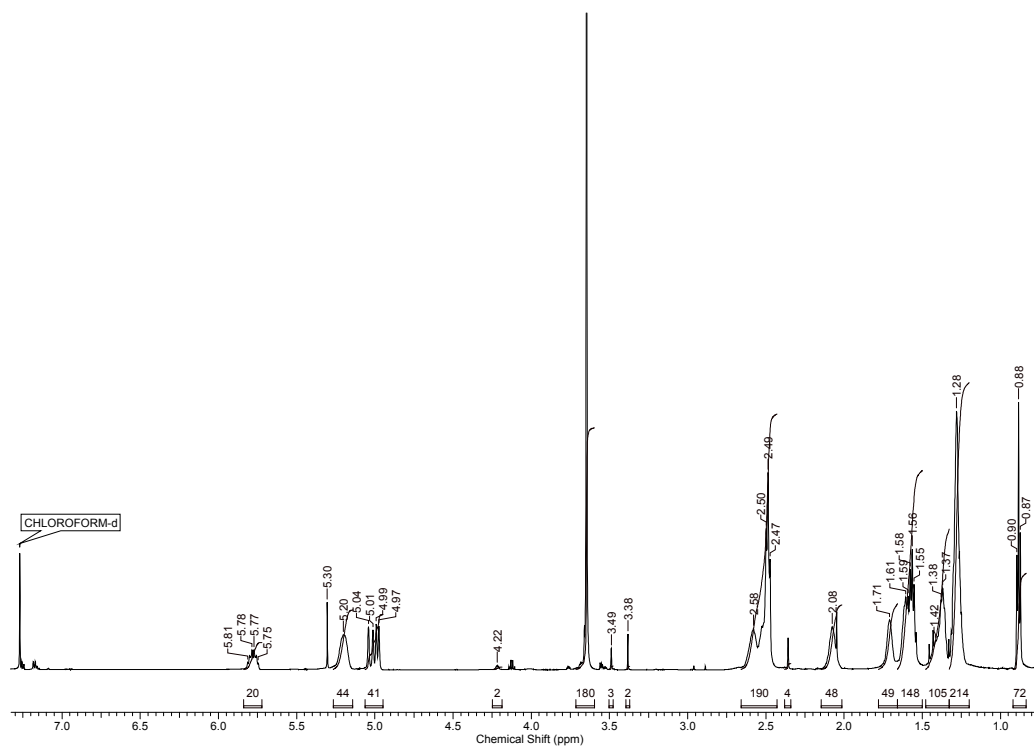


**Figure A1.7.** <sup>1</sup>H NMR spectrum of PEO<sub>45</sub>-b-PHEL<sub>45</sub>-octyl (600 MHz, CDCl<sub>3</sub>).

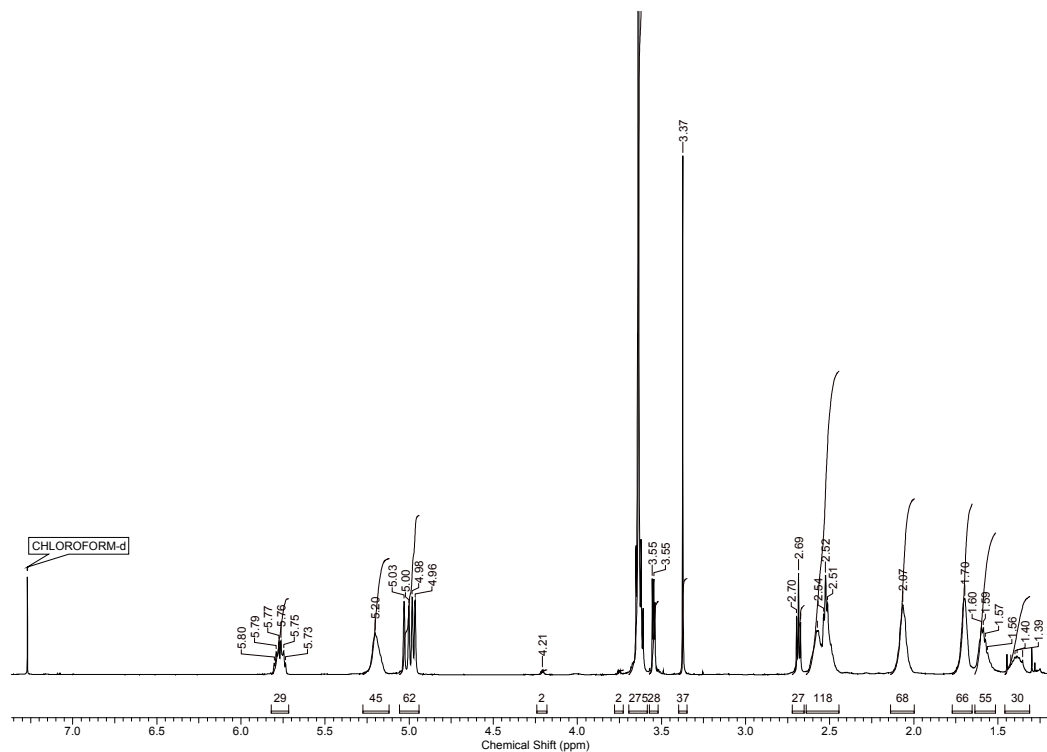


**Figure A1.8.** <sup>1</sup>H NMR spectrum of PEO<sub>45</sub>-b-PHEL<sub>45</sub>-TEG (600 MHz, CDCl<sub>3</sub>).

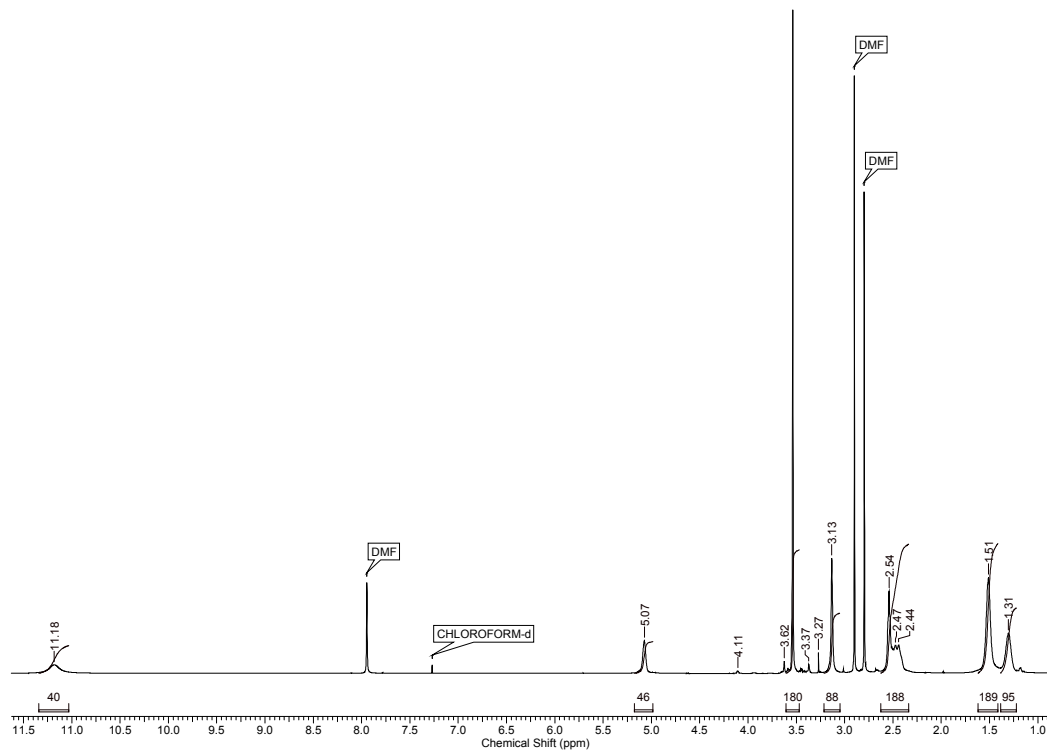


**Figure A1.9.** <sup>1</sup>H NMR spectrum of PEO<sub>45</sub>-b-PHEL<sub>45</sub>-acid (600 MHz, CDCl<sub>3</sub>).



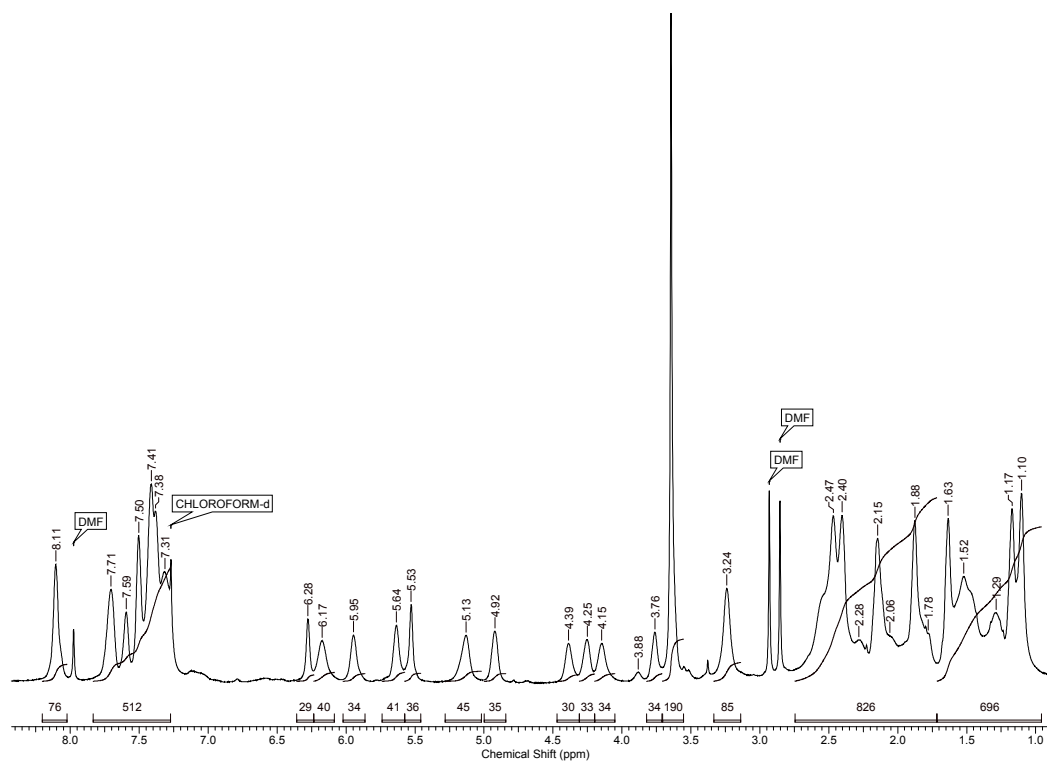


**Figure A1.10.** <sup>1</sup>H NMR spectrum of PEO<sub>45</sub>-b-PHEL<sub>45</sub>-PTX34 (600 MHz, CDCl<sub>3</sub>).

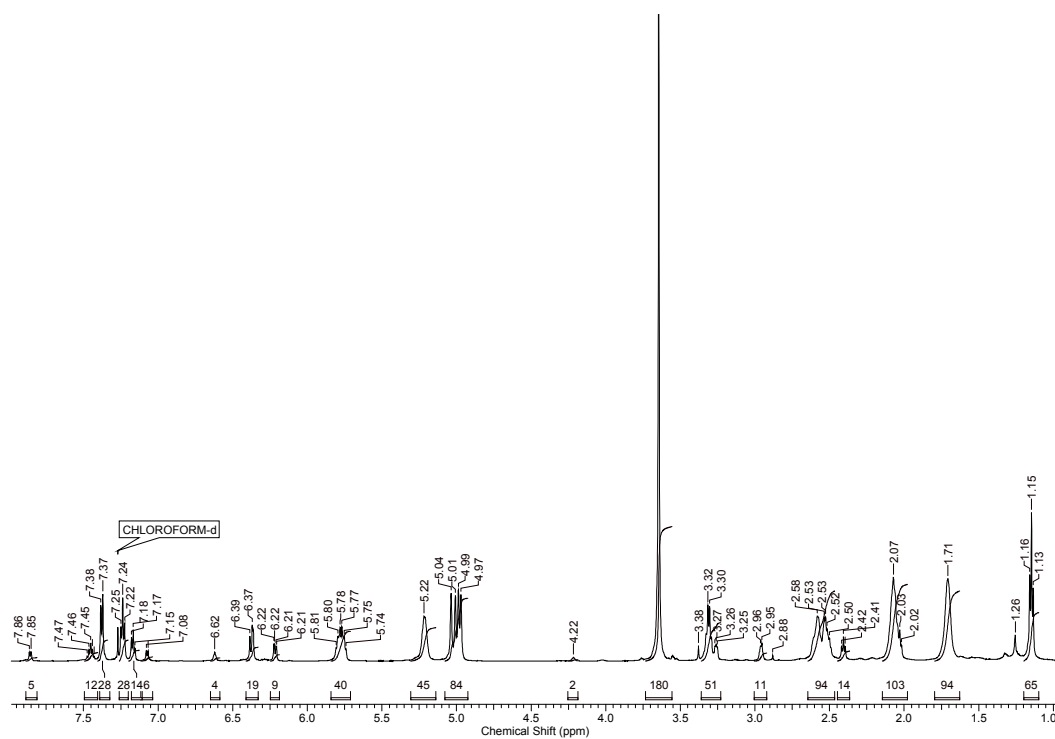


**Figure A1.11.** <sup>1</sup>H NMR spectrum of PEO<sub>45</sub>-b-PHEL<sub>45</sub>-RHD (600 MHz, CDCl<sub>3</sub>).

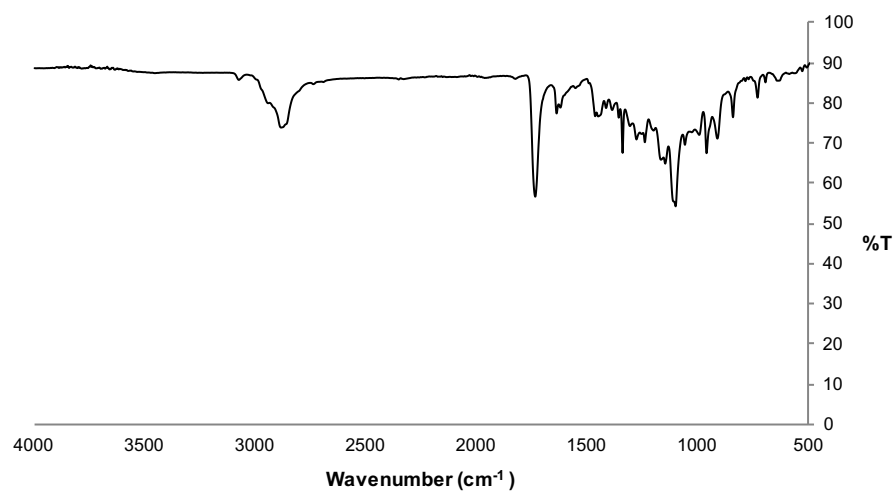


**Figure A1.12.** ATR-FTIR spectra of PEO<sub>45</sub>-b-PHEL<sub>23</sub>.

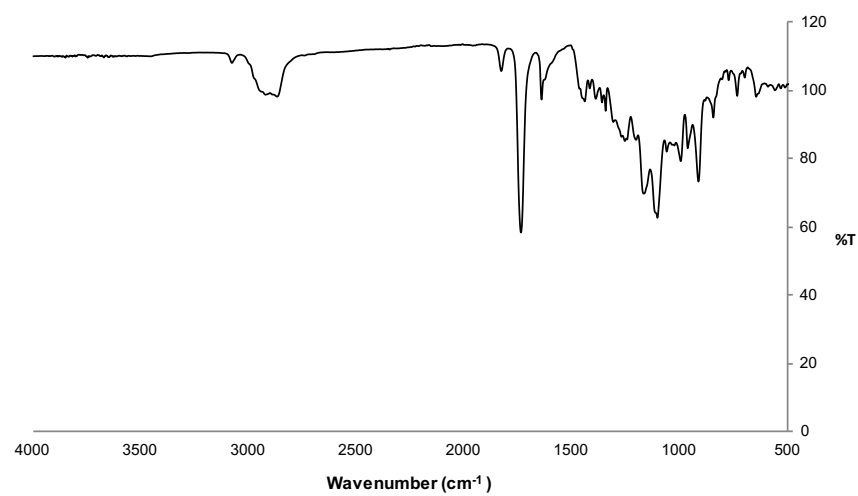


**Figure A1.13.** ATR-FTIR spectra of PEO<sub>45</sub>-b-PHEL<sub>45</sub>.

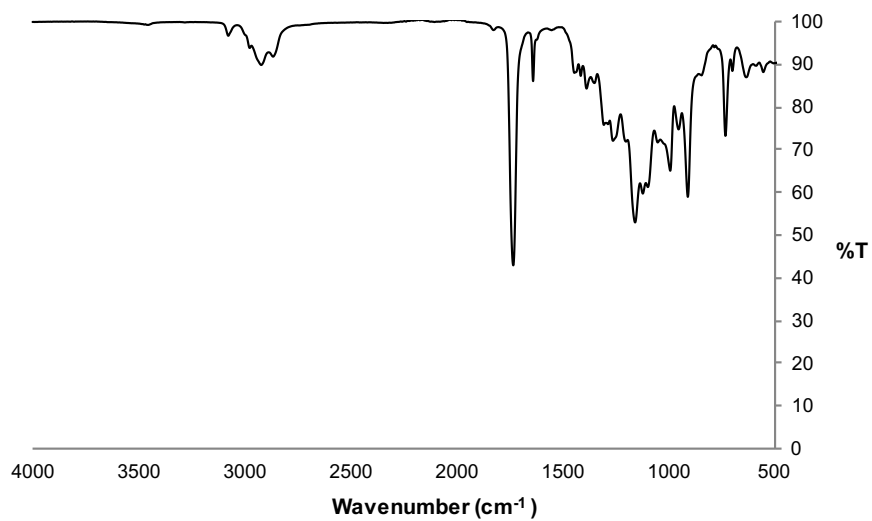


**Figure A1.14.** ATR-FTIR spectra of PEO<sub>45</sub>-b-PHEL<sub>79</sub>.

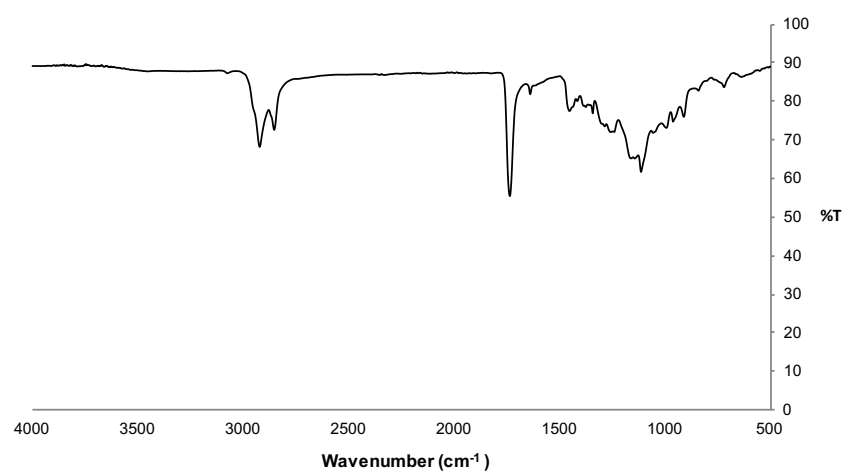


**Figure A1.15.** ATR-FTIR spectra of PEO<sub>45</sub>-b-PHEL<sub>45</sub>-octyl.

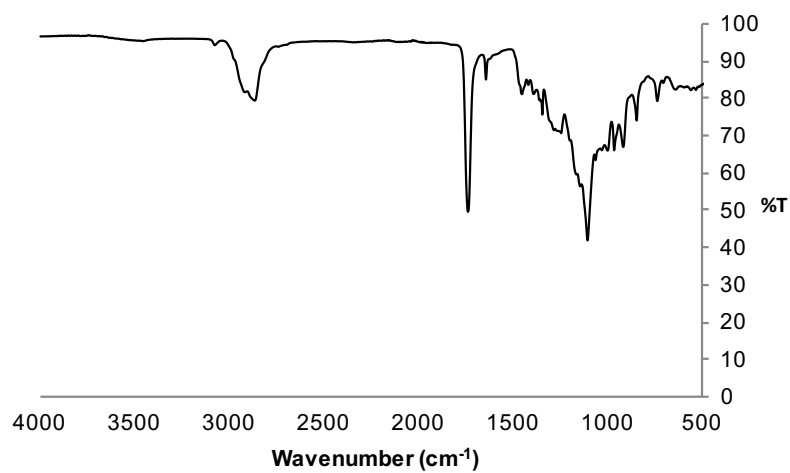


**Figure A1.16.** ATR-FTIR spectra of PEO<sub>45</sub>-*b*-PHEL<sub>45</sub>-TEG.

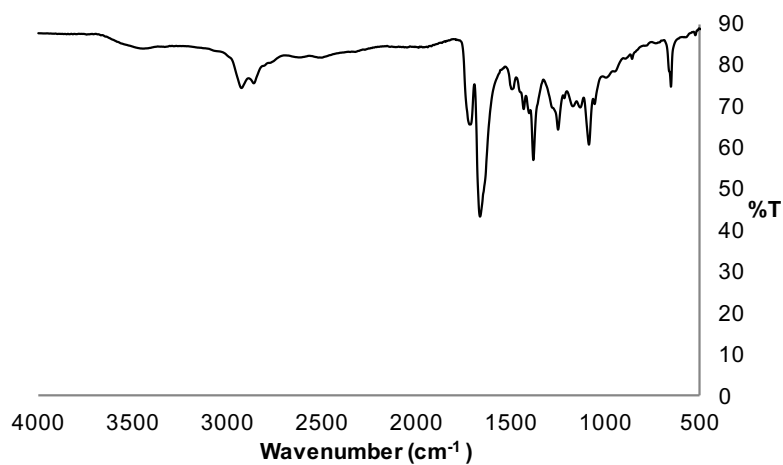


**Figure A1.17.** ATR-FTIR spectra of PEO<sub>45</sub>-*b*-PHEL<sub>45</sub>-acid.

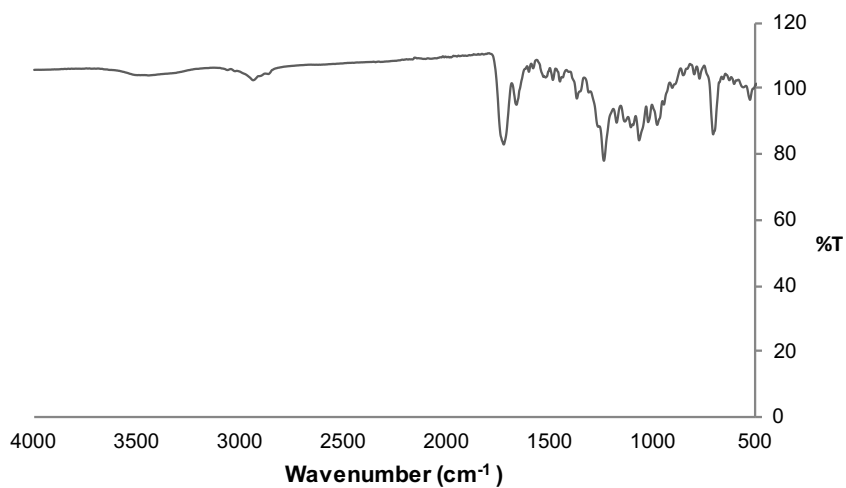


**Figure A1.18.** ATR-FTIR spectra of PEO<sub>45</sub>-*b*-PHEL<sub>45</sub>-PTX34.

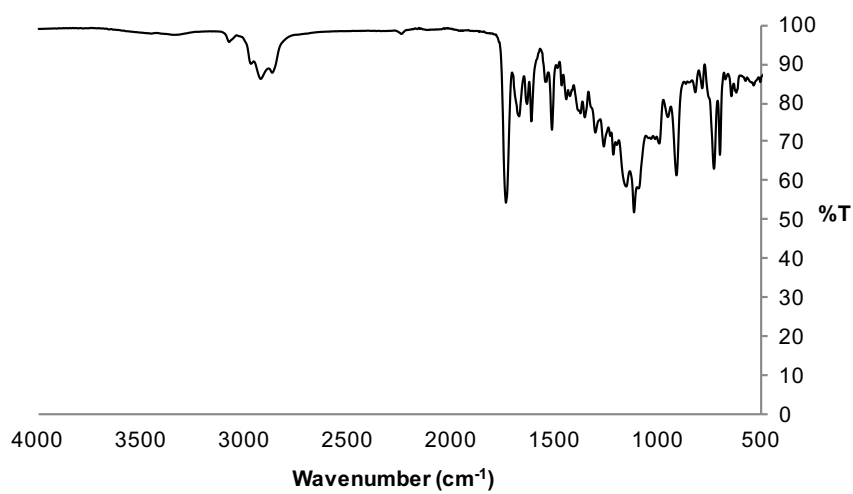


**Figure A1.19.** ATR-FTIR spectra of PEO<sub>45</sub>-*b*-PHEL<sub>45</sub>-RHD.

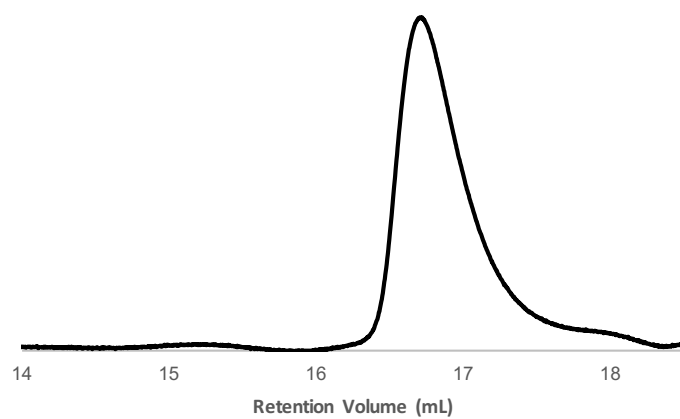


**Figure A1.20.** SEC trace for PEO<sub>45</sub>-*b*-PHEL<sub>23</sub>.

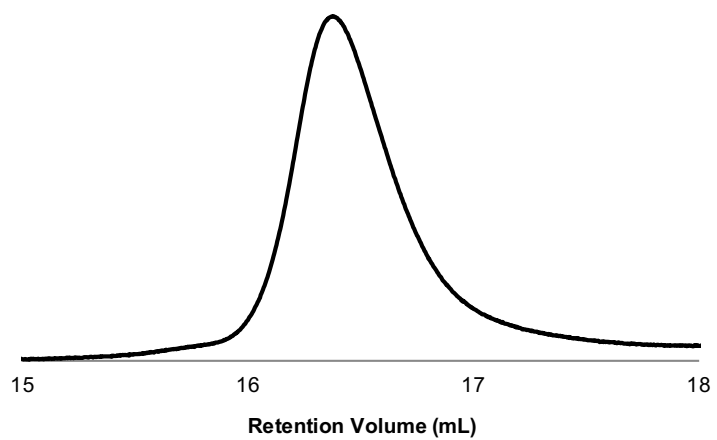


**Figure A1.21.** SEC trace for PEO<sub>45</sub>-*b*-PHEL<sub>45</sub>.

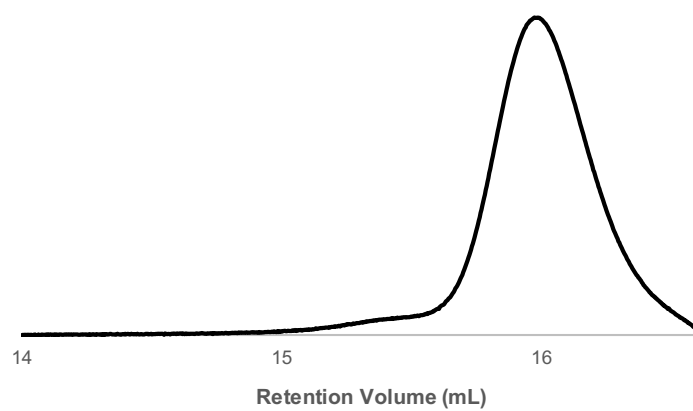


**Figure A1.22.** SEC trace for PEO<sub>45</sub>-*b*-PHEL<sub>79</sub>.

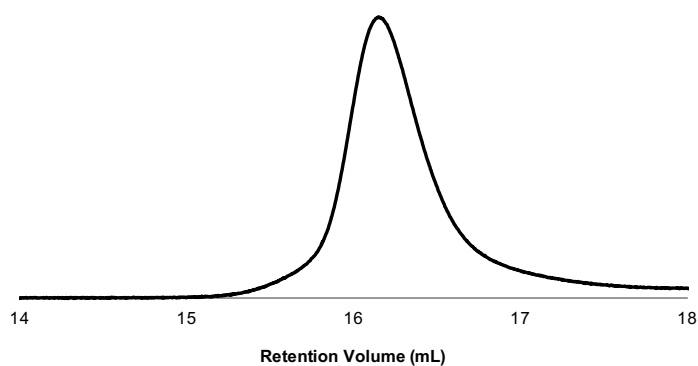


**Figure A1.23.** SEC trace for PEO<sub>45</sub>-*b*-PHEL<sub>45</sub>-octyl.

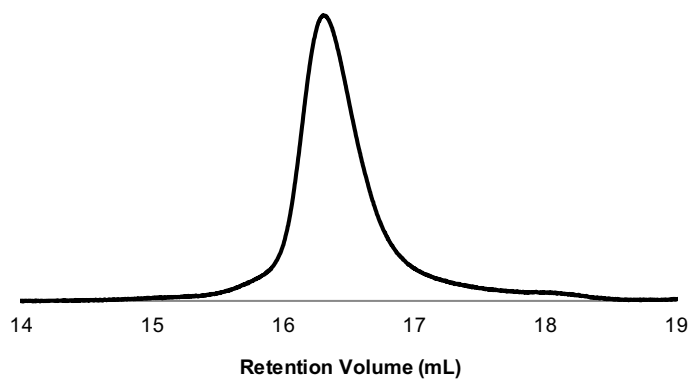


**Figure A1.24.** SEC trace for PEO<sub>45</sub>-*b*-PHEL<sub>45</sub>-TEG.

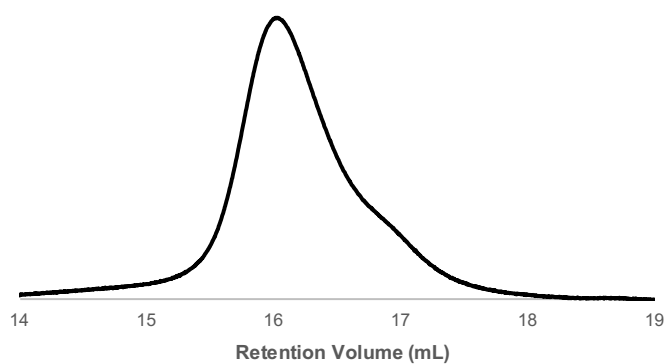


**Figure A1.25.** SEC trace for PEO<sub>45</sub>-*b*-PHEL<sub>45</sub>-PTX34.

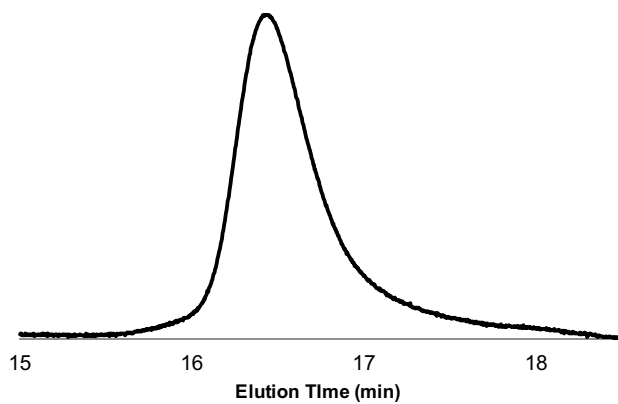


**Figure A1.26.** SEC trace for PEO<sub>45</sub>-*b*-PHEL<sub>45</sub>-RHD.

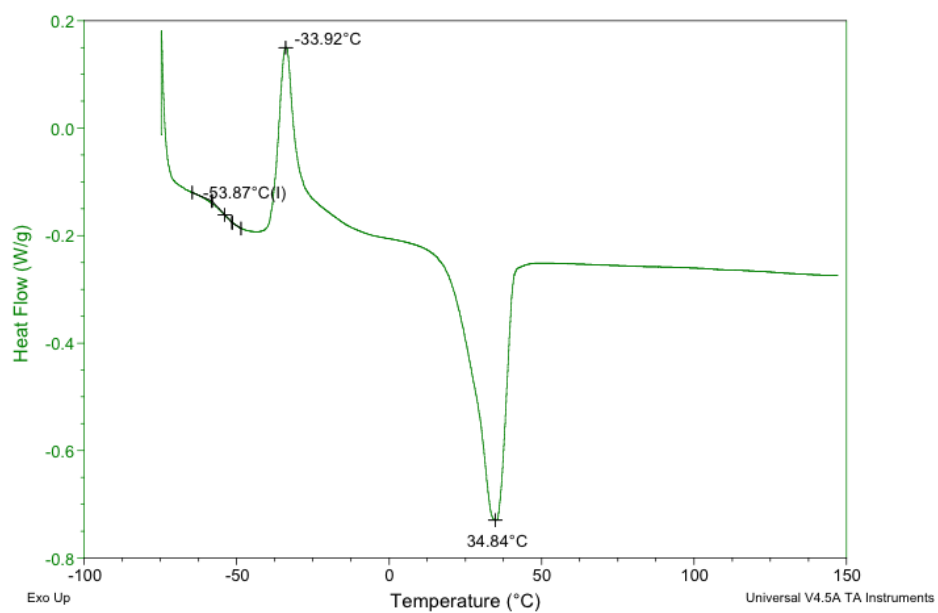


**Figure A1.27.** DSC curve for PEO<sub>45</sub>-*b*-PHEL<sub>23</sub> (obtained from third heating cycle).



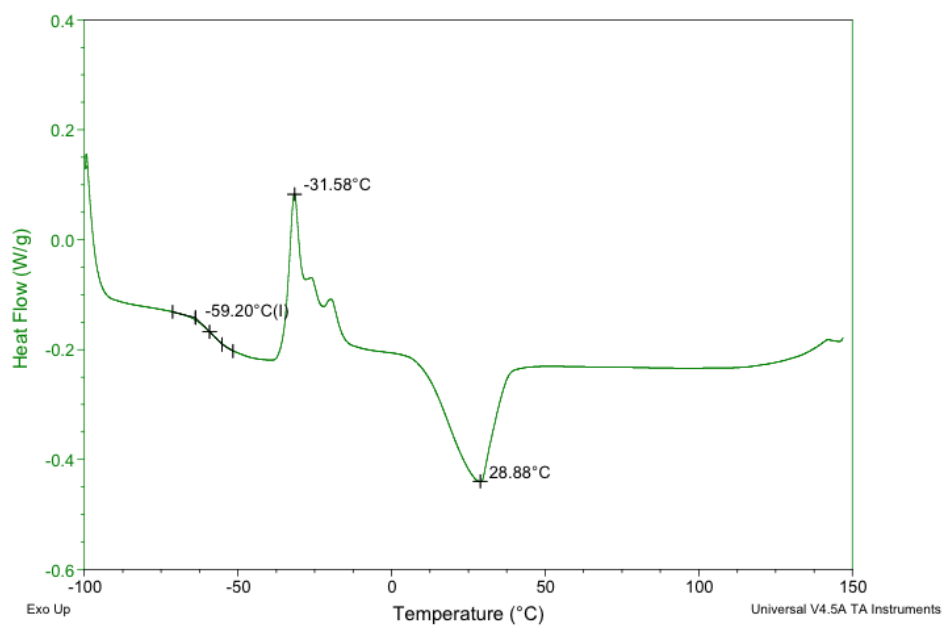


**Figure A1.28.** DSC curve for PEO<sub>45</sub>-*b*-PHEL<sub>45</sub> (obtained from third heating cycle).

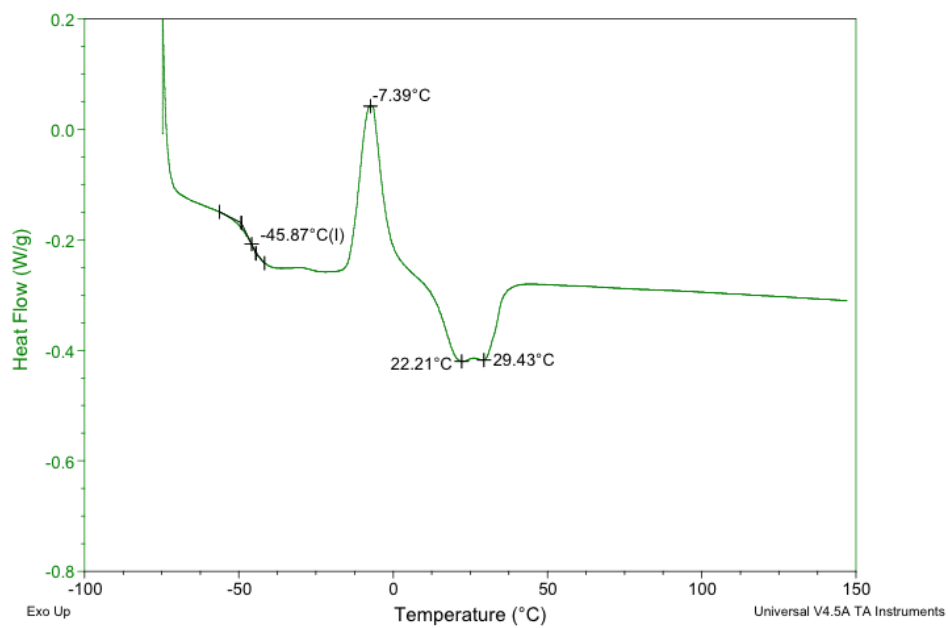


**Figure A1.29.** DSC curve for PEO<sub>45</sub>-*b*-PHEL<sub>79</sub> (obtained from third heating cycle).

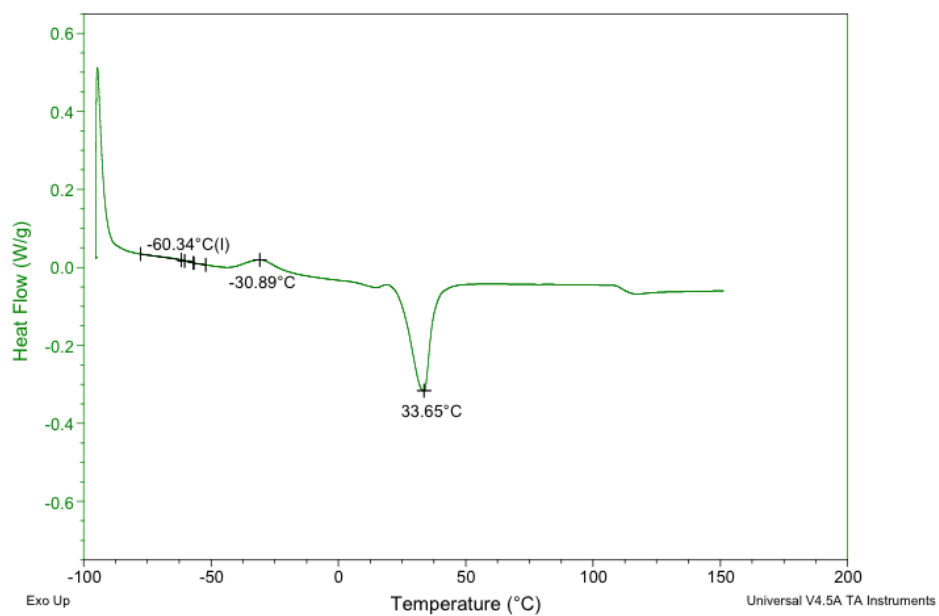


**Figure A1.30.** DSC curve for PEO<sub>45</sub>-*b*-PHEL<sub>45</sub>-octyl (obtained from fourth heating cycle).

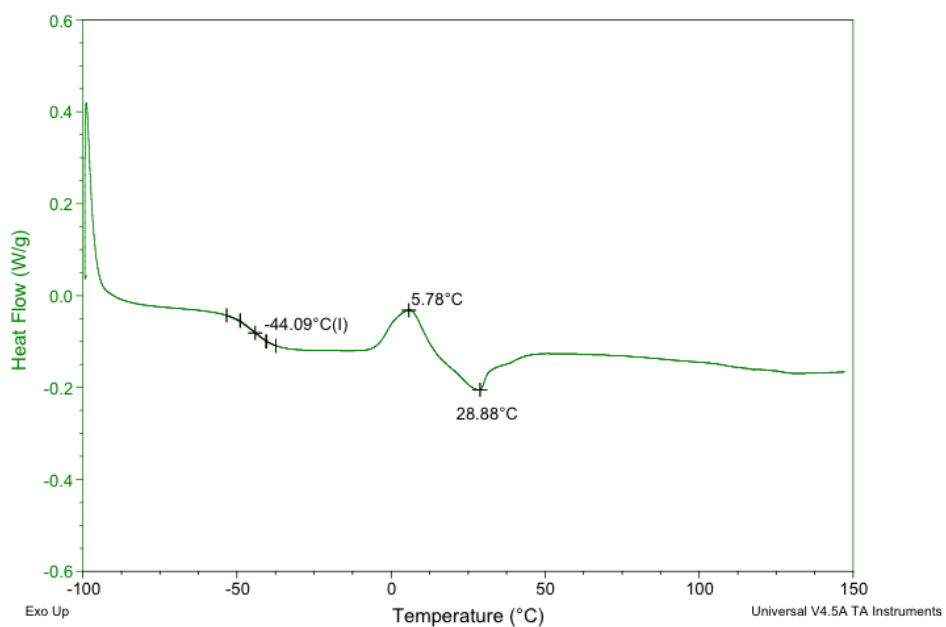


**Figure A1.31.** DSC curve for PEO<sub>45</sub>-*b*-PHEL<sub>45</sub>-TEG (obtained from fourth heating cycle).

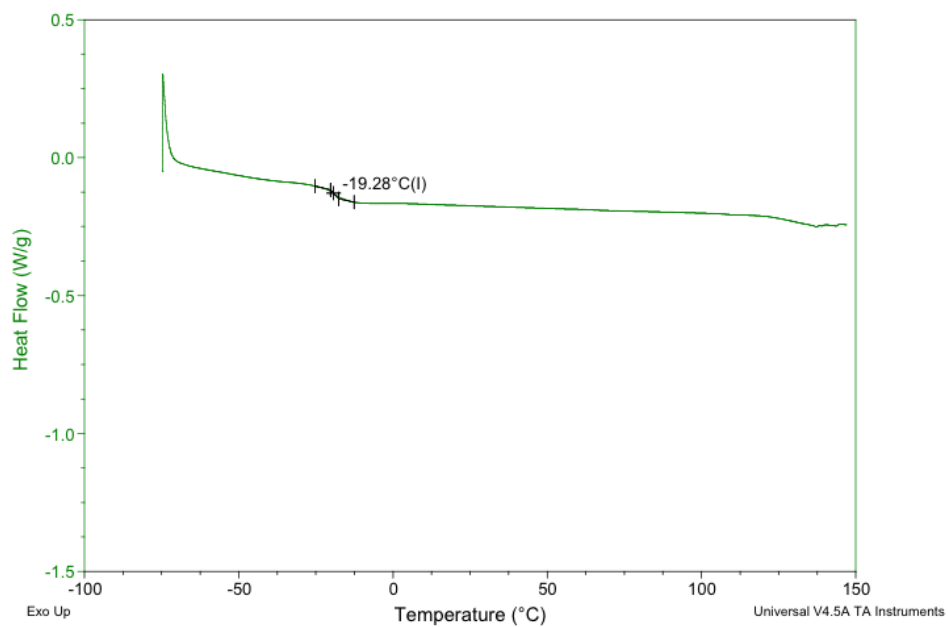


**Figure A1.32.** DSC curve for PEO<sub>45</sub>-*b*-PHEL<sub>45</sub>-acid (obtained from third heating cycle).

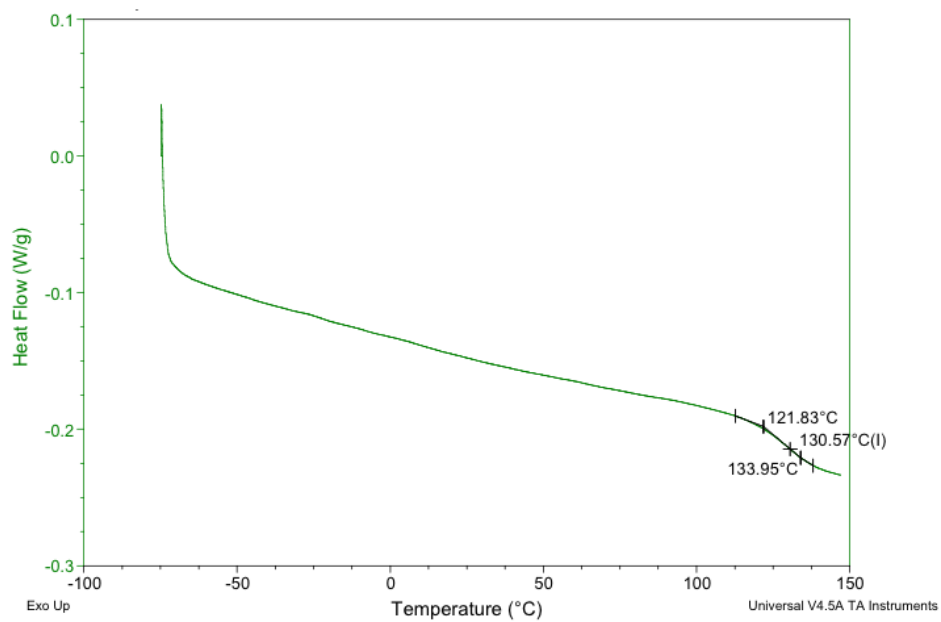


**Figure A1.33.** DSC curve for PEO<sub>45</sub>-*b*-PHEL<sub>45</sub>-PTX34 (obtained from third heating cycle).

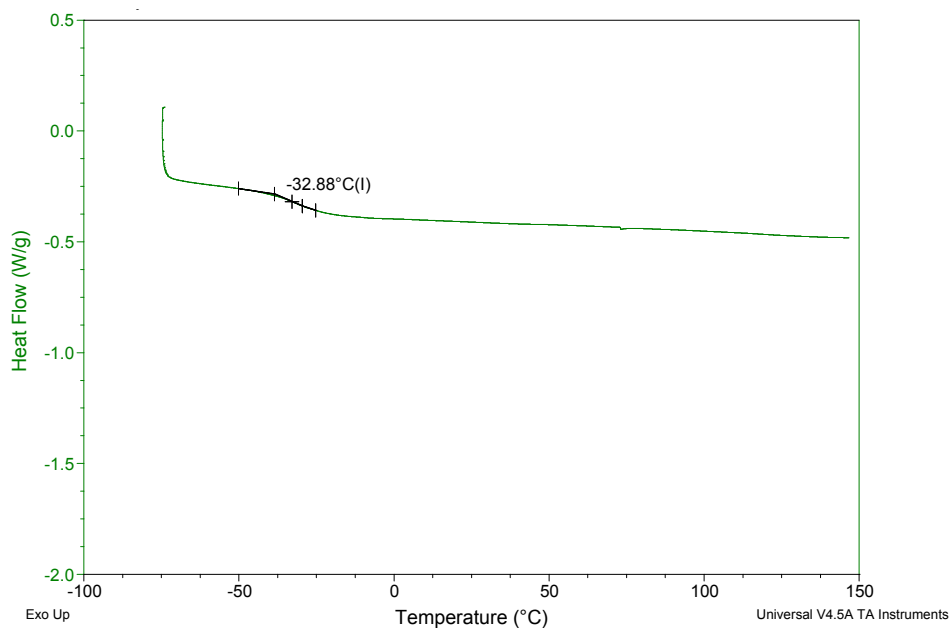


**Figure A1.34.** DSC curve for PEO<sub>45</sub>-*b*-PHEL<sub>45</sub>-RHD (obtained from third heating cycle).

**Table A1.1.** Summary of the thermal stabilities of PEO-*b*-PHELs measured by TGA.  
 T<sub>98%</sub> = maximum temperature at which 98% of mass is still present; T<sub>o</sub> = onset degradation temperature.

Polymer	T <sub>98%</sub> (°C)	T <sub>o</sub> (°C)
PEO <sub>45</sub> - <i>b</i> -PHEL <sub>23</sub>	223	262
PEO <sub>45</sub> - <i>b</i> -PHEL <sub>45</sub>	156	270
PEO <sub>45</sub> - <i>b</i> -PHEL <sub>79</sub>	243	262
PEO <sub>45</sub> - <i>b</i> -PHEL <sub>45</sub> -octyl	148	273
PEO <sub>45</sub> - <i>b</i> -PHEL <sub>45</sub> -TEG	142	258
PEO <sub>45</sub> - <i>b</i> -PHEL <sub>45</sub> -acid	232	246
PEO <sub>45</sub> - <i>b</i> -PHEL <sub>45</sub> -PTX34	114	221
PEO <sub>45</sub> - <i>b</i> -PHEL <sub>45</sub> -RHD	214	247

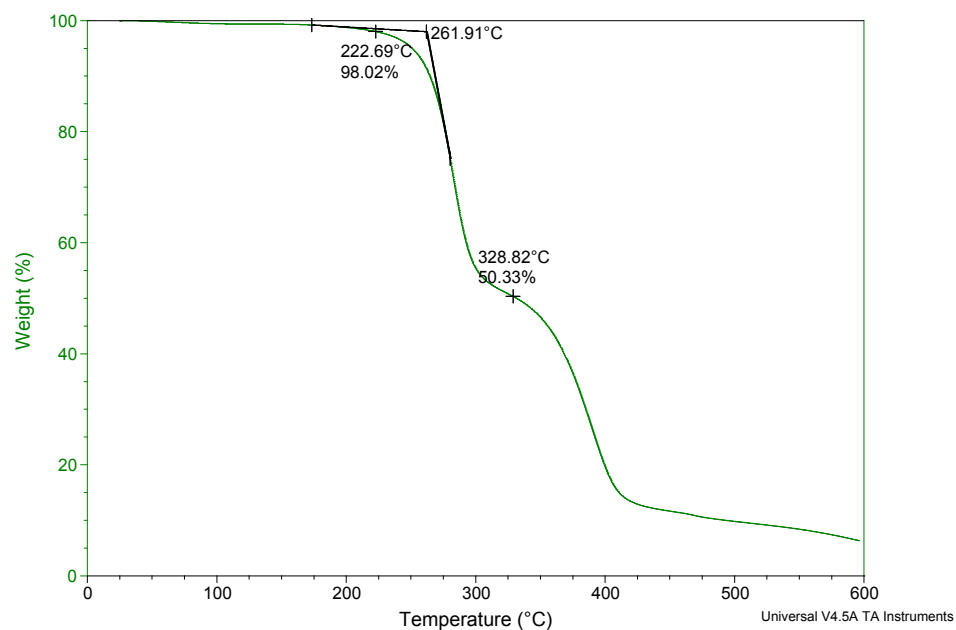


**Figure A1.35.** TGA curve for PEO<sub>45</sub>-*b*-PHEL<sub>23</sub>.

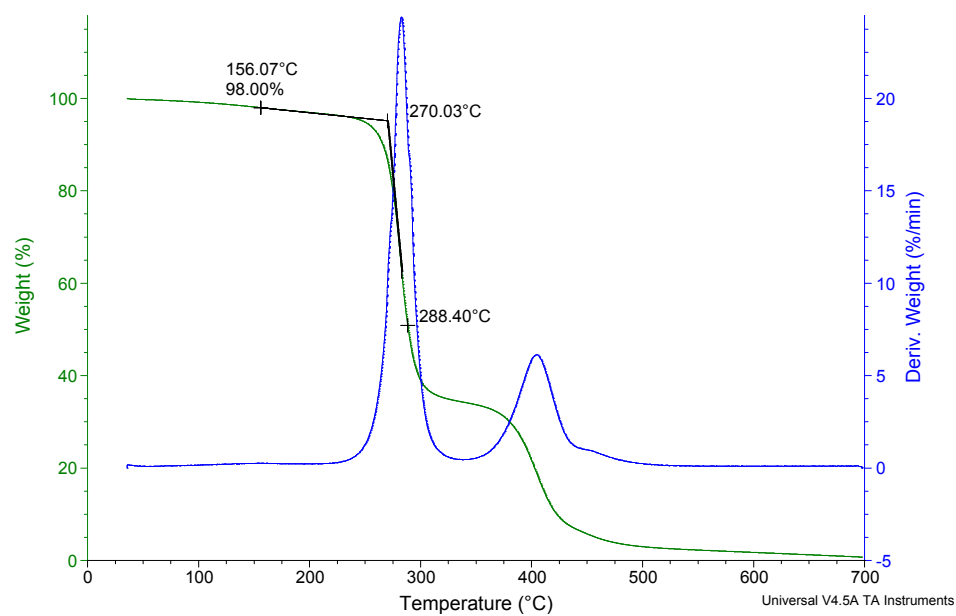


**Figure A1.36.** TGA curve for PEO<sub>45</sub>-*b*-PHEL<sub>45</sub>.

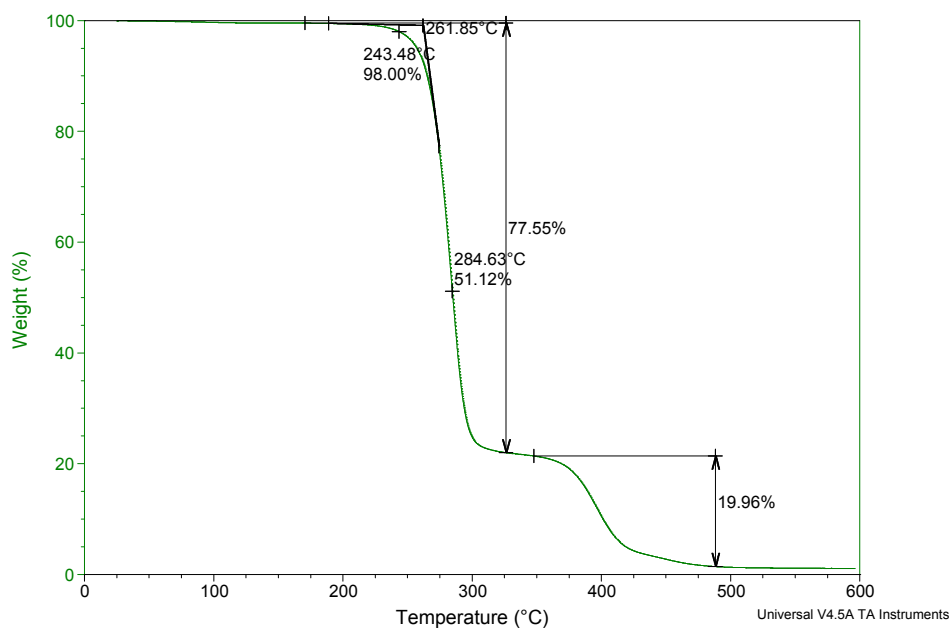


**Figure A1.37.** TGA curve for PEO<sub>45</sub>-*b*-PHEL<sub>79</sub>.

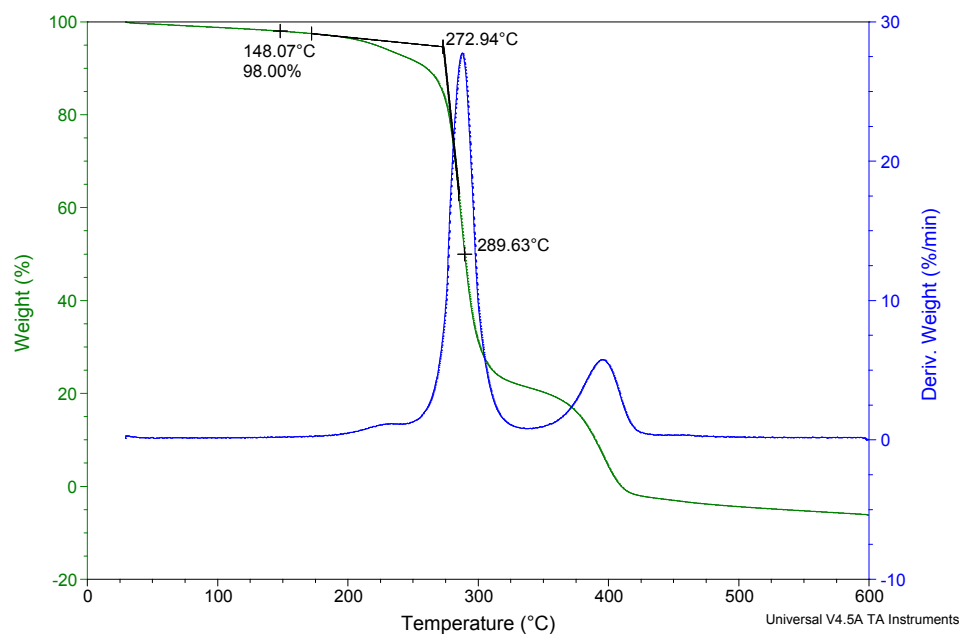


**Figure A1.38.** TGA curve for PEO<sub>45</sub>-*b*-PHEL<sub>45</sub>-octyl.

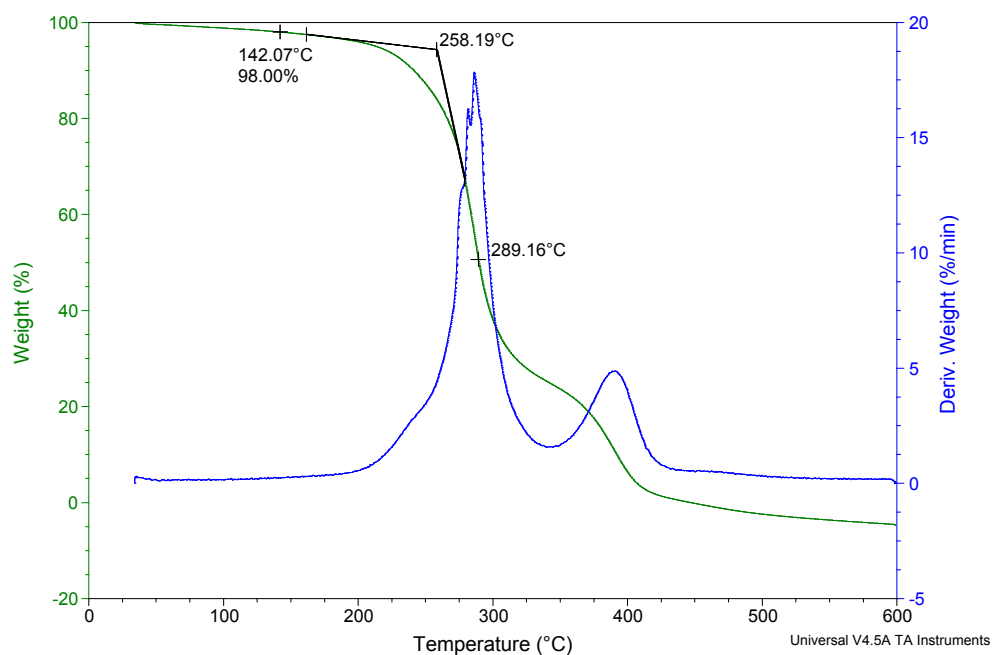


**Figure A1.39.** TGA curve for PEO<sub>45</sub>-*b*-PHEL<sub>45</sub>-TEG.

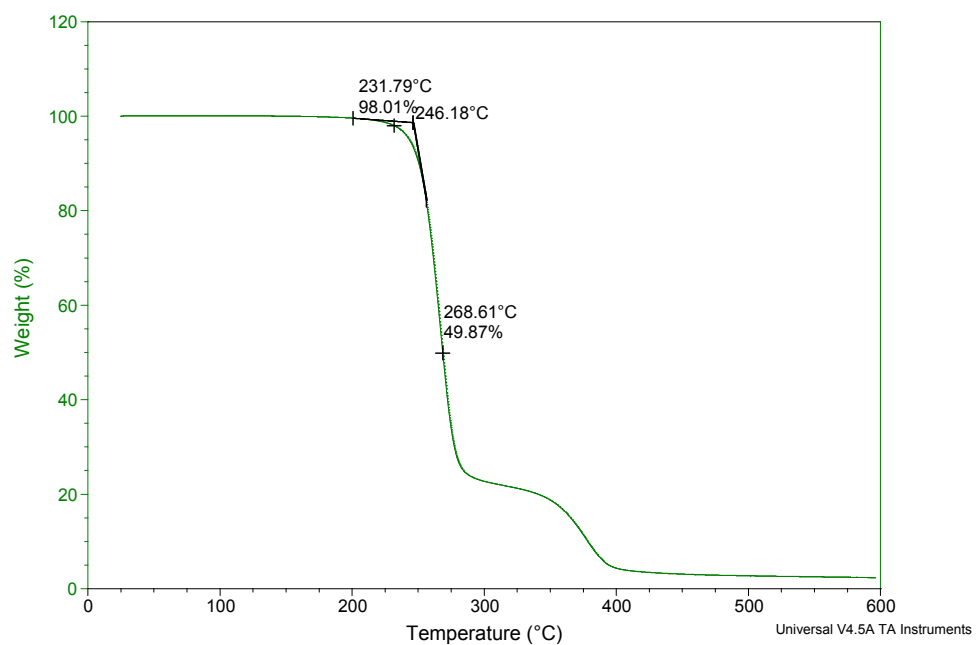


**Figure A1.40.** TGA curve for PEO<sub>45</sub>-*b*-PHEL<sub>45</sub>-acid.

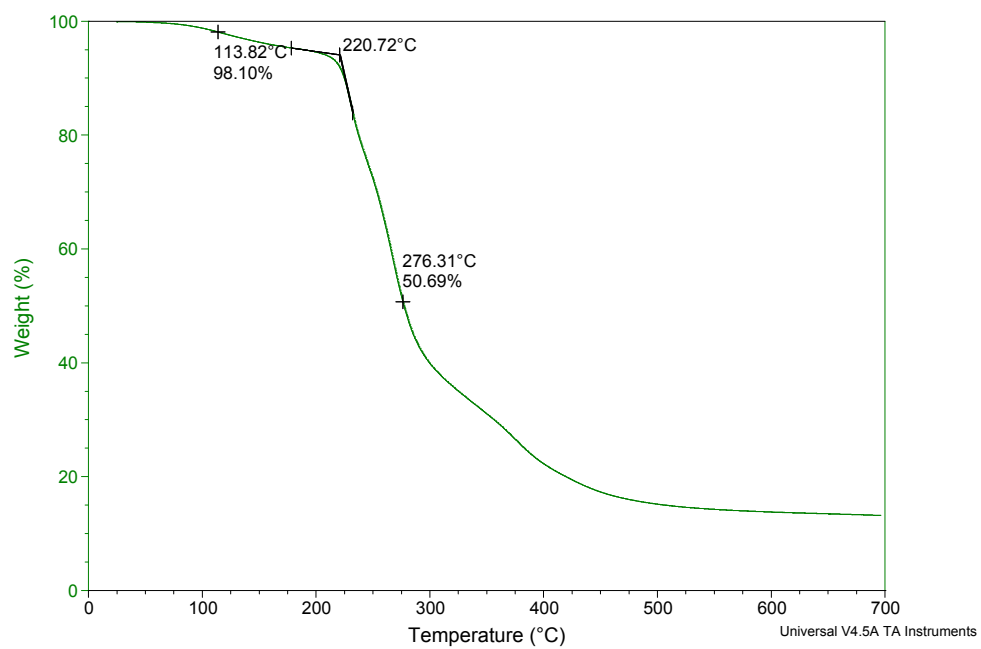


**Figure A1.41.** TGA curve for PEO<sub>45</sub>-*b*-PHEL<sub>45</sub>-PTX34.

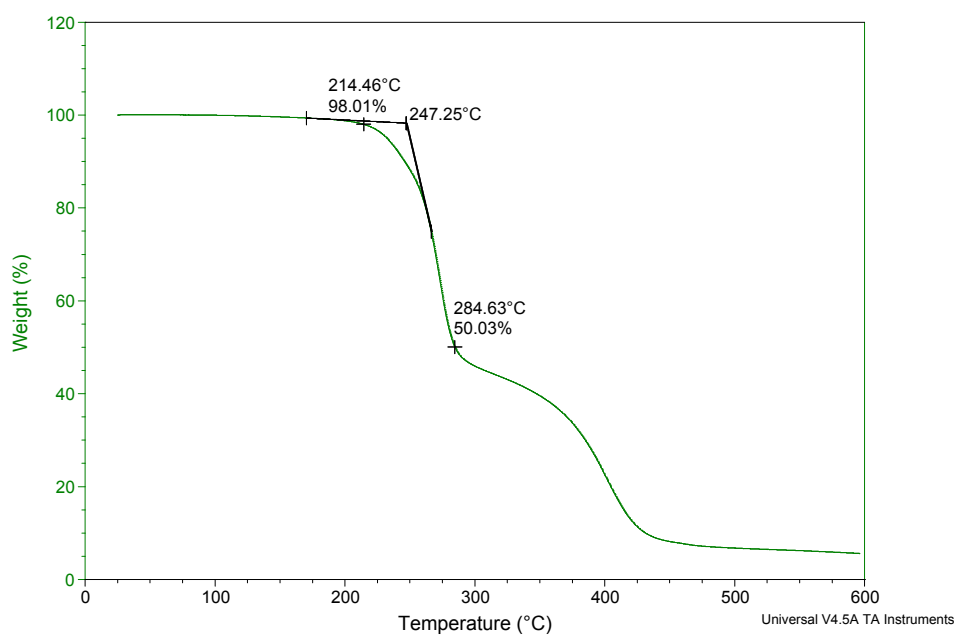


**Figure A1.42.** TGA curve for PEO<sub>45</sub>-*b*-PHEL<sub>45</sub>-RHD.



## Appendix 2

This appendix and compounds 1-7 included within correspond to the molecules described in Chapter 3.

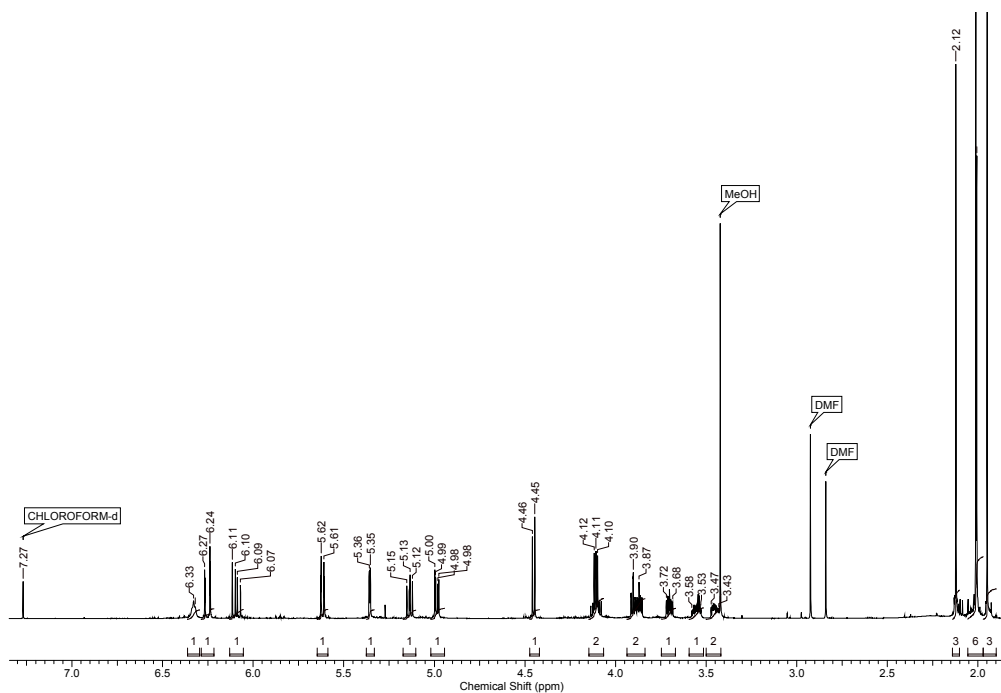


**Figure A2.1.**  $^1\text{H}$  NMR of acrylamide functionalized  $\beta$ -D-galactose pentacetate monomer (5) immediately before polymerization (600 MHz,  $\text{CDCl}_3$ ).

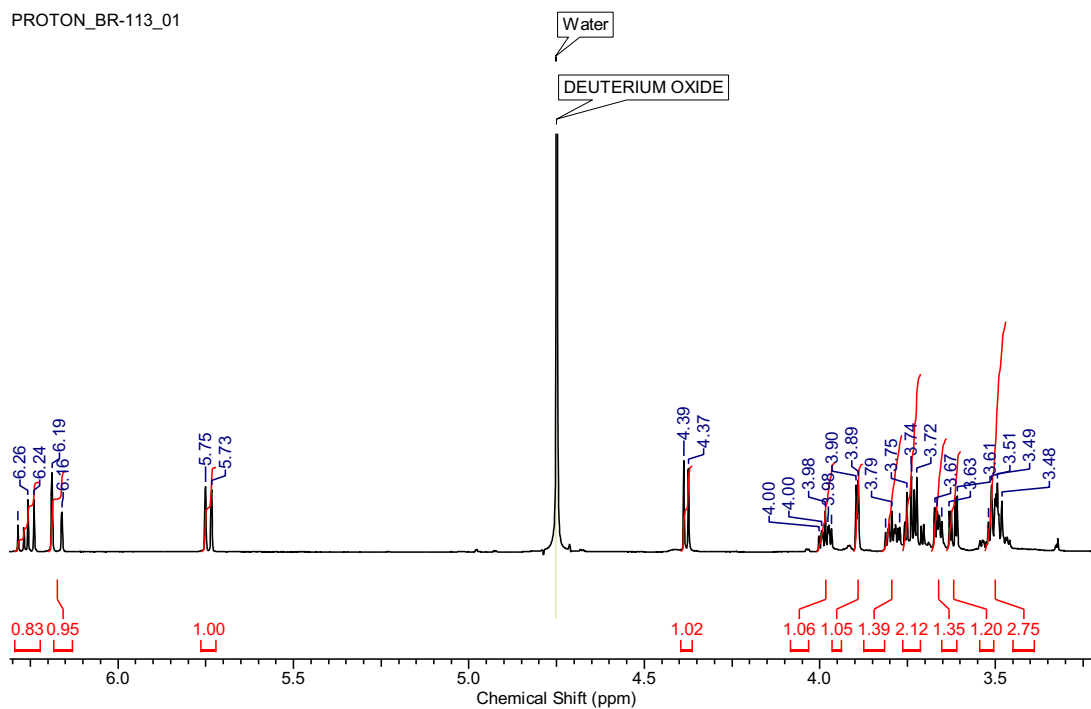


**Figure A2.2.**  $^1\text{H}$  NMR of purified  $\beta$ -D-galactose monomer possessing acrylamide functionality (**6**) (600 MHz,  $\text{D}_2\text{O}$ ).

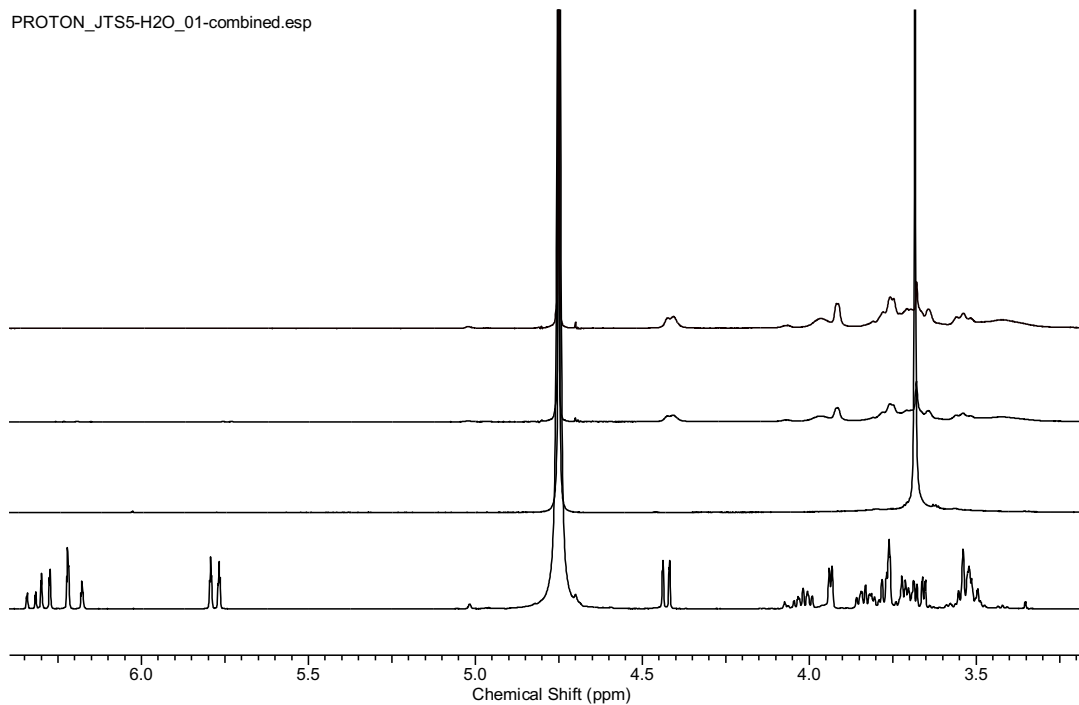


**Figure A2.3.**  $^1\text{H}$  NMR spectra of  $\beta$ -D-galactose monomer, CTA-functionalized PBD-*b*-PEO vesicles, polymerization at  $t = 18$  h, and  $t = 48$  h (bottom to top).

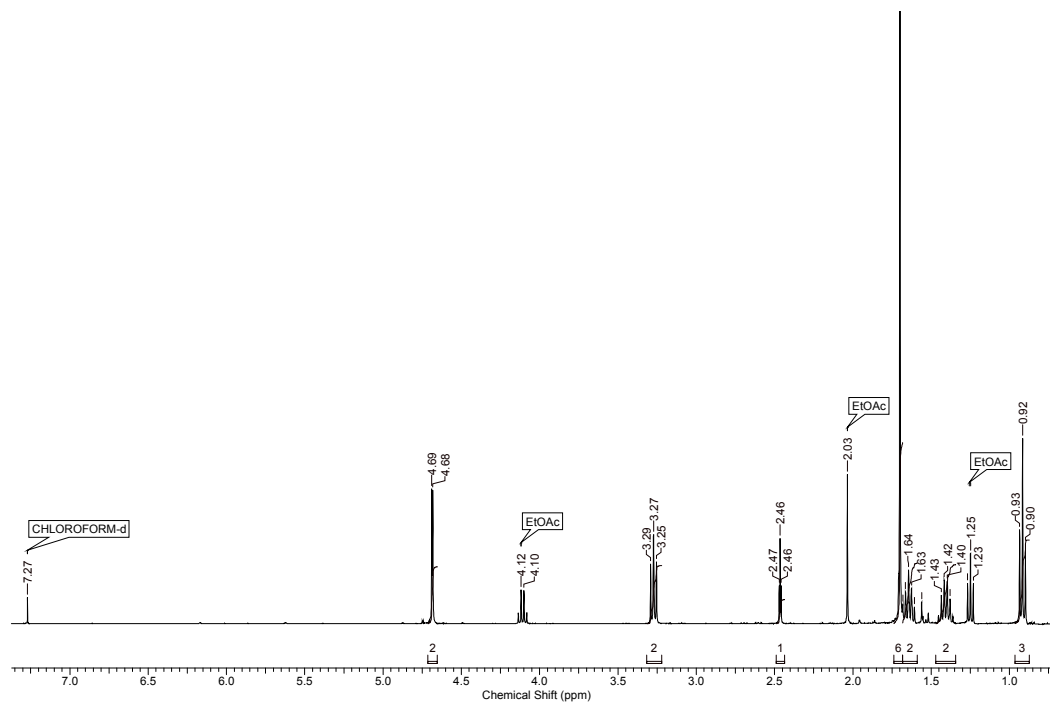


**Figure A2.4.**  $^1\text{H}$  NMR of prop-2-ynyl-2-(butylthiocarbonothiolthio)-2-methylpropanoate alkyne RAFT CTA (600 MHz,  $\text{CDCl}_3$ ).

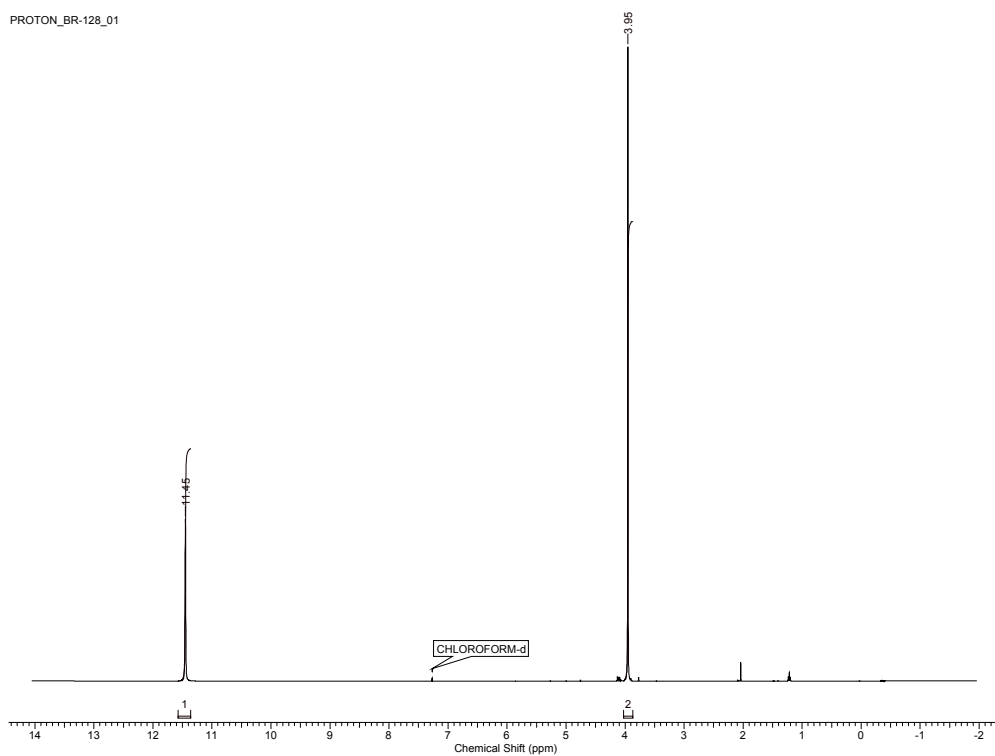


**Figure A2.5.**  $^1\text{H}$  NMR of 2-azidoacetic acid (600 MHz,  $\text{CDCl}_3$ ).

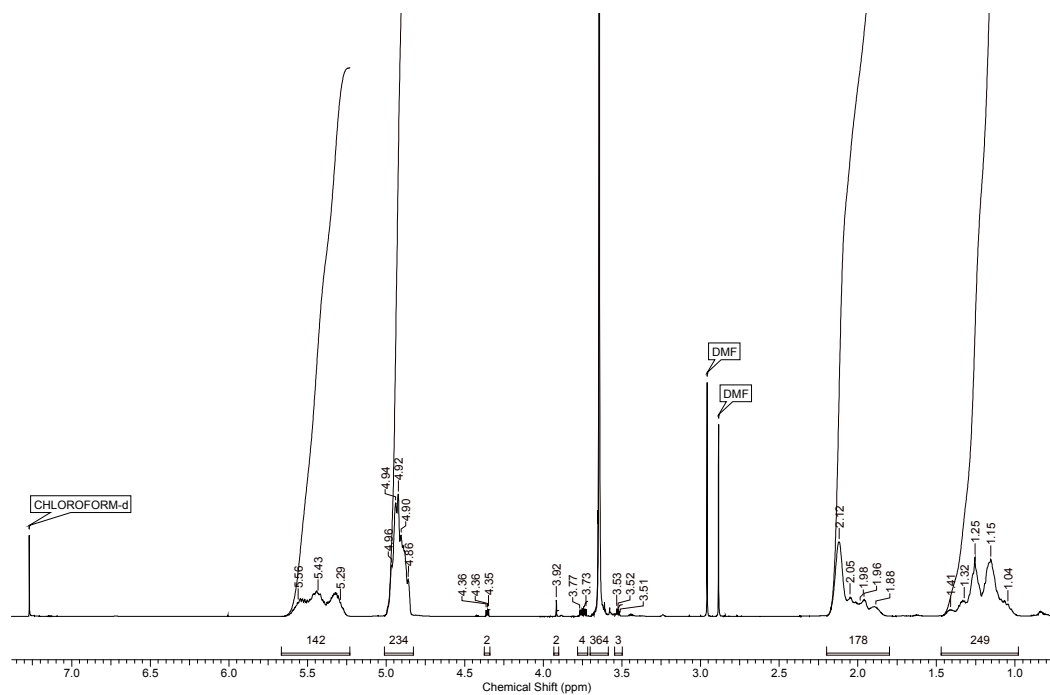


**Figure A2.6.** <sup>1</sup>H NMR of PBD-*b*-PEO-N<sub>3</sub> (600 MHz, CDCl<sub>3</sub>).

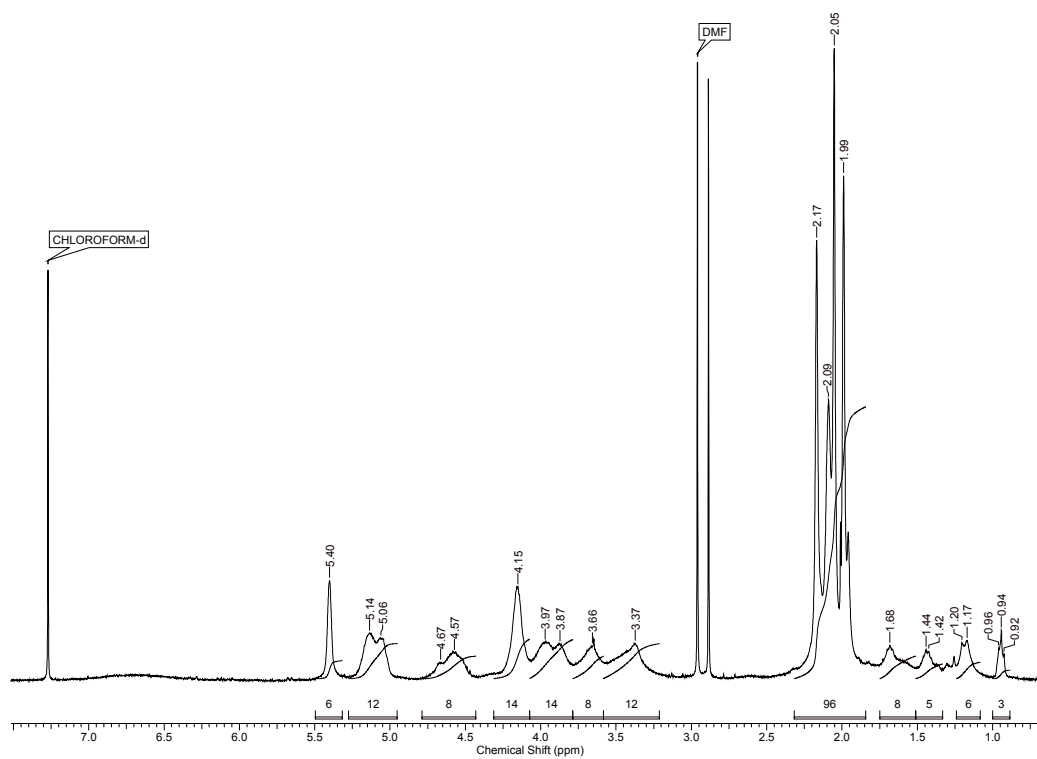


**Figure A2.7.** <sup>1</sup>H NMR of PAcGal<sub>6</sub> (600 MHz, CDCl<sub>3</sub>).

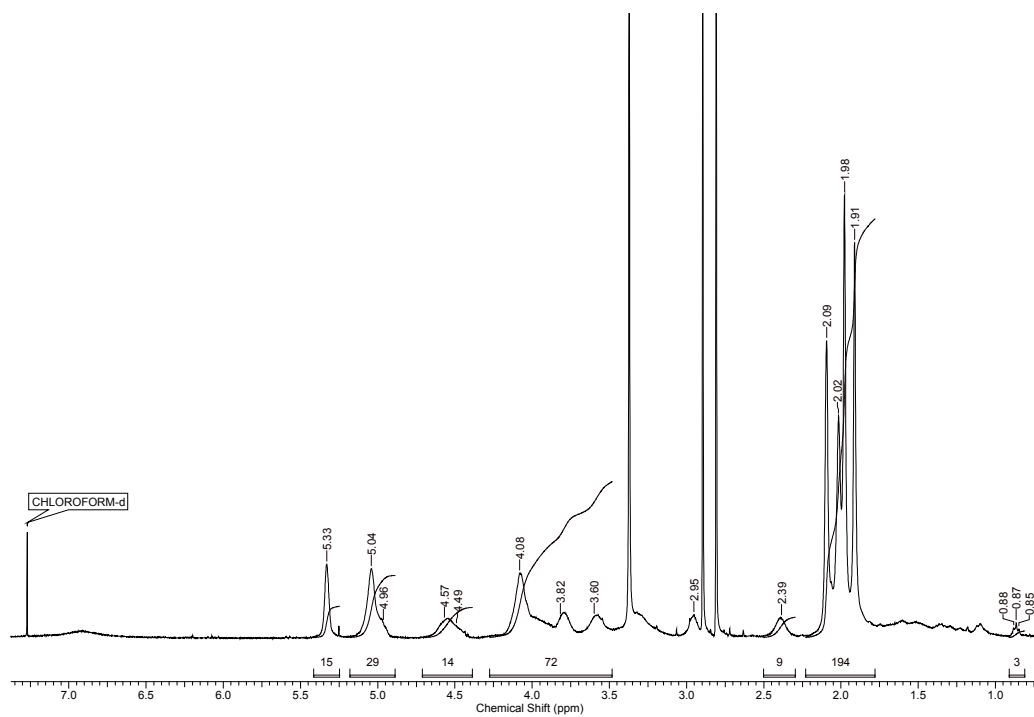


**Figure A2.8.** <sup>1</sup>H NMR of PAcGal<sub>15</sub> (600 MHz, CDCl<sub>3</sub>).

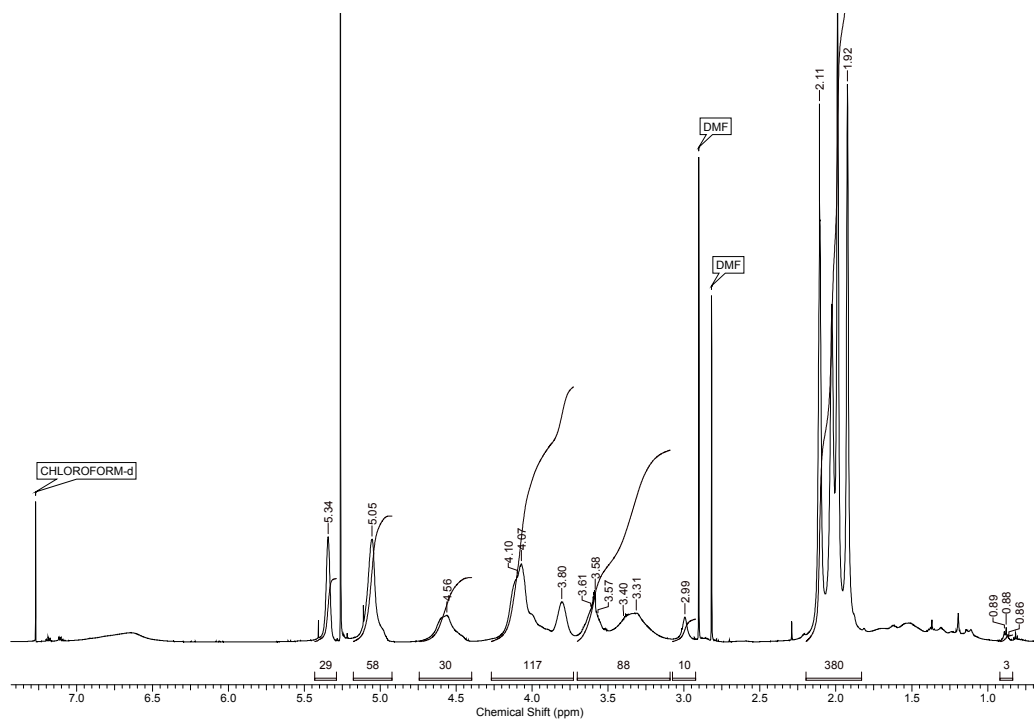


**Figure A2.9.** <sup>1</sup>H NMR of PAcGal<sub>29</sub> (600 MHz, CDCl<sub>3</sub>).

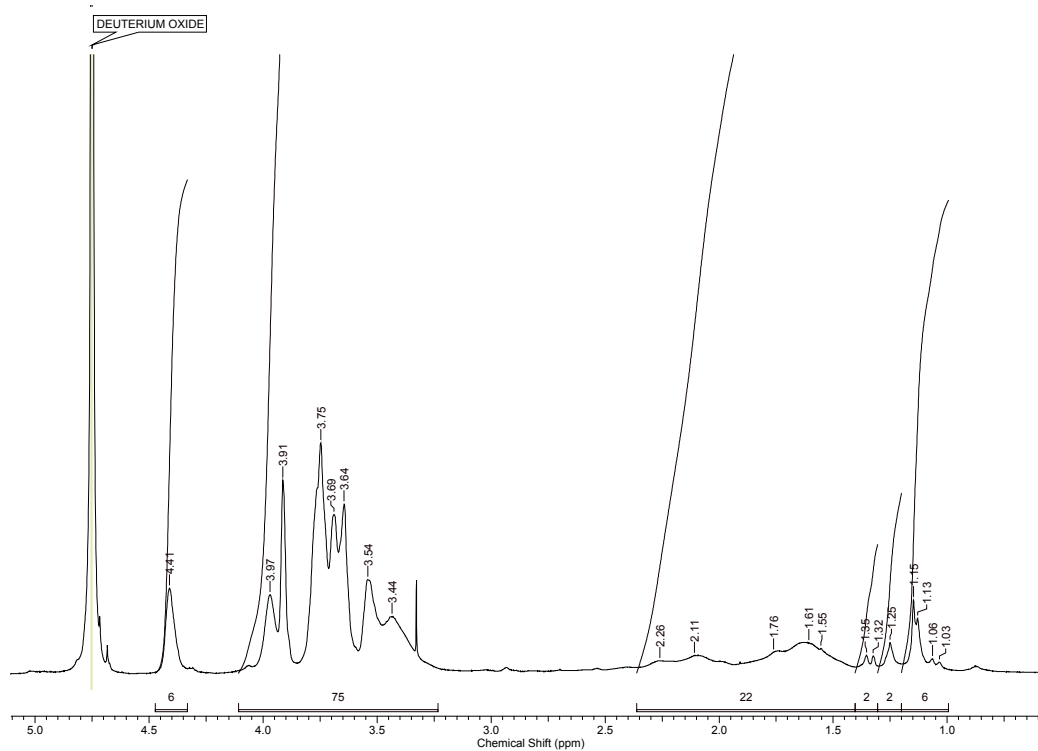


**Figure A2.10.** <sup>1</sup>H NMR of PGal<sub>6</sub> (600 MHz, D<sub>2</sub>O).

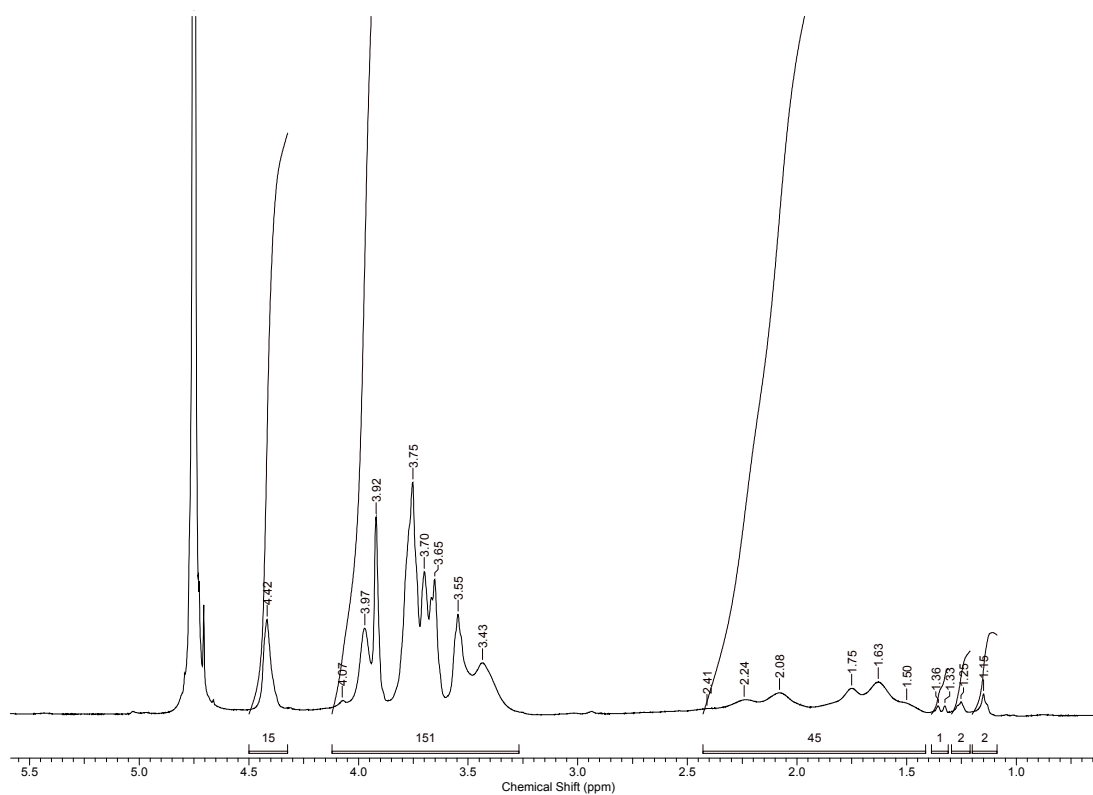


**Figure A2.11.** <sup>1</sup>H NMR of PGal<sub>15</sub> (600 MHz, D<sub>2</sub>O).

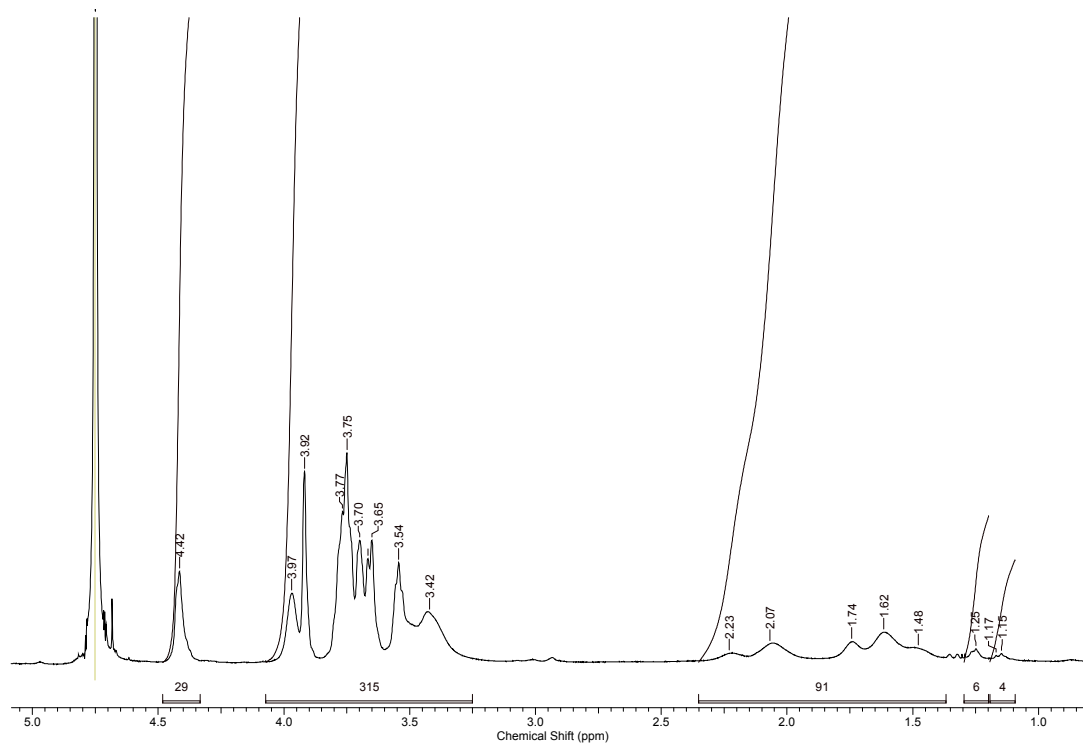


**Figure A2.12.** <sup>1</sup>H NMR of PGal<sub>29</sub> (600 MHz, D<sub>2</sub>O).

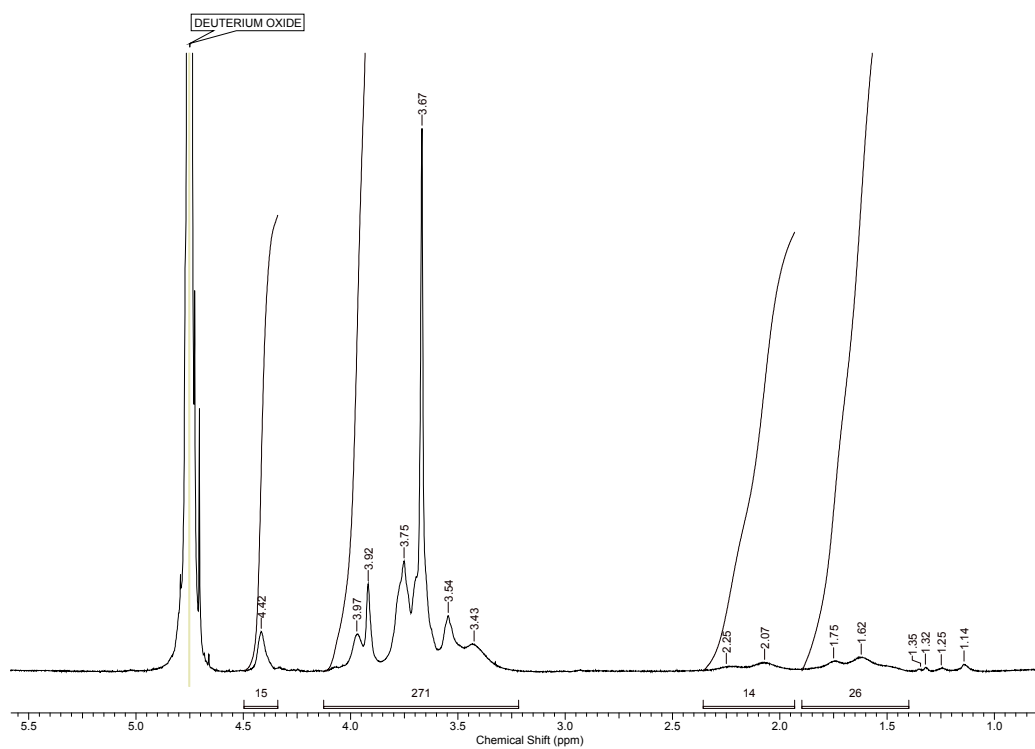


**Figure A2.13.** <sup>1</sup>H NMR of click reaction between PGal<sub>15</sub> and 10% azide-functionalized vesicles (600 MHz, D<sub>2</sub>O).

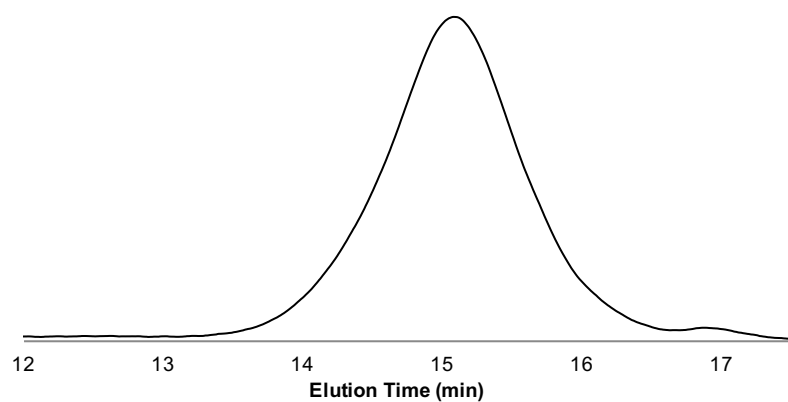


**Figure A2.14.** SEC trace for PAcGal<sub>6</sub>.

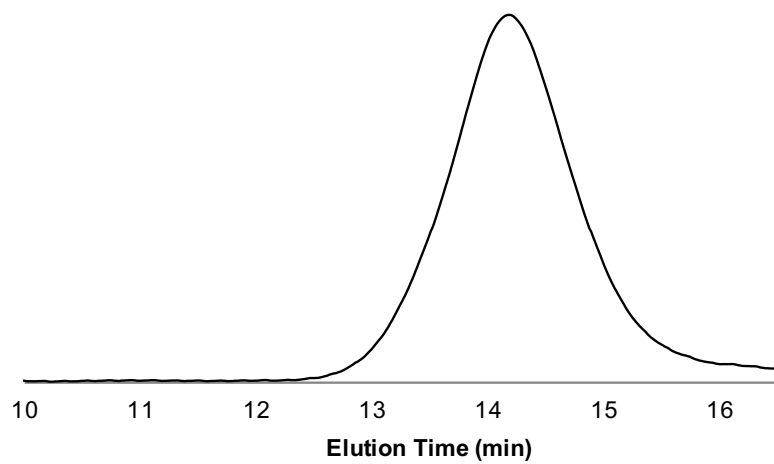


**Figure A2.15.** SEC trace for PAcGal<sub>15</sub>.

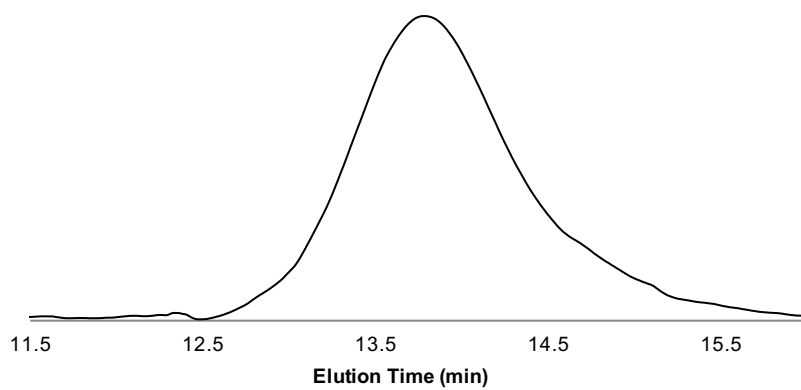


**Figure A2.16.** SEC trace for PAcGal<sub>29</sub>.



# Curriculum Vitae

**Name:** Brooke Marie Raycraft

## EDUCATION AND DEGREES

<b>Western University</b> M.Sc., Organic Chemistry	London, ON Sept 2014-Aug 2016
<b>Wilfrid Laurier University</b> Honours B.Sc., Health Sciences, Chemistry minor	Waterloo, ON Sept 2010-Apr 2014

## GRANTS AND AWARDS

<b>Fallona Family Interdisciplinary Showcase</b> • 1 <sup>st</sup> place poster in Materials and Biomaterials Division (\$100)	London, ON Dec 2015
<b>Western University</b> • Ontario Graduate Scholarship (\$15,000)	London, ON 2014-2015

## RELATED PROFESSIONAL EXPERIENCE

<b>Western University</b> Head Teaching Assistant, Introductory Organic Chemistry I and II	London, ON 2015-2016
<b>Western University</b> Teaching Assistant, Introductory Organic Chemistry I and II	London, ON 2014-2015
<b>Wilfrid Laurier University</b> Teaching Assistant, Introductory Organic Chemistry I and II	Waterloo, ON 2012-2014

## CONFERENCE PRESENTATIONS

**Raycraft, B.R.**, McIntosh, J.T., MacDonald, J.P., Gillies, E.R., Shaver, M.P. (2016). Functional polyester diblock copolymers possessing encapsulation and chemical conjugation capabilities. Talk delivered at the Canadian Chemistry Conference, Halifax, ON, June 2016.

**Raycraft, B.R.**, Whitton, G., Trant, J.F. and Gillies, E.R. (2015). Glycopolymer-functionalized vesicles via aqueous RAFT polymerization from vesicle surface. Poster

presentation delivered at the Fallona Family Interdisciplinary Research Showcase, London, ON, December 2015.

**Raycraft, B.R.**, Whitton, G., Trant, J.F. and Gillies, E.R. (2015). Glycopolymer-functionalized vesicles via aqueous RAFT polymerization from vesicle surface. Poster presentation delivered at the Canadian Chemistry Conference, Ottawa, ON, June 2015.

**Raycraft, B.R.**, Whitton, G., Trant, J.F. and Gillies, E.R. (2015). Glycopolymer-coated vesicles via aqueous RAFT polymerization. Poster presentation delivered at CAMBR, London, ON, April 2015.

**Raycraft, B.R.** and Maly, K.E. (2013). Synthesis and self-assembly of luminescent tetraoxadicyanopentacene derivatives. Poster presentation delivered at the Ontario-Quebec Physical Organic Mini-Symposium, Montreal, QC, November 2013.

**Raycraft, B.R.** and Maly, K.E. (2013). Synthesis, characterization and self-assembly of luminescent tetraoxadicyanopentacene derivatives. Oral presentation delivered at the Southern Ontario Undergraduate Student Chemistry Conference, Windsor, ON, March 2014.

## PUBLICATIONS

### Journal Articles

Raycraft, B.M., McIntosh, J.T., MacDonald, J.P., Gillies, E.R., Shaver, M.P. (2016). Functional polyester diblock copolymers possessing encapsulation and chemical conjugation capabilities. Manuscript in preparation.

### Magazine Entries

Co-Author. Whelan A\*, Kandiah J\*, Raycraft B\*. (2014). Altitude: Healthcare Mentoring – the importance of mentoring undergraduate students. Scrub-In. 9(3): 8-9.